DETERMINATION OF BRACE FORCES CAUSED BY CONSTRUCTION LOADS AND WIND LOADS DURING BRIDGE CONSTRUCTION

By

SAMUEL TAYLOR EDWARDS

A THESIS PRESENTED TO THE GRADUATE SCHOOL
OF THE UNIVERSITY OF FLORIDA IN PARTIAL FULFILLMENT
OF THE REQUIREMENTS FOR THE DEGREE OF
MASTER OF ENGINEERING

UNIVERSITY OF FLORIDA

2014

ACKNOWLEDGMENTS

This thesis would not be possible without the support of several individuals. I would like to express my sincere gratitude to my advisor, Dr. Gary Consolazio, for his motivation and guidance throughout my graduate education. He is an excellent role model and has greatly influenced my professional and technical skills as an engineer. Additionally, I would like to thank Dr. H.R. (Trey) Hamilton, Dr. Kurt Gurley, and Dr. Jennifer Rice for serving on my supervisory committee. Finally, I would like to thank my family and friends for providing support throughout this process.

TABLE OF CONTENTS

LIST OF TABLES

LIST OF FIGURES

Figure page

Abstract of Thesis Presented to the Graduate School
of the University of Florida in Partial Fulfillment of the
Requirements for the Degree of Master of Engineering

DETERMINATION OF BRACE FORCES CAUSED BY CONSTRUCTION LOADS AND WIND LOADS DURING BRIDGE CONSTRUCTION

By

Samuel Taylor Edwards

May 2014

Chair: Gary Consolazio
Major: Civil Engineering

The first objective of this study was to develop procedures for determining bracing forces during bridge construction. Numerical finite element models and analysis techniques were developed for evaluating brace forces induced by construction loads acting on precast concrete girders (Florida-I Beams) in systems of multiple girders braced together. A large-scale parametric study was performed with both un-factored (service) and factored (strength) construction loads (in total, more than 450,000 separate three-dimensional (3-D) structural analyses were conducted). The parametric study included consideration of different Florida-I Beam cross-sections, span lengths, girder spacings, deck overhang widths, skew angles, number of girders, number of braces, and bracing configurations (K-brace and X-brace). Additionally, partial coverage of wet (non-structural) concrete load and variable placement of deck finishing machine loads were considered. A MathCad calculation program was developed for quantifying brace forces using a database approach that employs multiple-dimensional linear interpolation. The accuracy of the database program was assessed by using it to predict end-span and intermediate-span brace forces for parameter selections not directly contained within the database, and then comparing the interpolated predictions to results obtained from finite element

analyses of corresponding verification models. In a majority of cases, the database-predicted brace forces were found to be less than ten percent (10%) in error.

The second objective of this study was to experimentally determine wind load coefficients (drag, torque, and lift) for common bridge girder shapes with stay-in-place (SIP) formwork and overhang formwork in place, and then to develop recommended global (system) pressure coefficients (e.g., for strength design of substructures). Wind tunnel tests were performed on reduced-scale models of Florida-I Beam (FIB), plate girder, and box girder cross-sectional shapes to measure aerodynamic forces acting on individual girders in the bridge cross-section. Tests were conducted at multiple wind angles, and corresponding tests with and without overhang formwork were conducted. Data from the wind tunnel tests were used to develop conservative procedures for calculating global pressure coefficients suitable for use in bridge design.

CHAPTER 1
INTRODUCTION

1.1 Overview

During the process of constructing a highway bridge, both the structure and the applied loading conditions will transition through several distinct stages, each of which warrants consideration from a structural safety perspective. Initially, individual girders are lifted by crane and placed into position atop flexible elastomeric bearing pads located on the bridge supports (e.g., abutments or piers). Placement of all girders into their final positions constitutes one of the earliest distinct structural stages that must be assessed for safety. In this structural configuration, it is typical for braces to be installed between the individual girders (Figure 1-1). Additionally, one or more girders may also be anchored to the bridge supports.

Structurally, the system at this stage consists of individual girders, bearing pads, braces, potentially anchors, and support structures (i.e., substructures). Loading conditions consist primarily of vertical gravity loads and horizontal wind loads (for individual girders as well for the collection of all girders as a whole). Primary structural design and safety concerns at this stage of construction focus on girder stability, adequate strength (and stiffness) of braces, and adequate global capacity of the substructure. Addressing these concerns requires that engineering calculation methods be available for quantifying girder buckling capacity, quantifying wind loads on the individual girders (due to predominantly horizontal wind), quantifying brace forces due to the same wind loads, and quantifying global wind-induced lateral loads on the bridge substructure (e.g., for strength design). All of these areas of concern were addressed in a previous study funded by the FDOT (BDK75-977-33, Consolazio et al., 2013) that involved the development of analytical methods for predicting structural forces and capacities, and

experimental wind tunnel testing to quantify aerodynamic girder wind load coefficients (drag, torque, and lift), including the effects of aerodynamic shielding.

After continued construction progress, another key stage will be reached wherein stay-in-place (SIP) forms have been installed between the girders and overhang formwork (and associated overhang support brackets) have been eccentrically attached to the exterior (fascia) girders of the bridge. Loading conditions at this stage consist primarily of horizontal wind loads and vertical 'construction loads' that are primarily associated with the process of placing the wet (plastic) concrete deck (Figure 1-2) and finishing it with a finishing machine (or a 'bridge paver'). During the deck placement process, most of the construction loads are applied eccentrically to overhang formwork and to stay-in-place forms. Consequently, torsional moments acting on the girders produce axial forces in the bracing system (diagonal and horizontal elements) that must be considered in the brace design process. Several geometric parameters influence the magnitude of brace forces caused by construction loads. A major component of the research presented in this report was carried out to quantify bracing forces caused by construction loads over a wide range of geometric parameters (i.e., span lengths, girder spacings, deck overhang widths, etc.).

Also of concern at this stage of construction are wind-induced lateral loads acting globally on the entire bridge cross section. Such loads generate lateral forces on the bridge substructure that must be considered in the design process. While the issue of global lateral wind load was addressed in the previous BDK75-977-33 study, the 'wind configuration' (or 'wind profile') of the bridge considered in the present study was distinctly different due to the aerodynamic blockage (between girders) that results from installation of SIP forms and overhangs. Therefore, in the study presented in this report, wind tunnel testing was once again

used quantify wind load coefficients (drag, torque, and lift) for multiple-girder systems, but this time *with* SIP forms (and possibly overhangs) present. The goal of measuring this data was to develop conservative methods for calculating global pressure coefficients and global lateral wind loads for substructure design.

1.2 Objectives

One objective of this research was to use finite element analysis of partially constructed bridge systems—consisting of multiple braced prestressed concrete girders (Florida-I beams)—to develop calculation procedures for quantifying brace forces caused by eccentric construction loads. A related objective was to experimentally determine wind load coefficients (drag, torque, and lift) for common bridge girder shapes with stay-in-place (SIP) forms and overhang formwork in place, and then to develop recommended global (system) pressure coefficients (e.g., for use in the strength design of substructures).

1.3 Scope of Work

- **Construction loads**: Numerical finite element bridge models and analysis techniques were developed for evaluating brace forces induced by construction loads acting on precast concrete girders (Florida-I Beams) in systems of multiple girders braced together. The construction loads considered were: wet concrete deck load, stay-in-place (SIP) form weight, overhang formwork weight, live load, worker line loads, and concentrated loads representing a deck finishing machine. A large-scale parametric study, involving more than 450,000 separate three-dimensional structural analyses, was performed to compute maximum brace forces for un-factored (service) and factored (strength) construction load conditions. The parametric study included consideration of different Florida-I Beam cross-sections, span lengths, girder spacings, deck overhang widths, skew angles, number of girders, number of braces, and bracing configurations (K-brace and X-brace). Maximum end-span brace forces and intermediate-span brace forces quantified from the parametric study were stored into a database and an ‘interpolated database approach’ to brace force prediction was developed and coded into a MathCad program for ease of use.

- **Wind loads**: Wind tunnel testing was used to quantify wind load coefficients (drag, torque, and lift) for systems of multiple bridge girders (FIB, plate girder, and box) with stay-in-place (SIP) forms and overhang formwork in place. Tests were conducted at multiple wind angles, and corresponding tests with and without overhang formwork were conducted so that the effects of overhang formwork on drag, lift, and torque coefficients could be quantified. Drag coefficients measured at each girder position in bridges with I-

shaped girders, and in bridges with box girders, were used to develop conservative methods for computing global (system) pressure coefficients suitable for use in bridge design (particularly, for use in calculating global lateral substructure load due to wind).

Figure 1-1. Prestressed concrete girders braced together for stability (photo courtesy of FDOT)

Figure 1-2. Bridge construction loads (photo courtesy of Gomaco)

CHAPTER 2
STRUCTURAL CONFIGURATION AND LOADING CONDITIONS DURING BRIDGE CONSTRUCTION

2.1 Overview

Braces used to stabilize girders during bridge construction must be designed to resist forces that are generated by construction loads and wind loads. The manner in which brace forces are distributed to the elements of the bracing system depends on geometric parameters (span length, girder spacing, deck overhang width, etc.), bracing configurations, and cross-sectional properties of the girders. In the present study, the girders under investigation are Florida-I Beams (FIBs), a group of standard cross-sectional shapes of varying depths that are commonly employed in Florida bridge designs. These beams are typically cast offsite, transported to the construction site by truck, then lifted into position one-at-a-time by crane, where they are placed on elastomeric bearing pads and braced together for stability. Formwork systems are then added to support the wet concrete deck and other construction loads encountered during the deck pouring process. In this chapter, a physical description of the 'construction-stage' structures under consideration will be provided along with the definition of relevant terminology.

2.2 Geometric Parameters

The term *girder system* will be used to refer to a group of two or more FIBs braced together in an evenly spaced row (Figure 2-1). In addition to span length and lateral spacing, there are several geometric parameters that define the shape and placement of the girders within a system:

- **Grade**: Longitudinal incline of the girders, typically expressed as a percentage of rise per unit of horizontal length (Figure 2-2).
- **Cross-slope**: The transverse incline (slope) of the deck, expressed as a percentage, which results in girders that are staggered vertically (Figure 2-3).

- **Skew angle**: Longitudinal staggering of girders, due to pier caps that are not perpendicular to the girder axes (Figure 2-4).
- **Camber**: Vertical bowing of the girder (Figure 2-5) due to prestressing in the bottom flange; expressed as the maximum vertical deviation from a perfectly straight line connecting one end of the girder to the other.
- **Sweep**: Lateral bowing of the girder (Figure 2-6) due to manufacturing imperfections, expressed as the maximum horizontal deviation from a perfectly straight line connecting one end of the girder to the other.

2.3 Bearing Pads

FIB bridge girders rest directly on steel-reinforced neoprene bearing pads which are the only points of contact between the girder and the substructure. There is generally sufficient friction between the pad and other structural components so that any movement of a girder relative to the substructure (with the exception of vertical uplift) must displace the top surface of the pad relative to the bottom surface. As a result, the girder support conditions in all six degrees of freedom (three translations, and three rotations) can be represented as finite stiffnesses that correspond to the equivalent deformation modes of the pad. These deformation modes fall into four categories: shear, compression (axial), rotation (e.g., roll), and torsion. Bearing pad stiffnesses in this study were quantified using calculation procedures developed and experimentally validated in a previous study (BDK75-977-33, Consolazio et al., 2013) for typical Florida bridge bearing pads.

2.4 Bracing

As adjacent girders are erected during the bridge construction process, girder-to-girder braces (henceforth referred to simply as *braces*) are used to connect the girders together into a single structural unit. At a minimum, braces are installed near the ends of the girders (close to the supporting piers); such braces are referred to as *end-span braces*. In addition, *intermediate-span braces* spaced at unit fractions (1/2, 1/3, 1/4) of the girder length may also be included. For

example, quarter-point (1/4 span) bracing divides the girder into four equal unbraced lengths (Figure 2-7). When skew is present, brace point locations are longitudinally offset (Figure 2-8) between adjacent girders because *FDOT Design Standard No. 20005: Prestressed I-Beam Temporary Bracing* (FDOT, 2014a) requires that all braces be placed perpendicular to the girders.

Braces are typically constructed from timber or steel members, but individual brace designs are left to the discretion of the contractor, so a variety of different bracing configurations are possible. The most common types of braces used in practice in Florida are X-braces (Figure 2-9a) and K-braces (Figure 2-9b). Therefore, in the present study, only these brace types are considered. Braces are typically attached to the girders using bolted connections or welded to cast-in steel plates.

2.5 Bridge Construction Loads

A major objective this study was to determine axial brace forces induced by bridge construction loads. In particular, the bridge deck placement (concrete application and finishing) process was the construction stage considered. Components of the bridge construction loads considered in this study were as follows:

- **Wind loads**: During bridge construction, wind loads are an important design consideration. However, severe wind loads and active construction loads (i.e., deck placement loads) are not likely to be encountered simultaneously. According to the FDOT Structures Design Guidelines (SDG; FDOT, 2013), the basic wind speed for active construction is specified as 20 mph. In this study, wind loads and construction loads were treated as separate design load cases. Wind loads on girders with stay-in-place forms were quantified experimentally with wind tunnel testing.

- **Concrete deck**: Throughout the deck pouring and finishing process, wet (plastic) concrete has *negligible stiffness*, which is beneficial for shaping the concrete into a smooth finished surface. Consequently, a non-composite girder system must support these construction loads. However, in the final bridge condition, the bridge deck works together with the girders as a composite system to resist and distribute loads to the supporting girders. Since the wet (nonstructural) concrete load is incrementally applied to bridges in the longitudinal direction, this load is treated as a variable length load in the

finite element analyses. Partial application of concrete deck loads to the girder system will be further explained later in this report.

- **Stay-in-place formwork**: Stay-in-place (SIP) formwork systems support intra-girder loads (wet concrete) that span transversely between girder top flanges (Figure 2-10). Stay-in-place forms consist of corrugated metal panels that are attached to the tips of the top flange of adjacent girders. The connection between the SIP forms and the girder flange is considered to be incapable of transmitting moments, therefore the SIP forms are essentially treated as being 'simply supported' on the girder flange tips.

- **Overhang formwork**: It is typical for the deck of a bridge to extend past the exterior (fascia) girder, thereby producing a cantilevered overhang (Figure 2-11). During construction, overhang brackets (Figure 2-12) are used to temporarily support the cantilever portion of the wet deck slab that extends beyond exterior girders. These temporary structural bracket systems support the overhang formwork, wet concrete, construction walkway, workers and concrete finishing machine. A survey of representative literature from overhang bracket manufacturers was conducted to quantify representative cross-sectional properties and longitudinal spacing requirements. Most commercially available formwork systems consist of timber joists and sheathing supported on steel bridge overhang brackets (Figure 2-13). It is important to note that all of the gravity loads supported by the overhang brackets are eccentric relative to the exterior girders, and as such apply torque loads to the exterior girders in the overall cross-sectional system.

- **Finishing machine**: Bridge deck finishing machines (Figure 2-14) spread, compact, and finish the freshly placed wet concrete deck surface. The finishing machine is an open steel frame that is supported at the extremities of the bridge width on the overhang brackets described above. Drive wheels (commonly referred to as bogies) move the paver longitudinally along the length of the bridge and are eccentrically supported by screed rails (Figure 2-13) on each side of the bridge. A suspended paving carriage with augers, drums, and floats finishes the concrete surface as it moves transversely from side to side across the width of the bridge (perpendicular to the longitudinal movement of the finishing machine along the length of the bridge). Concrete is typically placed just ahead of the travelling finishing machine using separate equipment, such as a pump. The most common finishing machine manufacturers are Terex Bid-Well and Gomaco.

- **Live loads**: Live loads that are present during the deck finishing process consist of workers, temporary materials, and supplementary construction equipment. For brace force calculation purposes, these loads are treated as either uniform pressure loads, or as line loads, as will be discussed in greater detail later in this report.

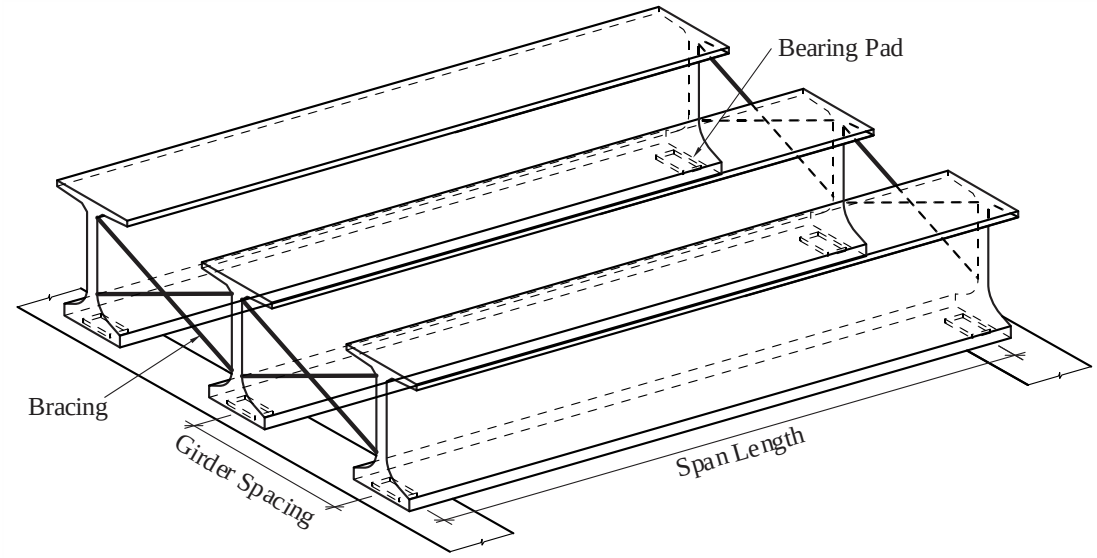

Figure 2-1. Girder system

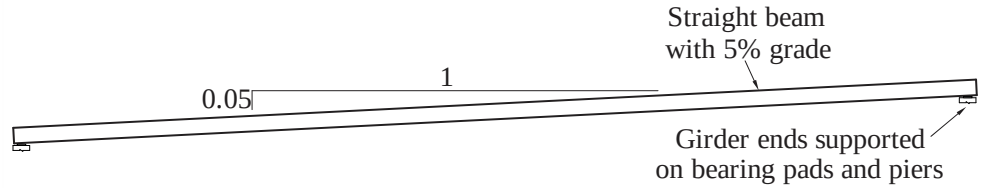

Figure 2-2. Definition of grade (elevation view)

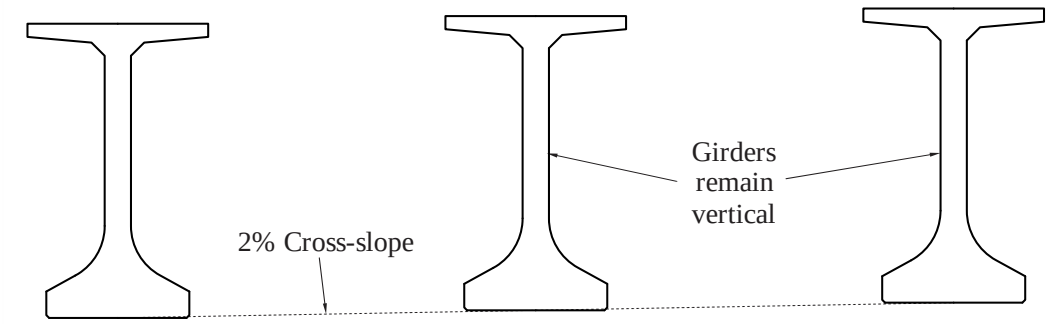

Figure 2-3. Definition of cross-slope (section view)

Figure 2-4. Definition skew angle (plan view)

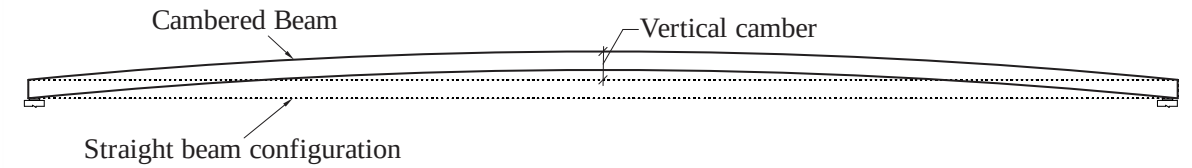

Figure 2-5. Definition of camber (elevation view)

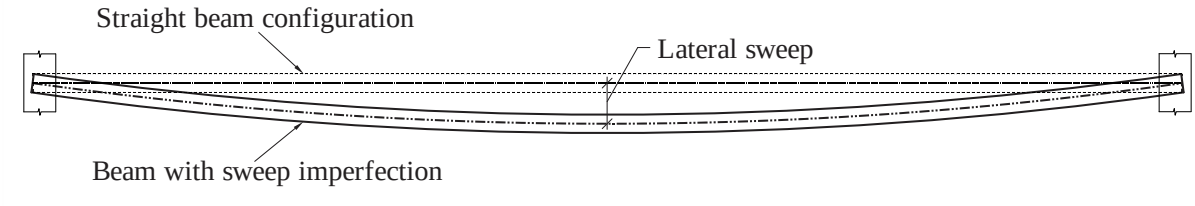

Figure 2-6. Definition of sweep (plan view)

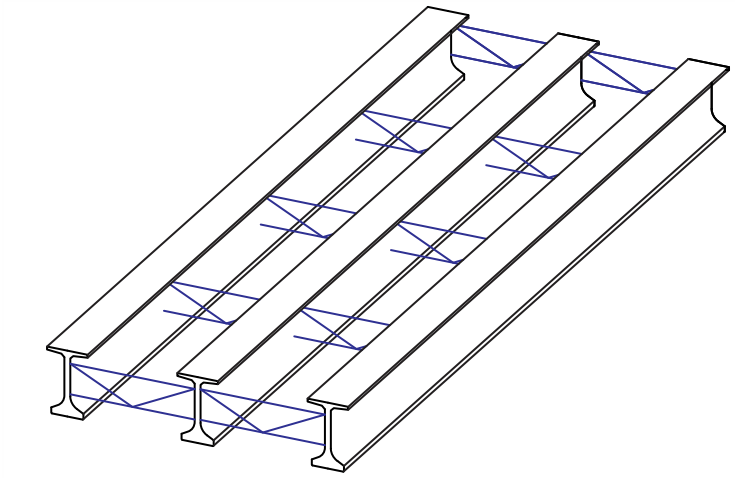

Figure 2-7. Girder system with quarter-point bracing

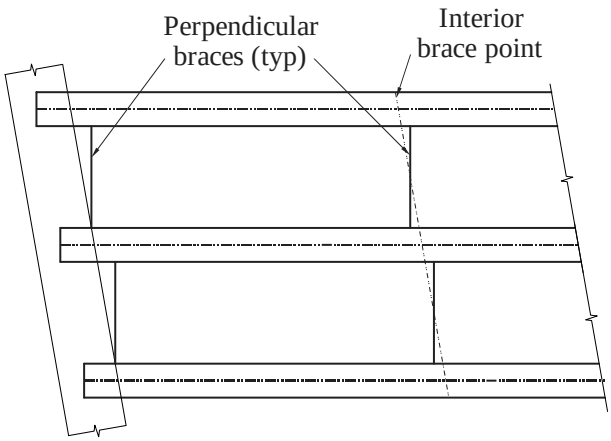

Figure 2-8. Perpendicular brace placement on skewed bridge (plan view)

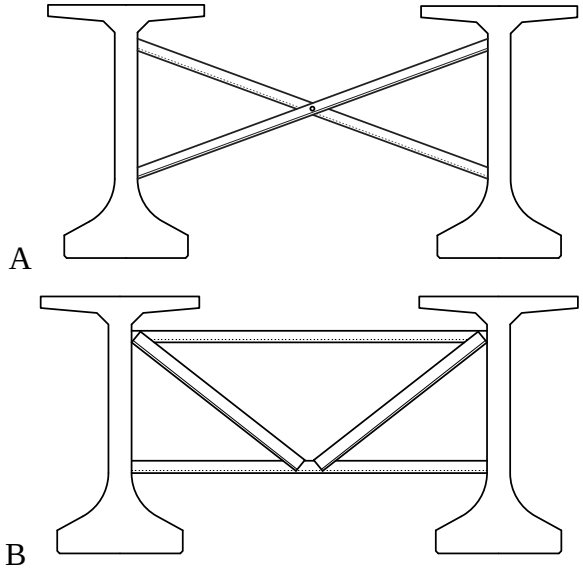

Figure 2-9. Common brace types. A) X-brace. B) K-brace.

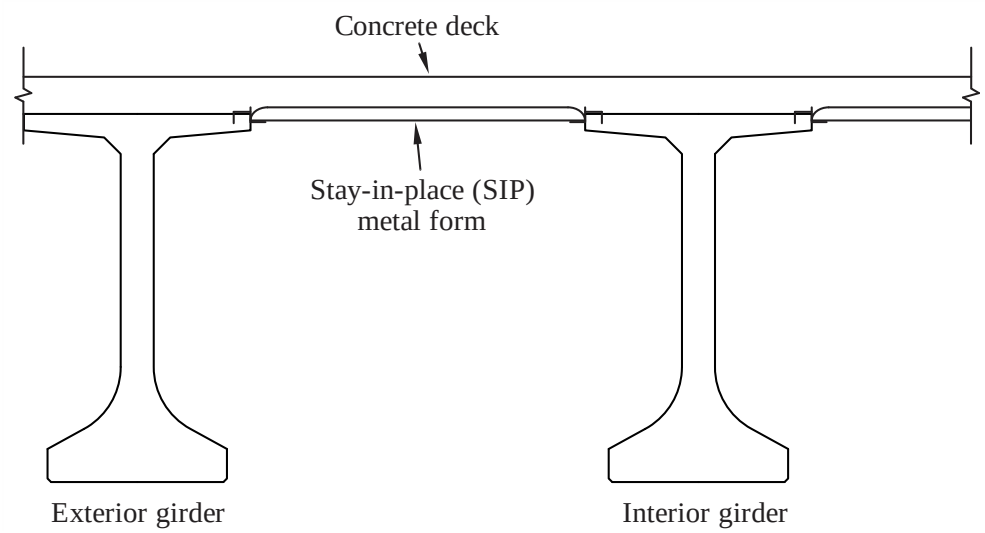

Figure 2-10. Stay-in-place formwork (section view)

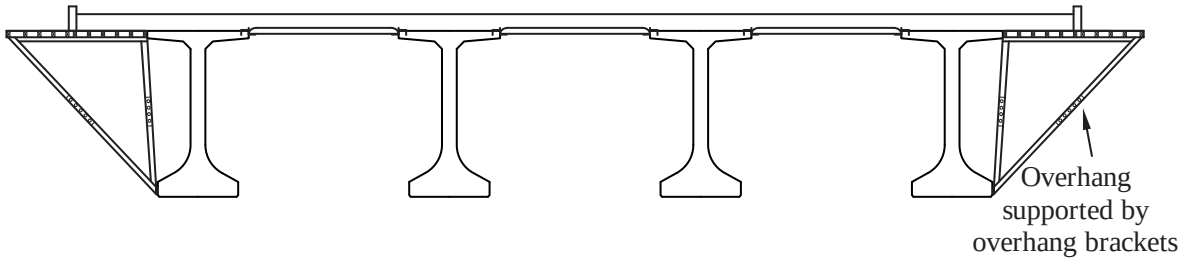

Figure 2-11. Temporary support brackets used to support deck overhangs during construction

Figure 2-12. Cantilever overhang supported by overhang brackets (Photo credit: Clifton and Bayrak (2008))

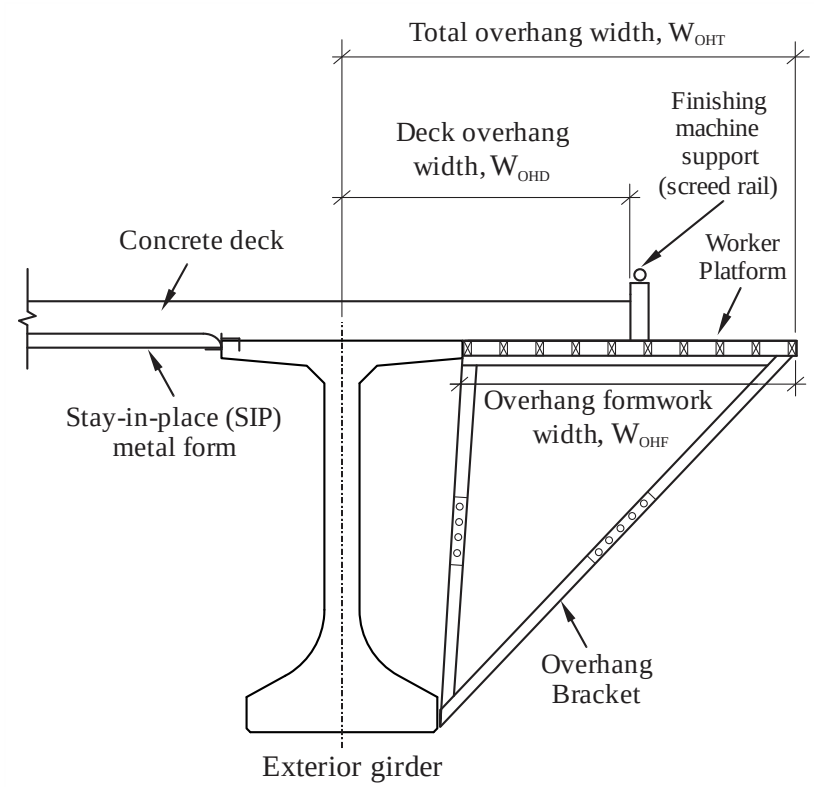

Figure 2-13. Details of overhang formwork support brackets and loads

Figure 2-14. Typical bridge deck finishing machine in operation (Photo credit: Gomaco)

CHAPTER 3
DEVELOPMENT OF STRUCTURAL ANALYSIS MODELS

3.1 Overview

To calculate brace forces induced by construction loads, braced systems of FIB girders were modeled and structurally analyzed using the ADINA (2012) finite element analysis code. The models were capable of capturing overall system-level behavior of braced FIB systems (including the influence of brace configuration, bearing pad stiffness, etc.), while remaining computationally efficient enough that hundreds of thousands of parametric analyses could be performed for the purpose of quantifying braces forces. In all cases, brace forces were determined using large-displacement (geometrically nonlinear) analyses, in which static loads were applied to the models in incremental steps, taking into account the deformed state of the structure at each step.

The parametric construction-stage bridge models analyzed in this study were developed in a semi-automated fashion by extending a modeling methodology developed in a previous study (BDK75-977-33, Consolazio et al., 2013) to further include the effects of construction loads and overhang brackets. In the following sections, key aspects of the model development process are summarized, and noteworthy modifications to the previously developed modeling methodology are described in detail.

3.2 Modeling of Bridge Girders

In the global coordinate system established for each bridge model, the X-axis corresponded to the transverse (lateral) direction; the Y-axis corresponded to the longitudinal (span) direction, and the Z-axis corresponded to the vertical direction. Bridge girders were modeled (Figure 3-1) using ‘warping beam elements’ which use an advanced beam element formulation type provided in ADINA that possess an additional degree of freedom at each end

node to represent the torsionally-induced out-of-plane warping of the cross-section. Warping beam elements are generally superior to standard Hermitian beam elements in that the bending and torsional deformation modes of the warping element are fully coupled together at the element formulation level. However, as a consequence, the use of warping beam elements requires the calculation of a comprehensive set of cross-sectional properties—many more than standard Hermitian beam elements—several of which require knowledge of the section 'warping function', which cannot be calculated in closed form and must instead be solved for numerically. Details relating to the section properties that were calculated in this study for the catalog of FDOT FIB cross-sectional shapes are provided in Appendix A. Throughout this study, material properties assumed for the prestressed concrete FIB girders were f'_c = 8.5 ksi, unit weight = 150 pcf, and Poisson's ratio = 0.2. Using these values and the PCI Design Handbook (PCI, 2010), the concrete elastic modulus was computed to be E = 5589 ksi.

Support conditions at each end of each girder were modeled with six (6) springs to represent the stiffnesses of the bearing pad in each degree of freedom. Each of the six (6) springs corresponded to one of four different pad deformation modes: shear, axial, torsion, and roll (Figure 3-2). Pad stiffnesses were determined using the calculation methods developed and validated in a previous study (BDK75-977-33, Consolazio et al., 2013). The roll stiffness springs (in both the overturning and bending directions) were assigned nonlinear moment-rotation curves that captured the softening effects of partial girder liftoff from the pad. All remaining pad stiffnesses were treated as linear.

Seven (7) standard types of elastomeric bearing pad are described in *FDOT Design Standard No. 20510: Composite Elastomeric Bearing Pads – Prestressed Florida-I Beams* (FDOT, 2014c) for use with FIB girders. During the design process, selection of the type of pad

that will be used in a particular bridge project is based on thermal expansion and live load deflection limit states of the completed bridge, neither of which can be predicted based solely on girder dimensions (cross-sectional properties or span length). As such, it is not appropriate to assume that for each unique type of FIB, there is a corresponding single type of bearing pad that would always be utilized.

In this study, bearing pad selection was instead based on ensuring that conservatively large values of *brace force* would be obtained for all analyses conducted. As bearing pad rotational stiffness decreases, the portion of the acting eccentric construction loads that is carried by a pad also decreases, thereby moderately increasing the forces that are developed in the braces. Consequently, the bearing pad with the minimum practical roll stiffness will produce the most conservative brace forces. Therefore, the FDOT Type J bearing pad was selected for use throughout this study. As documented in Consolazio et al. (2013), as the acting axial compressive load on a pad decreases, so does a component of the roll stiffness of the pad. Hence, for each FIB girder type considered in the present study, the *minimum* practical span length for that girder type was used to compute an axial pad load (equal to half of the total weight of a single girder). For each such axial load, the roll stiffness of the Type J pad was then computed and then subsequently used for all parametric analyses involving that type of FIB girder. Hence, a single minimized roll stiffness curve was calculated for each type of FIB, resulting in a total of seven (7) bearing pad moment-rotation curves. (For additional details on the bearing pad stiffness calculation procedures, see Consolazio et al., 2013, Chapter 6).

3.3 Modeling of Braces

In bridge construction, a wide variety of different bracing configurations are used in practice, consequently it was not possible for every possible configuration of brace to be included in the parametric studies that were conducted in this study. After carrying out a survey

of bracing designs used in the construction of bridges throughout Florida, two (2) representative brace configurations were identified:

- **X-brace**: Two diagonal members that cross in the middle to form an 'X' shape. A steel bolt typically passes through both members at the crossing point to create a hinge (Figure 3-3a).
- **K-brace**: Steel members (typically steel angles) welded together into a 'K'-shaped frame and welded or bolted to steel plates that are cast into the webs of the concrete girders. (Figure 3-3b).

Additionally, only the X-brace and K-brace configurations are currently recommended in the *FDOT Design Standard No. 20005: Prestressed I-Beam Temporary Bracing* (FDOT, 2014a) for end-span and intermediate-span bracing applications. For structural analysis purposes, all braces were modeled with beam elements, with each brace member represented by a single element. At the girder connection points, rigid links were used to connect the brace elements to the girder elements (i.e., the warping beam elements positioned at the centroid of the girders). Pins and hinges were modeled with beam moment end-releases and nodal constraints, respectively. Both X-brace and K-brace members included in the parametric studies were modeled as 4 in. x 4 in. x ⅜ in. steel angles, with an elastic modulus of E = 29000 ksi.

3.4 Modeling of Overhang Brackets

Construction loads applied beyond the lateral extents of an exterior girder are structurally supported during construction by *overhang brackets*. Specifically, the finishing machine, formwork, overhang wet concrete, and construction worker live loads are typical components of the supported overhang loads. To define the lateral eccentricity of the overhang construction loads, two offset parameters had to be established. To be consistent with the *FDOT Instructions for Design Standard No. 20010: Prestressed Florida-I Beams* (FDOT, 2014b), the concrete finishing machine was offset 2.5 in. from the overhang edge (Figure 3-4). In the *FDOT Concrete I-girder Beam Stability Program*, in addition to providing calculations for determining bracing

adequacy and girder stability, several recommended values for the overhang geometry are specified, including a 2-ft worker platform width. Therefore, for all the parametric studies conducted herein, the worker platform was assumed to extend 2-ft beyond the finishing machine supports (Figure 3-4).

In the girder system models, all components of the overhang brackets were modeled with beam elements, with representative cross-sectional properties that were obtained from a survey of overhang bracket manufacturers. To represent the offset eccentricities between the girder centroid and the bracket connection points, the deformable overhang bracket elements were connected to girder warping beam elements using rigid links (Figure 3-5). In order to model interaction between the overhang bracket and the girder bottom flange, two co-located but separate nodes were used: one at the bottom vertex of the metal overhang bracket, and a second at the end of the rigid link representing the surface of the girder bottom flange. At this location, the overhang bracket bears against (i.e., is in compressive contact with) the girder bottom flange. To model this behavior structurally, a constraint condition is defined such that the lateral (X-direction) translations of the two co-located nodes are constrained to match, while permitting independent movements (relative slip) in the vertical direction.

Overhang bracket nodes are positioned (Figure 3-5) to define: the three corners of the triangular system; and all locations of load discontinuities (i.e., deck overhang edge) and load application points (i.e., finishing machine and worker line load application points). The worker line load is conservatively applied to the center of the worker platform width. Thus, the load application of the worker line load is laterally offset in the X-direction 12 in. from the assumed finishing machine application point and 14.5 in. from the deck overhang edge (Figure 3-5). By combining each of the previously mentioned modeling components, an overall illustration of a

typical FIB system model is presented in Figure 3-6. Based on a review of literature obtained from typical overhang bracket manufacturers, brackets are commonly spaced between 4 ft and 6 ft on center longitudinally along the span length of a bridge. In the present study, therefore, an average longitudinal spacing of 5 ft was used for all brackets (Figure 3-7).

Also noted in Figure 3-6 and Figure 3-7 are rigid vertical elements (links)—extending from girder centroid to girder top surface—which are included in the model for application of construction loads on each girder. These rigid elements account for the vertical eccentricity between the girder centroid and the girder top surface (where loads are applied). It was determined that brace forces induced by construction loads were not sensitive to changes in the longitudinal spacing of the rigid vertical elements; consequently, the rigid links were given an arbitrary longitudinal spacing of 1-ft in the span direction.

3.5 Application of Construction Loads

In this section, the magnitudes and methods of application for construction loads considered in this study are described. In Figure 3-8, a summary of the superimposed construction loads that will be described in more detail below is provided. Additionally, self-weight (i.e., gravity loads from girders, braces, and overhang brackets) were included in the models.

An important consideration in this study was the application of the concrete finishing machine loads. Finishing machines are supported near the extremities of the bridge width by several wheels. The common Terex Bid-Well 4800 machine has a total wheel base of approximately 8 feet in the longitudinal (bridge span) direction. Since this wheel base is small relative to the typical span lengths of prestressed girder bridges, the finishing machine wheel reaction forces were idealized as single concentrated loads (one load on each side of the bridge equal to half the total machine weight).

During bridge deck placement, a concentration of live load will be located at the extremities of the bridge deck. To account for this loading, the *AASHTO Guide Design Specifications for Bridge Temporary Works* (2008) recommends that a worker line load be applied along the outside edge of all deck overhangs. In addition, the line load shall be applied as a moving load but with a fixed length of 20-ft so as to not introduce excessive conservatism. In the girder system models analyzed in this study, the worker line load was centered longitudinally at the concrete finishing machine such that the line load extended 10-ft behind and ahead of the finishing machine.

Since temporary bracing must be designed for service and strength limit states, two separate parametric studies were conducted: un-factored (service) loads and factored (strength) loads. A summary of un-factored and factored construction loads is provided in Table 3-1 along with applicable references.

Construction loads that are applied between adjacent girders (i.e., on the stay-in-place forms) produce vertical reaction forces that act on the tips of the girder top flanges. Since all Florida-I beams have a top flange width of 48 in., the lateral eccentricity between the girder centroid and the formwork reaction force (Figure 3-9) is 24 inches (half of the girder top flange width). For analysis purposes, each eccentric reaction forces of this type was converted into a statically equivalent combination of force and moment (Figure 3-9) which were then applied along the centerlines of the girders.

Consequently, all intra-girder distributed loads that were applied over the width of the stay-in-place formwork were converted into equivalent nodal forces and moments. Other types of construction loads, such as the overhang loads (overhang formwork, worker line load, etc.),

were applied directly to nodes in the structural model based on the appropriate tributary areas (Figure 3-10).

During the process of placing and finishing of a concrete bridge deck, wet concrete pressure load is applied to the bridge (by way of SIP forms) over incrementally increasing lengths of the structure. Consequently, loading conditions corresponding to the placement of concrete deck loads over *partial lengths* of the bridge—less than the total span length—were considered in this study. For all such partial coverage cases, the position of the finishing machine was taken to coincide with the location of the furthest placed concrete. Wet concrete is typically placed just ahead of the moving finishing machine (Figure 2-14) using a pump, therefore, in vast majority of paving situations, the location of the finishing machine and the end of the concrete coverage will generally coincide. (Although it is feasible for a finishing machine to be moved to a location other than then end of the placed concrete, it was determined that such situations are generally rare and/or non-controlling, and thus were not considered in this study). By analyzing several 'test' bridge models in which the finishing machine and the end of the concrete deck coverage area were moved in small increments along the bridge length, it was determined that maximum end-span brace and intermediate-span brace forces occurred when the web slab load terminated at one of the bracing points (e.g., end point, 1/2 point, 1/3 point, 1/4 point). However, depending on the bridge configuration parameters (deck overhang width, girder spacing, etc.) the controlling coverage of concrete loads and finishing machine loads that produced the maximum brace forces varied from case to case. For example, full span concrete coverage with the finishing machine at the end-span often produced the highest end-span brace forces. However, a partially placed deck terminating at an interior brace point typically produced the largest interior brace forces. To ensure that maximum brace forces were quantified from the parametric studies,

multiple load cases were analyzed (Figures 3-11, 3-12, 3-13, and 3-14) for each bridge, depending on the number of interior bracing lines that were present. Note that for each geometric configuration (span length, girder spacing, deck overhang width, etc.), maximum end-span brace and intermediate-span brace forces were quantified for each loading condition.

According to *AASHTO Guide Design Specifications for Bridge Temporary Works* (2008), a worker line load (75 lb/ft [un-factored] over a length of 20 ft) should be included as a design load during the deck placement. This line load accounts for additional workers that are standing on the overhang platform during deck placement. For load cases where the finishing machine was at either the start or the end of the bridge, the worker line load was applied over the first or last 20-ft of the structure. For all other cases, where the concrete deck terminated at an interior brace point, the 20-ft line load extended longitudinally 10-ft to either side of the brace point (and finishing machine location).

Table 3-1. Summary of construction loads applied in parametric studies

Construction loads	Load type	Un-factored loads	Load factor	Factored loads	Reference
Wet concrete deck	Permanent	106.25 psf (8.5" thick, 150 pcf)	1.25	132.8 psf (8.5" thick, 150 pcf)	I
Wet concrete build-up	Permanent	50 lb/ft	1.25	62.5 lb/ft	I
Stay-in-place forms	Permanent	20 psf	1.25	25 psf	I
Overhang formwork	Temporary	10 psf	1.5	15 psf	II
Live load	Temporary	20 psf	1.5	30 psf	III
Worker line load	Temporary	75 lb/ft for 20 ft	1.5	112.5 lb/ft for 20 ft	III
Finishing machine	Temporary	10 kip total (5 kip each side)	1.5	15 kip total (7.5 kip each side)	II

I: per FDOT Structures Design Guidelines (FDOT, 2013)
II: per FDOT recommendations
III: per AASHTO Guide Design Specifications for Bridge Temporary Works (AASHTO, 2008)

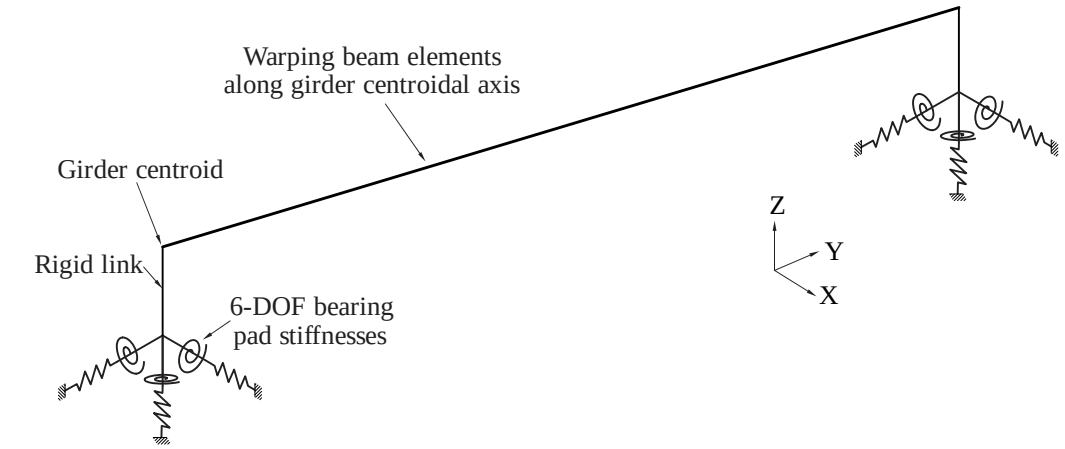

Figure 3-1. Finite element model of a single FIB (isometric view)

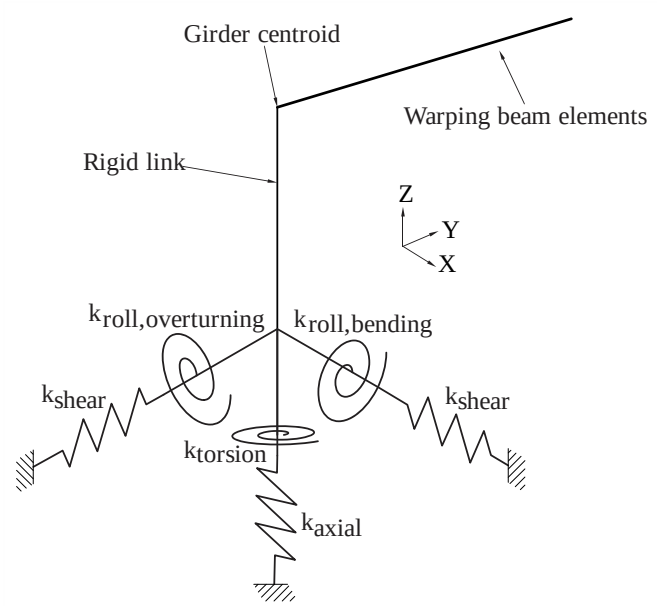

Figure 3-2. Modeling of bearing pad stiffness springs at end of girder

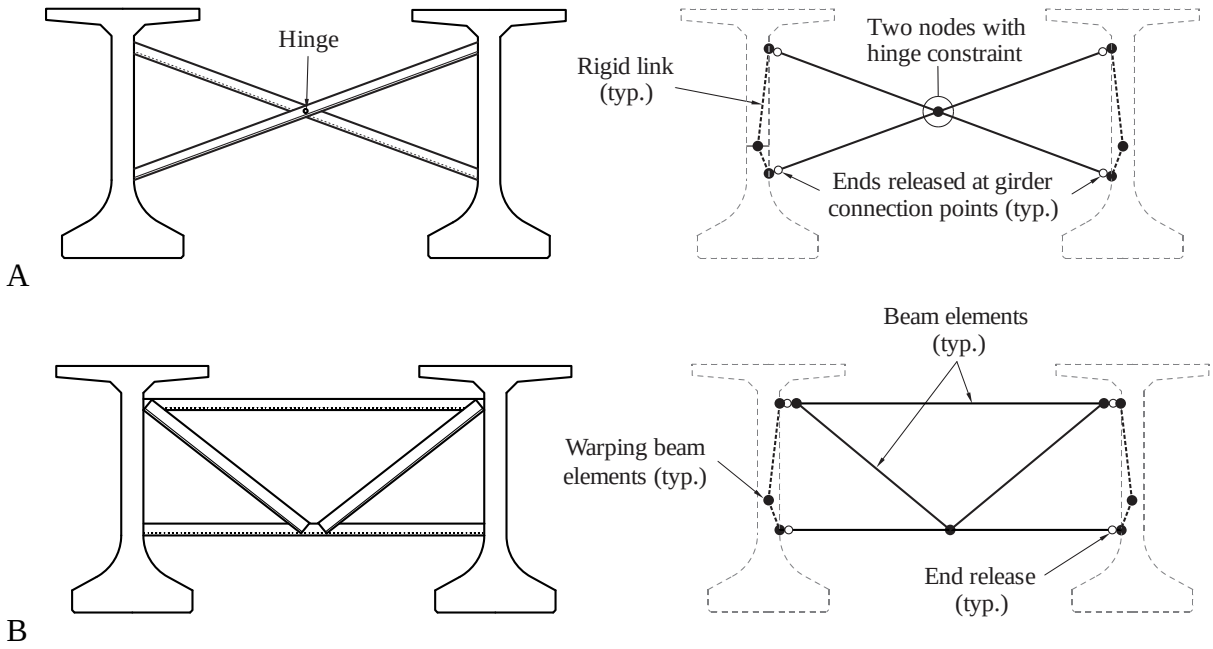

Figure 3-3. Modeling of brace configurations in FIB system models. A) X-brace. B) K-brace.

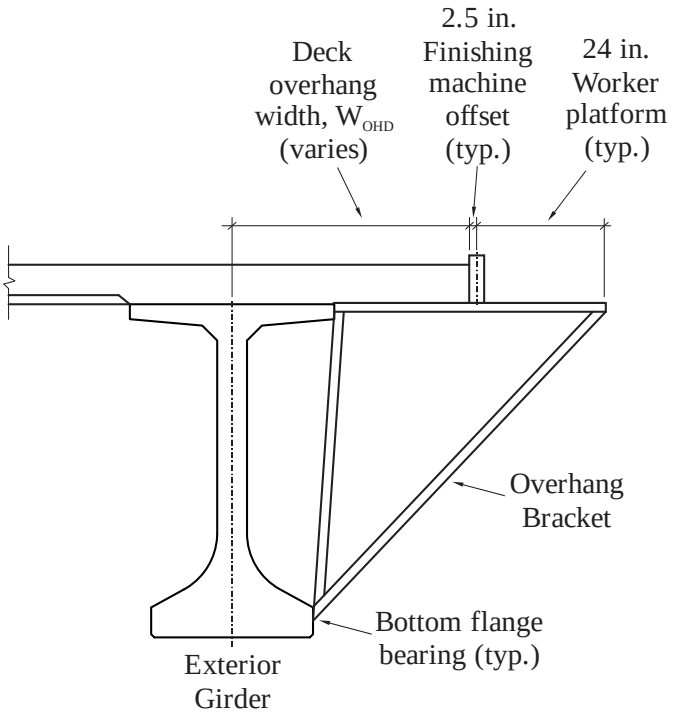

Figure 3-4. Overhang bracket components and geometry

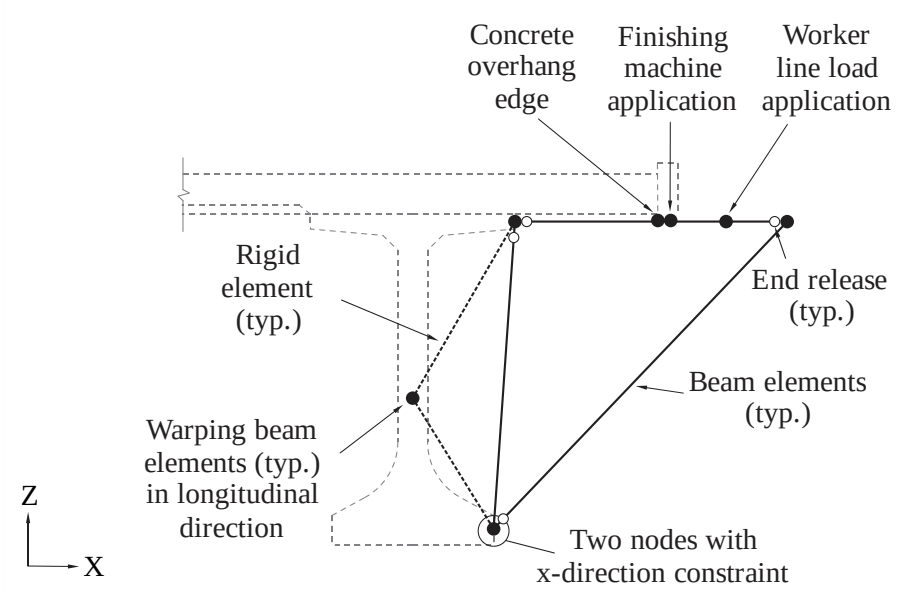

Figure 3-5. Details of overhang bracket model

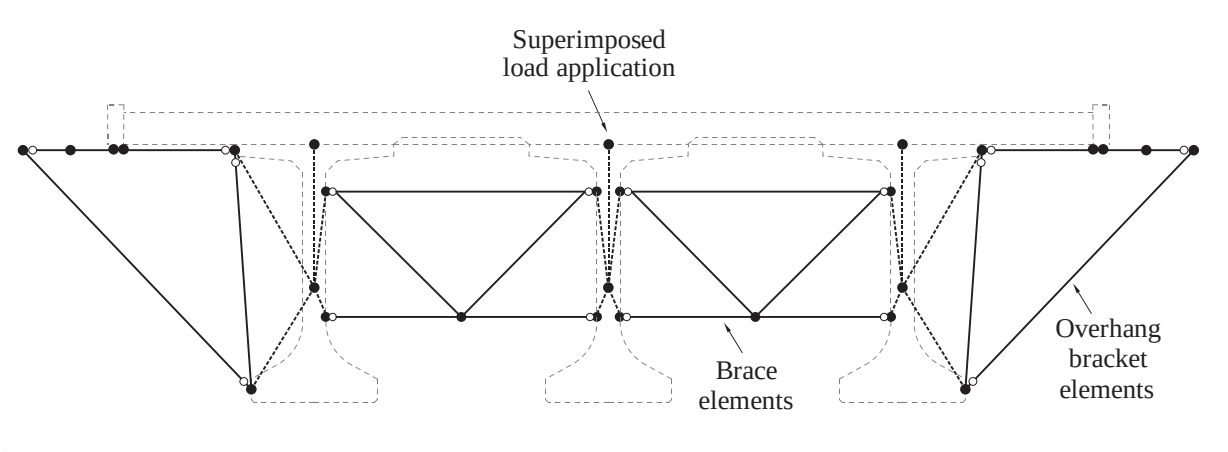

Figure 3-6. Cross-sectional view of overall braced girder system model

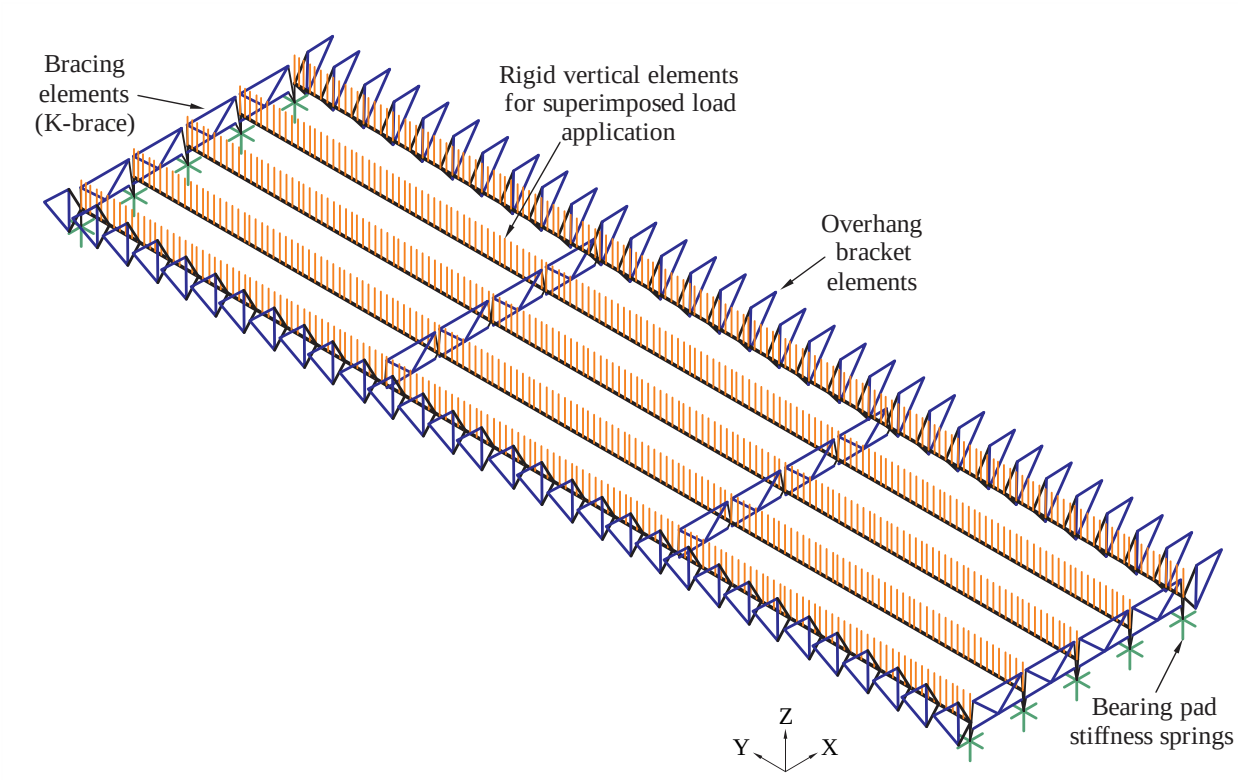

Figure 3-7. Isometric view of overall braced girder system model

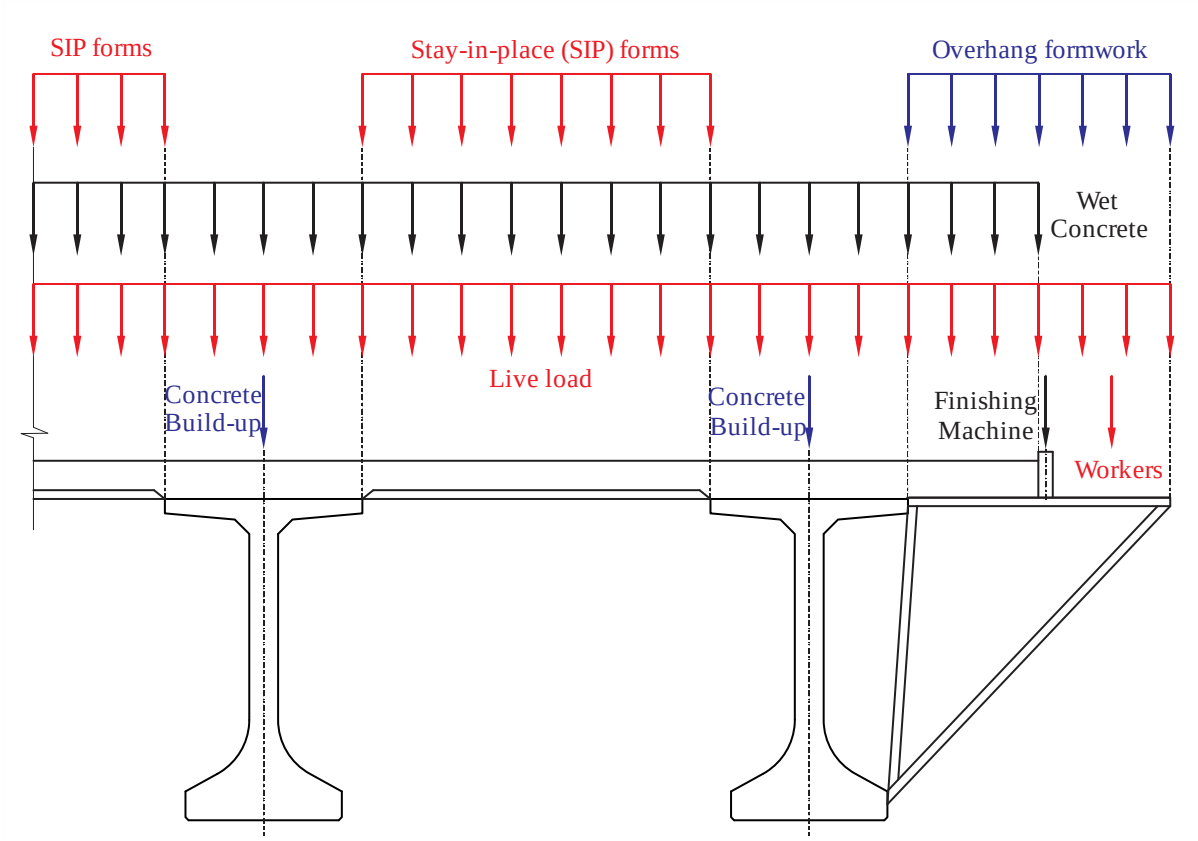

Figure 3-8. Summary of construction loads considered

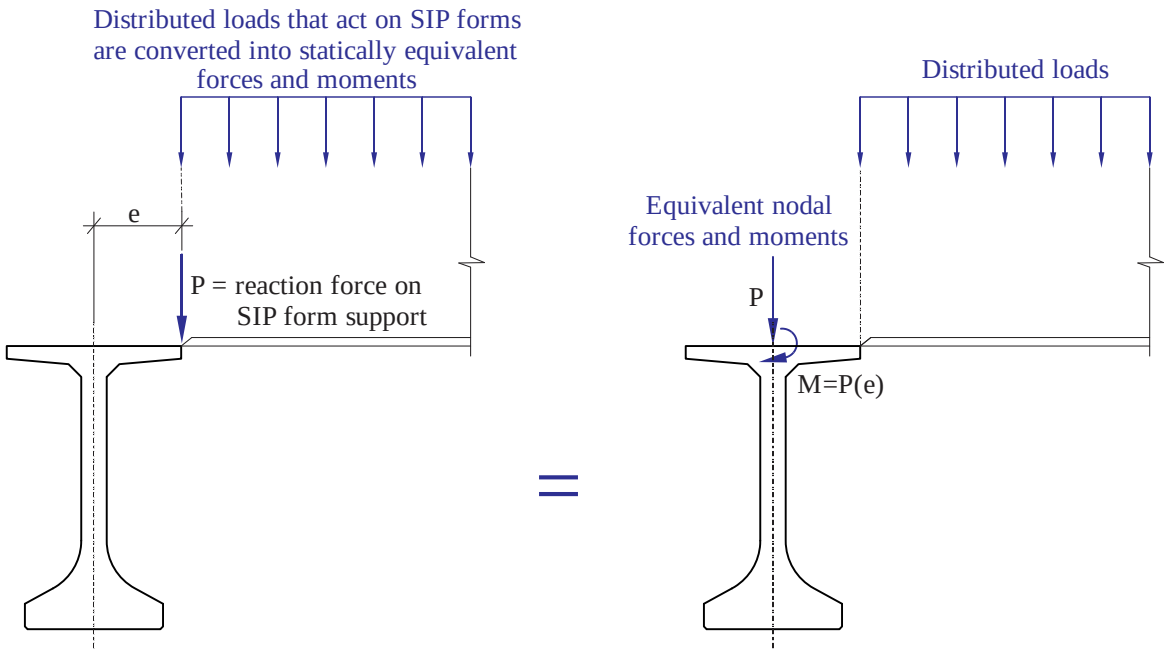

Figure 3-9. Eccentric reaction forces from loads applied to SIP forms, and statically equivalent nodal force and moment applied to top of girder

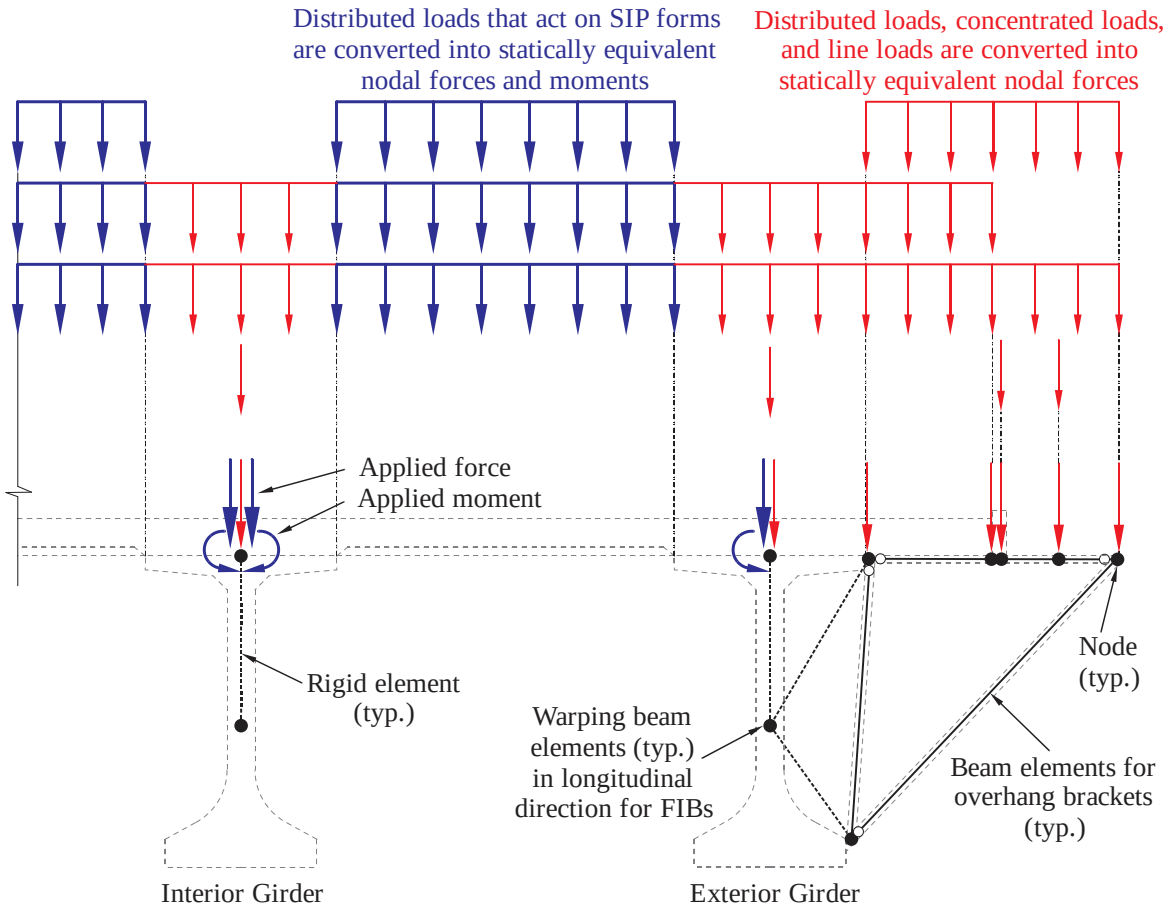

Figure 3-10. Construction loads converted to equivalent nodal loads

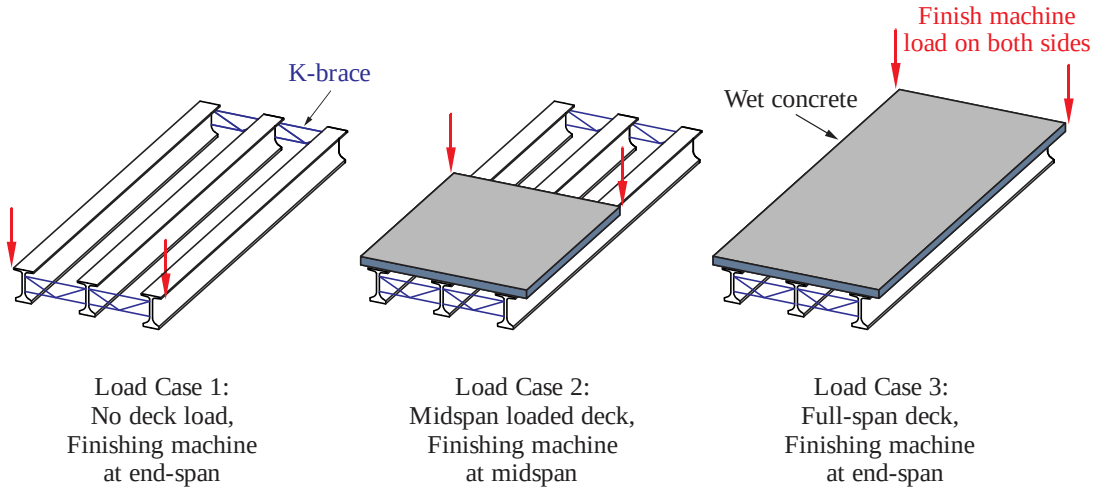

Figure 3-11. Coverage of deck loads as a function of finishing machine location (Bridges with only end-span braces; no interior braces)

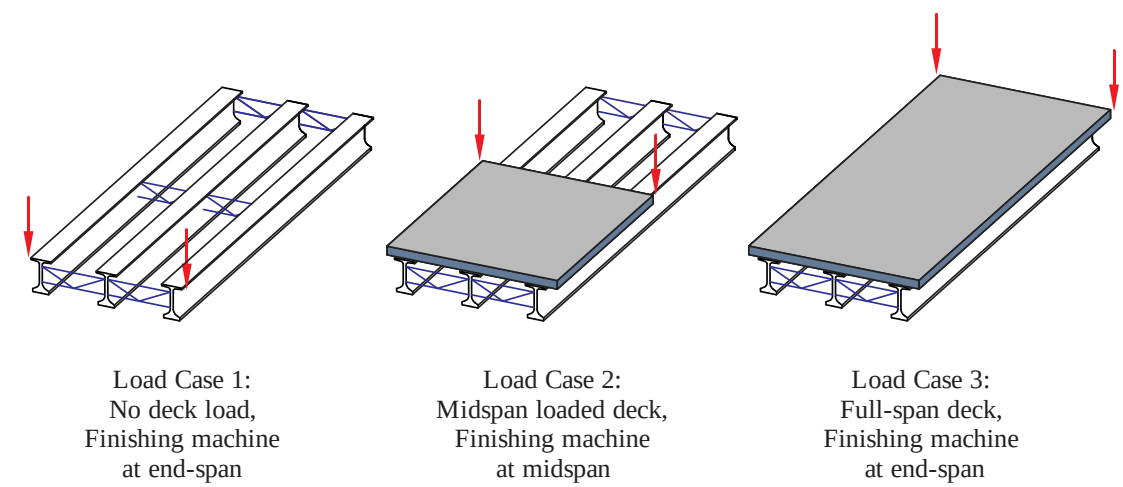

Figure 3-12. Coverage of deck loads as a function of finishing machine location (Bridges with end-span and midspan bracing)

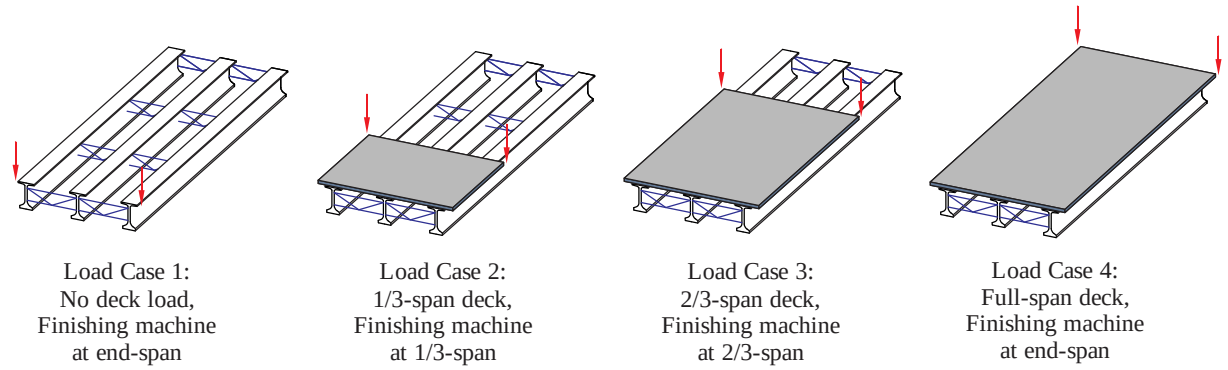

Figure 3-13. Coverage of deck loads as a function of finishing machine location (Bridges with third-point bracing)

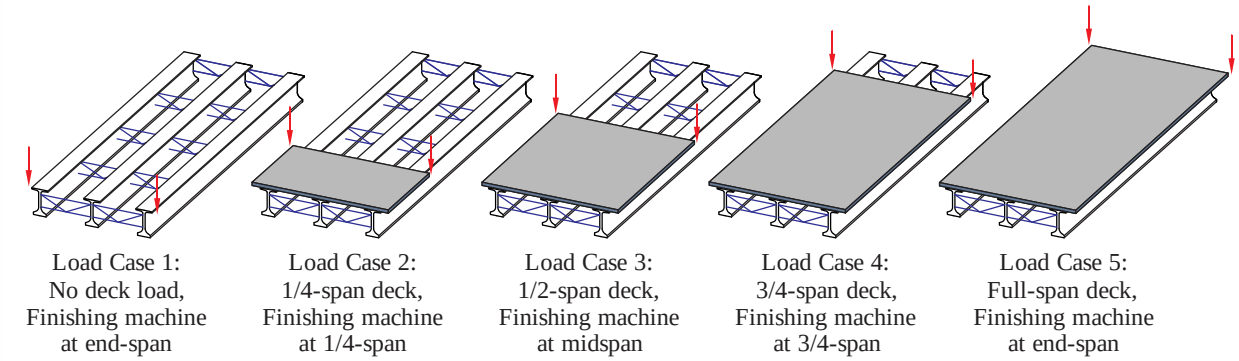

Figure 3-14. Coverage of deck loads as a function of finishing machine location (Bridges with quarter-point bracing)

CHAPTER 4
DEVELOPMENT OF BRACE FORCE PREDICTIONS

4.1 Overview

To investigate brace forces caused by eccentric construction loads, a large-scale parametric study was performed using finite element models of braced systems of Florida-I Beams (FIBs). As discussed in the previous chapter, several load cases were considered depending on the number of bracing lines present in the bridge. From the parametric study, maximum end-span brace forces and intermediate-span brace forces (if present) were quantified for both factored and un-factored construction loads. In bridge construction, different types of bracing may be provided at the end-span versus at intermediate-span (interior) bracing points due to relative differences in brace forces at these locations. However, it is also typical practice to use a consistent type of bracing throughout the interior portion of the bridge (i.e., longitudinally away from the ends). Therefore, for each bridge analyzed in the parametric study, maximum brace forces were quantified once for all end-span braces, and a second time for all intermediate-span (interior) braces.

For X-brace (cross-brace) models, the maximum diagonal brace forces were quantified at end-span and intermediate-span bracing locations. However, K-braces typically have smaller diagonal element forces as compared to the top and bottom horizontal element forces. Therefore, for K-brace models, maximum diagonal forces were quantified separately from the maximum horizontal element forces (and, as noted above, separately for end-span and intermediate-span bracing locations).

Ultimately, the goal in performing the parametric study was to develop a method by which engineers can rapidly compute brace forces for varying system parameters (girder type, span length, number of bracing locations, etc.). One approach to achieving this goal would be to

perform a moderate size parametric study, use the resulting brace force data to attempt to identify key relationships between forces and system parameters, and then form empirical brace force prediction equations. Such an approach must balance several—often competing—issues: the need for the empirical prediction equations to be mathematically simple in form; conservative in their prediction of brace force; but not *overly* conservative (since this outcome could lead to uneconomical bracing designs). The alternative approach taken here was to conduct a large-scale (and relatively 'fine-grain') parametric study (in total, approximately 450,000 three-dimensional (3-D) structural analyses of FIB bridges were conducted); store the summarized results data into a simple database; and then subsequently access and interpolate that database whenever brace forces need to be computed (i.e., predicted for design). By including a sufficiently large number of incremental values of each system parameter (e.g., span length, skew angle, number of braces, etc.), the error introduced in brace force prediction by database interpolation was kept to an acceptably small level. In verification tests demonstrated later in this chapter, it will be shown that the interpolated database approach yields results which are, in a majority of cases, less than ten percent (10%) in error.

4.2 Limited-scope Sensitivity Studies

Fully characterizing a braced multi-girder bridge system requires a large number of geometric parameters. Consequently, conducting a parametric study in which *all possible* combinations of these parameters were considered (even if only a few discrete values were selected per parameter) would require millions of individual structural analyses to be performed. To avoid such a situation, several limited-scope sensitivity studies were performed to help guide the design of an efficient final 'database-production' parametric study. As a result of these preliminary investigations, several geometric parameters were identified as having negligible influence on bracing forces due to construction loads and were therefore excluded from the

database-production parametric study. Additionally, sensitivity studies were performed to address the influence of K-brace configuration type (i.e., inverted K-brace, horizontally offset diagonal connections, etc.) on brace forces so that a conservative, representative brace type could be selected for use in the database-production parametric study. Also, in order to achieve an efficient number of construction load cases (due to the longitudinal variability of the finishing machine and concrete deck loads), the critical loading conditions to be used in the database-production parametric study were also determined.

4.2.1 Effect of Geometric Imperfections on Brace Forces

Geometric deviations (i.e., deviations from perfectly horizontal, straight girders) were considered in several limited-scope sensitivity studies to quantify the effects of the geometric deviations on maximum brace forces. In total, approximately 500 analyses were conducted for a variety of FIB bridge configurations. Bridge geometric parameters that did not have a significant effect on brace forces were not included in the database-production parametric study. Similar trends of brace force sensitivity—for both maximum end-span and intermediate-span bracing—were observed for all tested cases. Therefore, representative results for an example girder system [three (3) 78" FIB girders, quarter-point K-braces, 9 ft girder spacing, 4 ft deck overhang, 0 deg. bridge skew, service construction loads (no load factors)] are provided below for each geometric imperfection parameter:

- **Grade**: Longitudinal incline of the girders (recall Figure 2-2), typically expressed as a percentage of rise per unit of horizontal length. As evident in the example presented in Figure 4-1, the increase of grade by 2% had no effect on brace forces. Consequently, 0% grade was assumed for all cases in the database-production parametric study.
- **Cross-slope**: Transverse incline (slope) of the deck (recall Figure 2-3), typically expressed as a percentage, which results in girders that are staggered vertically. As evident in the example presented in Figure 4-2, an increase of cross-slope by 2% had a negligible effect on brace forces. Other girder systems with higher and lower cross-slopes showed similarly negligible influences on brace forces (for both end-span and

intermediate-span brace forces). Therefore, a cross-slope of 0% was assumed for all cases in the database-production parametric study.

- **Camber**: Vertical bowing of the girder (recall Figure 2-5) due to prestressing in the bottom flange, expressed as the maximum vertical deviation from a perfectly straight line connecting one end of the girder to the other. Girder camber was implemented as a vertical parabolic shape with a maximum vertical deviation at midspan. As evident in the example presented in Figure 4-3, an increase of camber of 6 inches (at midspan) for all girders in the system had no effect on maximum end-span brace and interior-span brace forces. Note that camber sensitivities for other girder systems with higher and lower maximum cambers were similar. Therefore, zero inches of camber was assumed in the database-production parametric study.

- **Sweep**: Lateral bowing of the girder (recall Figure 2-6) due to manufacturing imperfections, expressed as the maximum horizontal deviation from a perfectly straight line connecting one end of the girder to the other. Construction tolerances for FIBs are specified in the *FDOT Standard Specifications for Road and Bridge Construction* (FDOT, 2010), which limits girder sweep to ⅛ in. for every 10 ft of girder length, but not to exceed 1.5 in. Therefore, both maximum end-span and intermediate-span brace forces were compared between girder systems without sweep and girder systems with the *maximum* possible sweep of 1.5 inches (applied to all girders). By extending the modeling methodology developed in BDK75-977-33 (Consolazio et al., 2013), sweep was implemented using a half-sine function, with the maximum allowable sweep at midspan. In the example presented in Figure 4-4, increasing sweep from zero to the maximum permitted value increased the intermediate-span brace forces by approximately five percent (5%). In all tested cases, the percent differences of end-span and intermediate-span brace forces—caused by maximum girder sweep—were less than 5%. Due to the relatively small influence of sweep on brace forces, girder sweep imperfections were omitted from the database-production parametric study (i.e., lateral girder sweep was assumed to be zero at midspan).

4.2.2 Effect of K-brace Configuration on Brace Forces

Sensitivity studies were performed to assess the influence of K-brace configuration (inverted K-brace, horizontally offset diagonal connections, etc.) on brace forces so that a conservative, representative brace type could be selected for the database-production parametric study. In total, approximately 300 sensitivity analyses were conducted for a variety of different bridge configurations. From a survey of typical bracing types used in modern Florida bridges, four typical K-brace types were selected (Figure 4-5). Each K-brace configuration was given a letter designation (*Type-A, Type-B,* etc.) for comparison purposes.

This limited-scope sensitivity study assessed the effects of K-bracing configuration on brace forces for a broad range of geometric parameters (e.g., span length, girder spacing, deck overhang width, etc.). In the *FDOT Design Standard No. 20005: Prestressed I-Beam Temporary Bracing* (FDOT, 2014a), the *Type-A* K-brace configuration (Figure 4-5) is recommended for both end-span and intermediate-span bracing applications. Therefore, it was used as a *reference brace*, by which other K-brace forces in the sensitivity study could be compared by normalization.

As evident in Figure 4-6, the *Type-A* K-brace had normalized maximum brace force results that were approximately equal to *Type-C* (i.e., normalized values were approximately 1.0 indicating that the brace forces were very similar). Additionally, the *Type-A* K-brace had conservatively higher, but not overly-conservative, maximum brace forces compared to the offset diagonal configurations of *Type-B* and *Type-D* (Figure 4-7, normalized values were slightly greater than 1.0 in most cases). Note that the average conservatism of Type A compared to both *Type-B* and *Type-D* was approximately five percent (5%). Therefore, the *Type-A* configuration was selected as the representative K-brace configuration to be used for all cases in the database-production parametric study.

4.2.3 Effect of Partial Application of Construction Loads on Brace Forces

As discussed previously, during the process of placing and finishing a concrete bridge deck, wet concrete pressure loads are applied to a bridge (by way of SIP forms) over incrementally increasing lengths of the structure. Consequently, loading conditions corresponding to the placement of concrete deck loads over *partial lengths* of the bridge—less than the total span length—were considered in the database-production parametric study. For all such partial deck coverage cases, the position of the finishing machine was taken to coincide with the location of the furthest placed concrete. As discussed in Chapter 3, wet concrete is

typically placed just ahead of the finishing machine (recall Figure 2-14) using a pump, therefore, in the vast majority of paving situations, the location of the finishing machine and the end of the concrete coverage will generally coincide.

A limited-scope sensitivity study was conducted to determine the critical locations—those that cause maximum brace forces—of the wet slab and finishing machine. In total, approximately 900 analyses were conducted where the concrete deck coverage area was moved in small increments along the bridge length. For this sensitivity study, the increments corresponded to the bridge 10^{th} points (i.e., increments of ten percent (10%) of the bridge span length). In all cases, the maximum end-span brace and intermediate-span brace forces occurred when the web slab load terminated close to one of the bracing points (e.g., end point, 1/2 point, 1/3 point, 1/4 point). Conversely, it was determined that partially placed deck loads terminating *between* the locations of the braces did not control maximum end-span or intermediate-span brace forces. Therefore, for purposes of quantifying maximum brace forces in the database-production parametric study, it was found to be adequate to consider the multiple deck load cases illustrated earlier in Figures 3-11, 3-12, 3-13, and 3-14 for each bridge, with the specific number of load cases depending on the number of intermediate-span bracing lines present in the bridge.

4.3 Scope of the 'Database-Production' Parametric Study

To develop a comprehensive database of brace forces for use in the brace force prediction program, a final 'database production' parametric study was conducted. Three-dimensional (3-D) structural analyses were conducted to quantify maximum end-span and intermediate-span brace forces for combinations of the following parameters:

- FIB cross-section depth (in.)
- Span length (ft)
- Girder spacing (ft)
- Deck overhang width (ft)

- Skew angle (deg.)
- Brace type (K-brace or X-brace)
- Number of brace points (end-span only, 1/2 point, 1/3 point, 1/4 point)
- Number of girders
- Construction load factors (un-factored service loads; factored strength loads)

Specific parameter values that were included in the database-production parametric study—which involved 453,600 separate analyses—are listed in Tables 4-1 and 4-2. For the factored construction load analyses, the load factors previously listed in Table 3-1 were used. (Note that seven (7) of the eight (8) standard FIB cross-sections were included in the study. The 36″ FIB, however, was excluded because the cross-section is so shallow that use of moment-resisting X-braces and K-braces is not likely to be feasible or warranted).

Maximum and minimum span lengths used in the parametric study were based on design aids included in the *FDOT Instructions for Design Standard No. 20010: Prestressed Florida-I Beams* (IDS 20010; FDOT, 2014b), which provide estimated span lengths (Table 4-4) for FIBs with different lateral spacings, based on representative bridge design calculations. Maximum lengths were conservatively based on a lateral girder spacing of 6 ft and an environment classified as ‘'Moderately Aggressive’, while minimum lengths assumed a 12-ft spacing and an ‘Extremely Aggressive’ environment. To ensure that the considered length ranges included all reasonable beam designs, the basic ranges taken from FDOT IDS 20010 were extended to cover a total span range of 50 ft. The parametric study included span lengths chosen at 10-ft intervals over the final ranges.

It was also determined from a survey of typical bridges (and FDOT recommendations) that the range of other geometric parameters, such as deck overhang widths, girder spacings, and skew angles, would cover most design scenarios. Additionally, preliminary analyses indicated that as the number of interior brace points increases beyond three (3) interior braces (i.e., 1/4

point bracing), changes in maximum brace forces become small (i.e., the brace forces converged). Similarly, increasing the number of girders in the system beyond nine (9) girders did not significantly change maximum brace forces in the construction load analyses. Therefore, bridges with more than nine girders were not expected to have significantly different brace forces induced by construction loads than would a bridge with nine (9) girders.

For each Florida-I beam in the parametric study, a single bracing depth (Figure 4-8) was assigned based on available web height. For FIB sections, as the overall girder depth increases, so does the available web depth (since the top and bottom flange dimensions remain constant). Therefore, deeper girders in the parametric study allowed for larger brace depths. Additionally, as brace depth increases, the bracing system becomes more effective in resisting torsional moments induced by eccentric construction loads. Therefore, the representative brace depths chosen for the parametric study (Table 4-4) were selected so as to avoid producing overly-conservative brace force data.

4.4 Calculation of Brace Forces by Database Interpolation

As noted earlier, the approach to brace force prediction (calculation) taken in this study was to conduct a large-scale parametric study; store the brace force results into a database; and then access and interpolate that database when forces are needed for bracing design. The overall database of information generated by the database-production parametric study was stored into two text-file ‘databases’—one for K-braced systems, and the other for X-braced systems. Within each database file, maximum brace forces were stored both for *un-factored* service loads and for *factored* strength loads. Additionally, for K-braced systems, diagonal element forces and horizontal element forces were computed and stored separately. Data contained within the database files are organized in such a manner that particular cases of interest can be efficiently located.

To make the process of accessing and interpolating the database simple and user-friendly, a MathCad-based program was developed. The program allows the user to specify the following key system parameters:

- FIB cross-section depth (in.)
- Span length (ft)
- Girder spacing (ft)
- Deck overhang width (ft)
- Skew angle (deg.)
- Brace type (K-brace or X-brace)
- Number of brace points (end-span only, 1/2 point, 1/3 point, 1/4 point)
- Number of girders

and reports back the maximum end-span and intermediate-span brace forces for un-factored (service) and for factored (strength) loading conditions. Of the eight (8) parameters listed above, three (3) are never interpolated since intermediate values are not possible—FIB depth, number of interior brace points, and brace type (K-brace or X-brace). For the five (5) remaining parameters (span length, girder spacing, deck overhang width, skew angle, and number of girders), the corresponding data are extracted directly from the database, if an exact match is available. If, however, an exact match is not available, then interpolation (and in some cases, extrapolation) is used to estimate the brace force. To accomplish this outcome, the program implements a five-dimensional linear interpolation algorithm.

When user-specified parameter values lie outside the scope of the database-production parametric study (Tables 4-1 and 4-2), one of three possible actions will occur: 1) data extrapolation; 2) data bounding; 3) generation of an error message. For some parameters, limited linear extrapolation outside the scope of the database is appropriate. However, for some parameters, it is more appropriate to report brace forces for the *bounding* value from Table 4-1 and Table 4-2, rather than to perform extrapolation. For example, when the number of girders exceeds nine (9), it is more appropriate to estimate the brace forces using data corresponding to a

bridge with nine (9) girders than to perform linear extrapolation. Note that whenever data extrapolation or data bounding are necessary to compute brace forces, a message is generated by the program indicating to the user which process was used. Finally, selected parameter values are not permitted to be outside the range indicated in Tables 4-1 and 4-2. Specifically, skew angles larger than 45 degrees and deck overhang widths larger than 6 ft are not permitted and will result in an error message being generated.

4.5 Verification of Database Approach

To evaluate the level of accuracy and conservatism produced by the interpolated database approach (and to verify correct functioning of the associated calculation program that was developed), a limited-scope sensitivity study was conducted. System parameters used in the sensitivity study (e.g., span length, deck overhang width, skew, girder spacing, number of girders) were specifically chosen to fall *between* the parameter values (Tables 4-1 and 4-2) that were used to generate the brace force database. Additionally, for each set of intermediate system parameters that were chosen, an additional—and corresponding—finite element bridge model was constructed and analyzed to provide a datum for brace force comparison.

Approximately 200 unique geometric configurations of bridges with end-span and mid-span bracing (involving approximately 600 separate analyses with multiple construction *loading* conditions) were tested for a broad range of girder types. The level of accuracy and conservatism was quantified for each case by normalizing the database-predicted maximum brace forces by the maximum brace forces computed from the additional finite element analyses. Normalized results for K-brace cases are illustrated in Figure 4-9 for end-span braces and Figure 4-10 for intermediate-span braces. Similarly, results for X-brace cases are illustrated in Figure 4-11 for end-span braces and Figure 4-12 for intermediate-span braces. For all four sets of data presented, the majority of the database predicted brace forces were within ±10% of the corresponding finite

element computed values. Furthermore, in all four sets of data, the distributions of normalized predictions were clearly biased (skewed) toward the side of producing conservative results. Overall, the level and bias of the conservatism produced by the interpolated database approach was considered to be appropriate and reasonable for purposes of designing braces.

Note that these analyses included different combinations of intermediate parameters (i.e., parameters not in parametric study scope) from one intermediate parameter to all five parameters (skew, number of girders, span lengths, girder spacings, and deck overhang width).

Table 4-1. Span length values used in the database-production parametric study

Span length, L (ft)						
45″ FIB	54″ FIB	63″ FIB	72″ FIB	78″ FIB	84″ FIB	96″ FIB
80	100	110	120	130	150	160
90	110	120	130	140	160	170
100	120	130	140	150	170	180
110	130	140	150	160	180	190
120	140	150	160	170	190	200
130	150	160	170	180	200	210

Table 4-2. Other parameter values used in the database-production parametric study

Deck overhang width, (in.)	Skew angle	Intermediate-span brace points, n_i	Girder spacing, (ft)	Girders, n_g
25	0°	0	6	3
36	15°	1	9	5
48	30°	2	12	9
60	45°	3	-	-
72	-	-	-	-

Table 4-3. Range of allowable span lengths for FIBs

	Values from FDOT IDS 20010		
Section	Min length (ft)	Max length (ft)	Span length range
45″ FIB	98	126	80–130
54″ FIB	113	142	100–150
63″ FIB	124	155	110–160
72″ FIB	142	173	120–170
78″ FIB	151	182	130–180
84″ FIB	159	191	150–200
96″ FIB	175	208	160–210
Spacing	12 ft	6 ft	
Environment	Extremely aggressive	Moderately Aggressive	

Table 4-4. Brace depths used in construction load parametric study

Girder type	Brace depth, (in.)
45” FIB	18
54” FIB	22
63” FIB	27
72” FIB	36
78” FIB	41
84” FIB	48
96” FIB	60

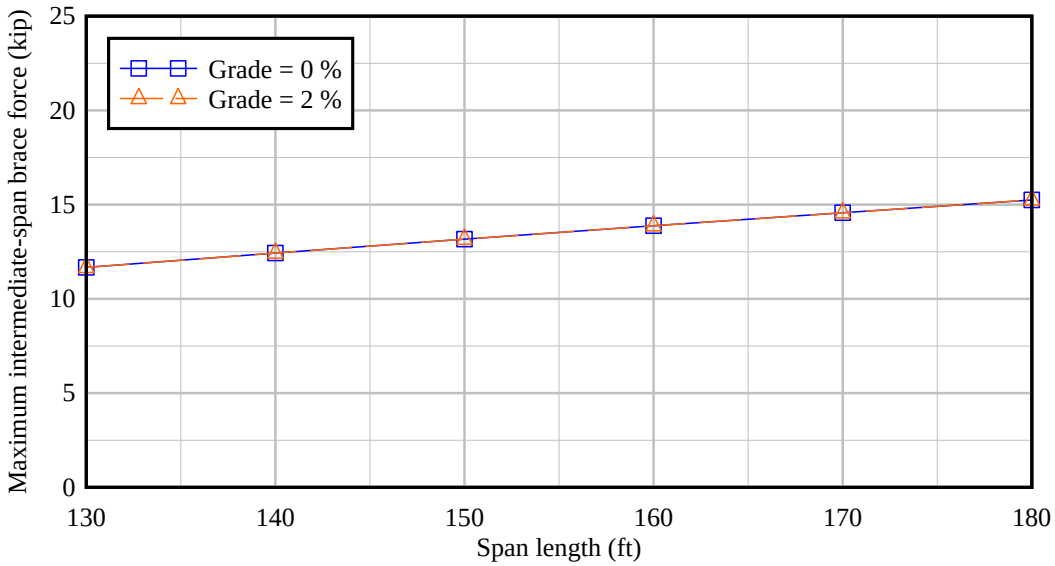

Figure 4-1. Effect of bridge grade on brace forces for an example 78” FIB system

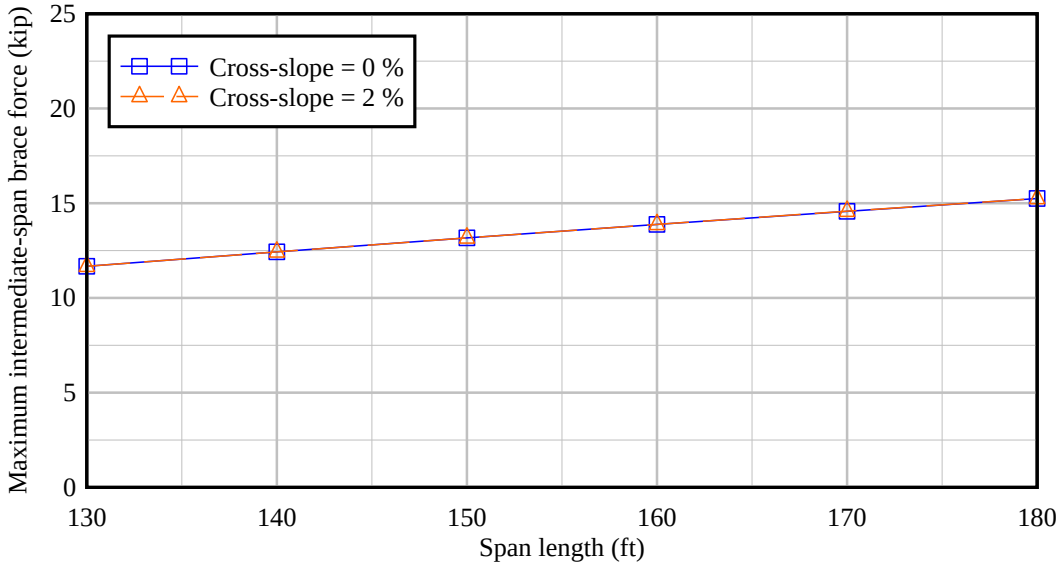

Figure 4-2. Effect of cross-slope on brace forces for an example 78" FIB system

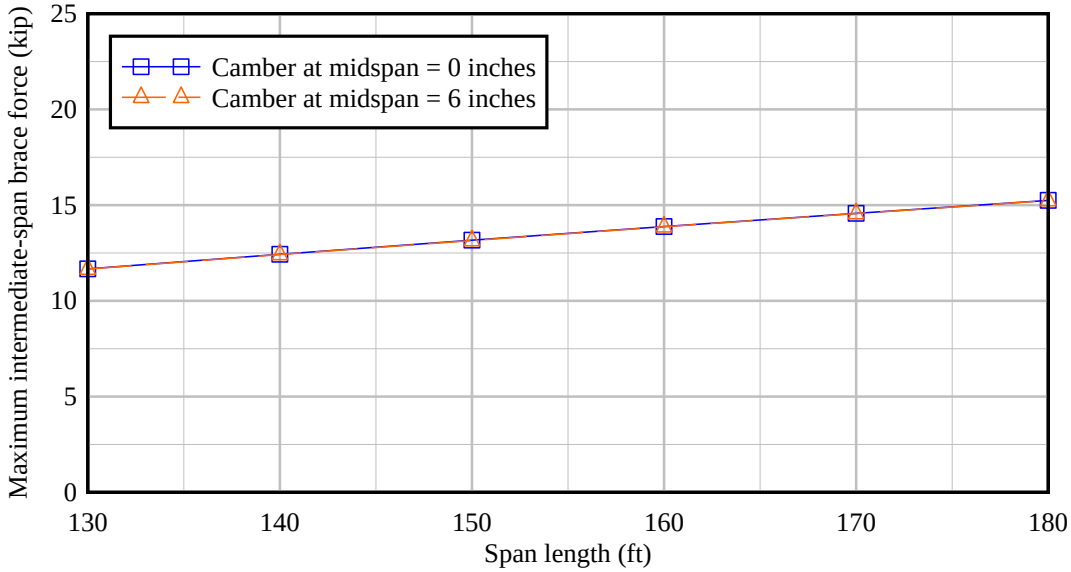

Figure 4-3. Effect of camber on brace forces for an example 78" FIB system

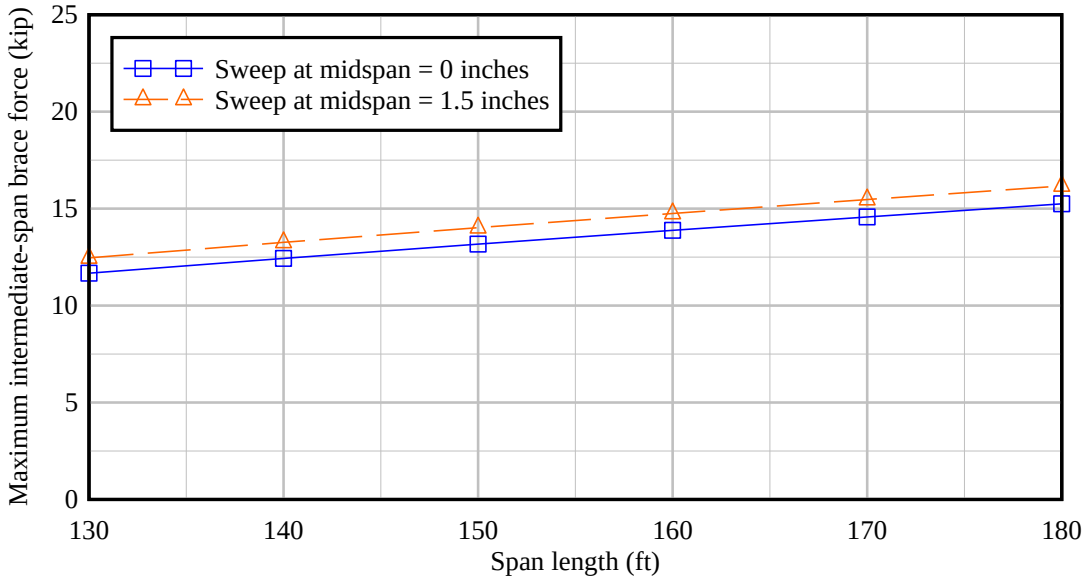

Figure 4-4. Effect of sweep on brace forces for an example 78" FIB system

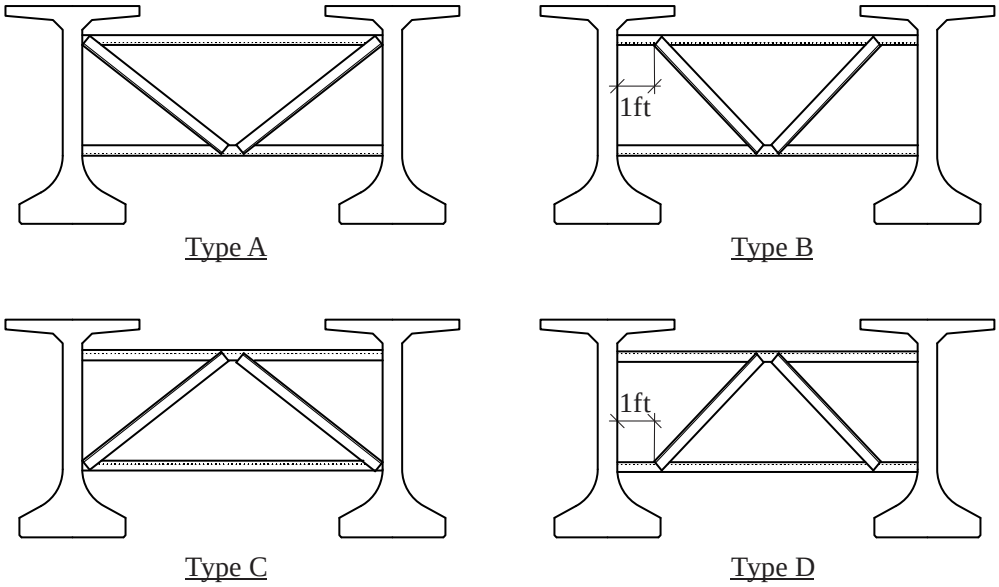

Figure 4-5. K-brace configurations analyzed in limited-scope sensitivity study

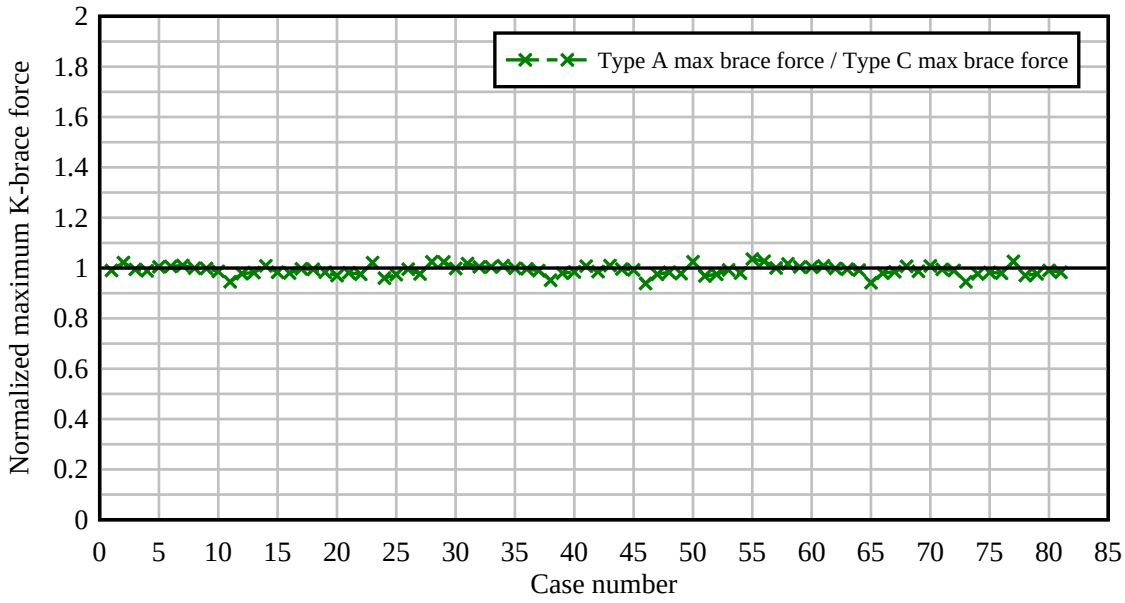

Figure 4-6. Conservatism of selected K-brace configuration (compared to inverted K-brace)

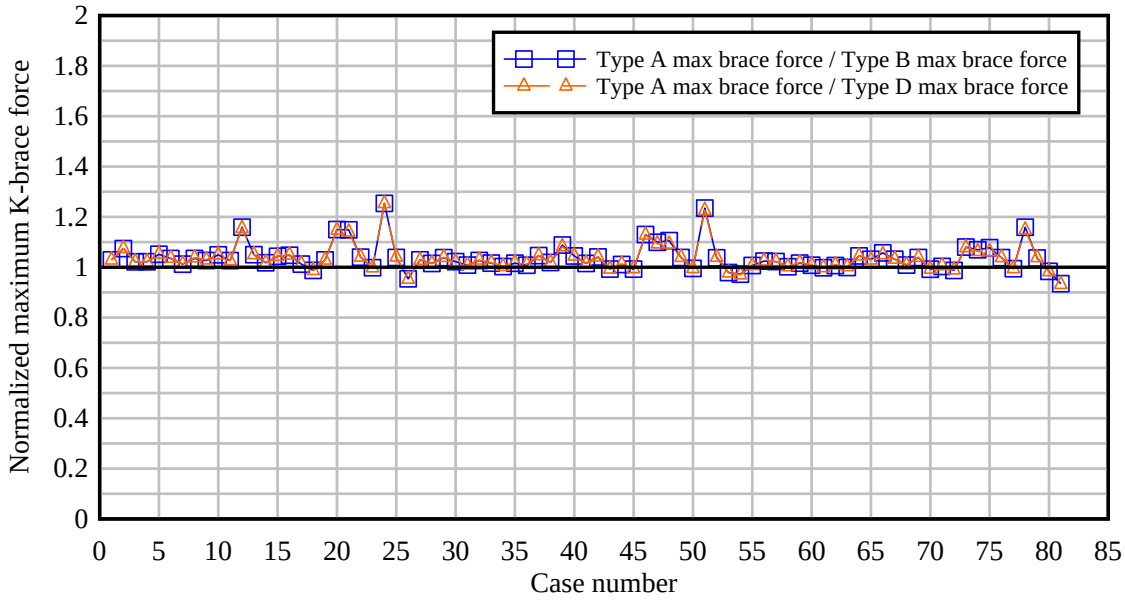

Figure 4-7. Conservatism of selected K-brace configuration (compared to offset ends)

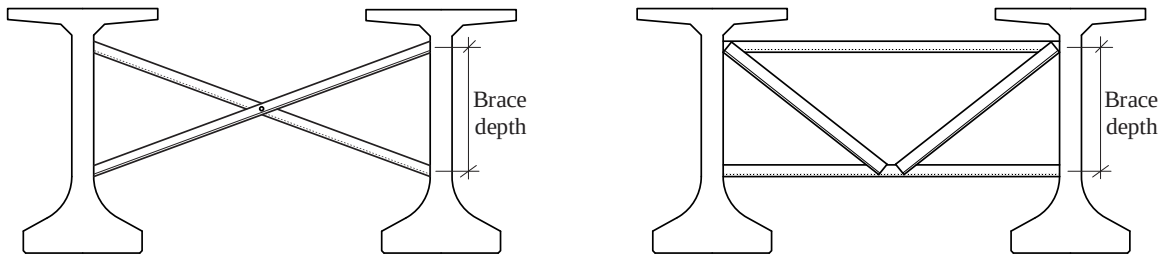

Figure 4-8. Definition of brace depth

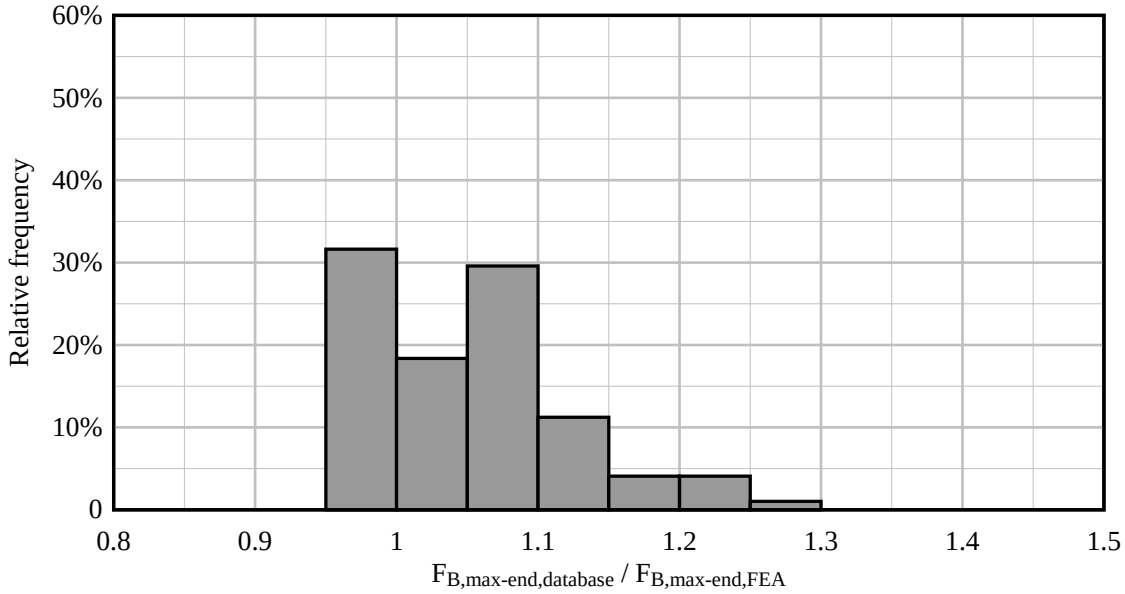

Figure 4-9. Accuracy of interpolated database approach for maximum end-span K-brace force

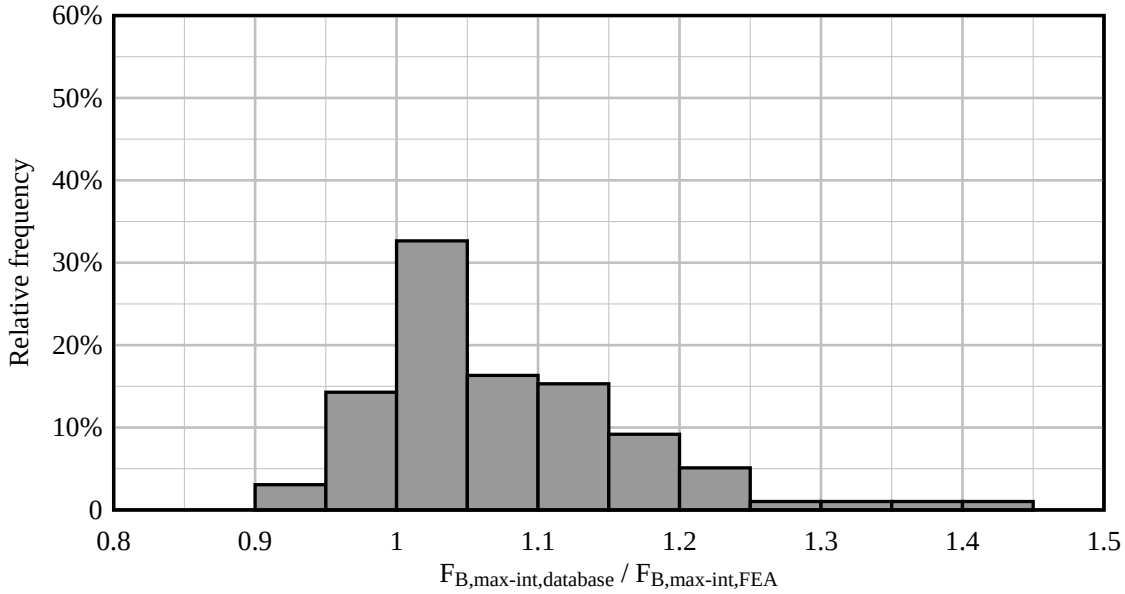

Figure 4-10. Accuracy of interpolated database approach for maximum intermediate-span K-brace force

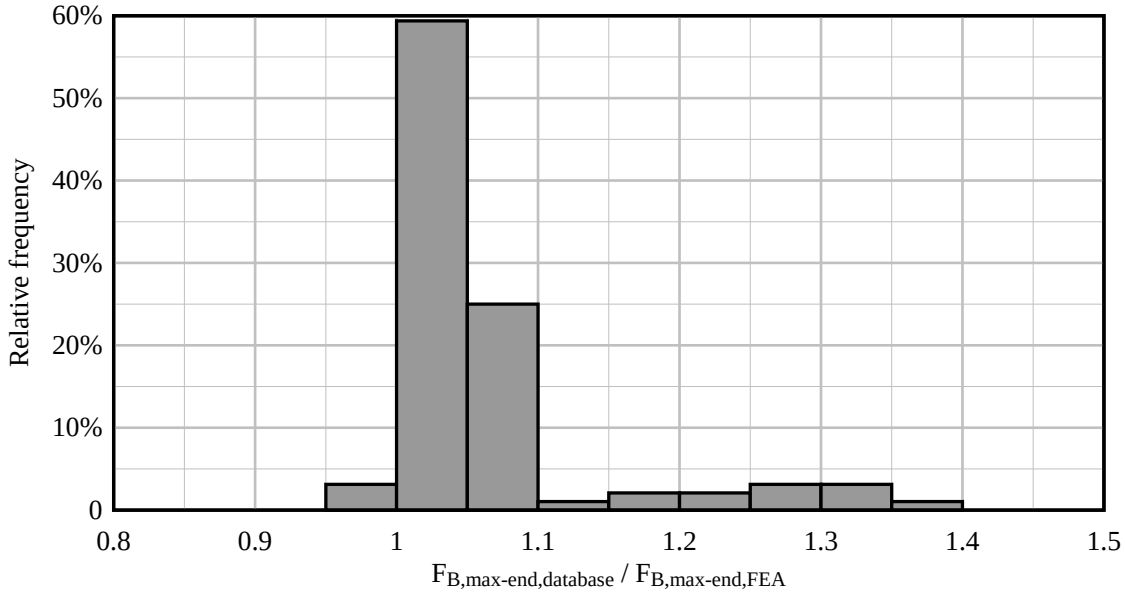

Figure 4-11. Accuracy of interpolated database approach for maximum end-span X-brace force

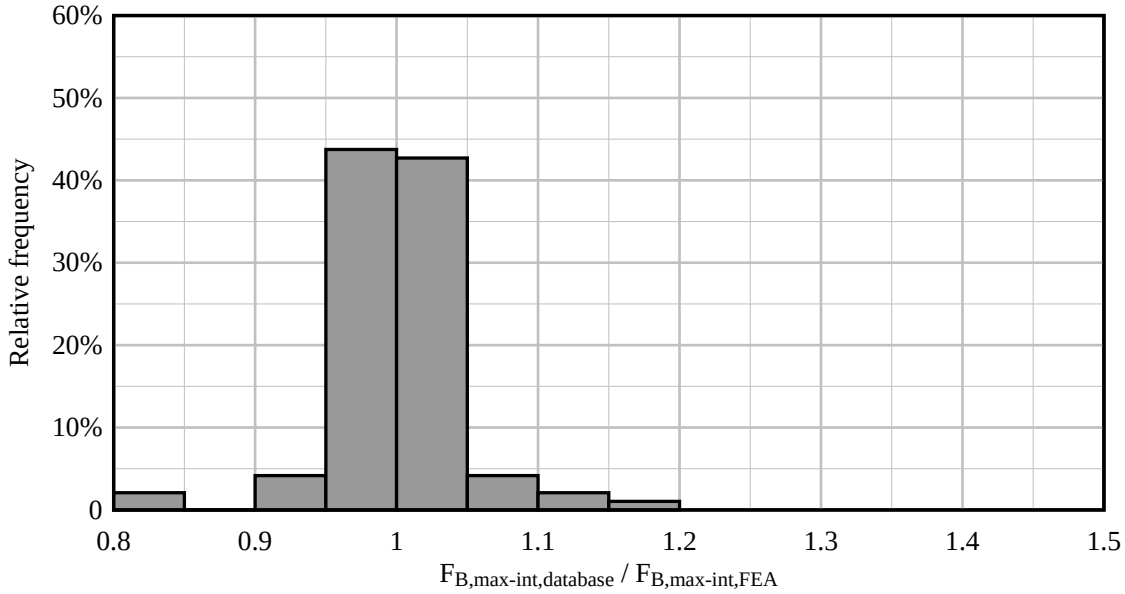

Figure 4-12. Accuracy of interpolated database approach for maximum intermediate-span X-brace force

CHAPTER 5
WIND TUNNEL TESTING

5.1 Overview

In addition to the construction loads discussed in previous chapters, wind loads must also be accounted for when quantifying brace forces for bracing system design. In a previously conducted study (BDK75-977-33, Consolazio et al., 2013) wind tunnel tests were conducted to quantify girder drag coefficients for partially constructed bridges at the stage where only the girders and bracing are present. When stay-in-place forms and overhang formwork are subsequently added to the bridge—as part of the ongoing construction process—they introduce new barriers to wind flow (e.g., between adjacent girders) and therefore have the potential to alter the drag coefficients for the individual girders within the bridge cross-section. A goal of the present study was to therefore to quantify drag coefficients for individual girders in bridges that are at the construction stage where stay-in-place forms and overhang formwork have been installed. To achieve this goal, wind tunnel tests were conducted on bridges with stay-in-place forms present (and in some cases overhangs) to generate data that would complement data previously measured in BDK75-977-33. By comparing data measured in the current study to data from the previous study, the influences of stay-in-place forms and overhangs on girder drag coefficients could be quantified and appropriate drag coefficients for wind-load brace force design could be determined.

Additionally, since practical bridge structures almost always consist of *multiple* girders positioned side by side, it was also necessary to investigate the effects of *shielding* (i.e., aerodynamic interference), in which the windward girder acts as a wind break and reduces the total force on subsequent leeward girders. The wind tunnel tests conducted in this study were

therefore performed on bridge cross-sections with variations in the number of girders, variations in girder spacing, and variations as to the presence of stay-in-place forms and overhangs.

5.2 Background on Drag Coefficients

In order to calculate wind load on a bridge girder, it is necessary to know the drag coefficient for the girder cross-sectional shape. The drag coefficient is a type of *aerodynamic coefficient*: a dimensionless factor that relates the magnitude of the fluid force on a particular geometric shape to the approaching wind speed. Drag coefficients are typically a function of the relative orientation of the object relative to the direction of the impinging wind.

5.2.1 Dimensionless Aerodynamic Coefficients

Fluid forces arise when a solid body is submerged in a moving fluid. As the fluid flow is diverted around the body, a combination of inertial and frictional effects generates a net force on the body. It is observed that this force—called aerodynamic force (F) when the fluid under consideration is air—is directly proportional the dynamic pressure (q) of the fluid:

$$q = \frac{1}{2}\rho V^2 \tag{5-1}$$

where ρ is the mass density of the fluid and V is the flow velocity (Çengel and Cimbala, 2006). Dynamic pressure can be considered as the *kinetic energy density* of the fluid. This offers an intuitive explanation for its proportional relationship to aerodynamic force, which is, at the most fundamental level, the cumulative effect of innumerable microscopic collisions with individual fluid particles. Similarly, if the dimensions of the body are scaled up, it is observed that the aerodynamic force increases quadratically, reflecting the fact that the increased surface area results in a greater total number of collisions.

These proportional relationships can be combined and expressed as:

$$F = C_F q L_0 L_1 \tag{5-2}$$

where, L_0 and L_1 are arbitrary reference lengths, and C_F is a combined proportionality factor, called a *force coefficient*. The selection of L_0 and L_1 does not affect the validity of Equation 5-2 as long as they both scale with the structure. However, it is important to be consistent; force coefficients that use different reference lengths are not directly comparable, and a coefficient for which the reference lengths are not explicitly known is useless for predicting aerodynamic forces. In structural applications, it is common for the product $L_0 L_1$ to be expressed in the form of a reference area, A, which is typically taken as the *projected area* of the structure in the direction of wind.

By an analogous process, it is possible to derive a *moment coefficient* (C_M), which normalizes aerodynamic moment load in the same way that the force coefficient normalizes aerodynamic force. The only difference is that aerodynamic moment grows cubically with body size rather than quadratically (because the moment arms of the individual collisions grow along with the surface area). Therefore, the moment proportionality expression is:

$$M = C_M q L_0 L_1 L_2 \tag{5-3}$$

As with the force coefficient, the reference lengths must be known in order to properly interpret the value of C_M. However, with moment coefficients, it is equally important to know the center of rotation about which the normalized moment acts. Together, C_F and C_M are called *aerodynamic coefficients*, and they can be used to fully describe the three-dimensional state of aerodynamic load on a structure (for a particular wind direction).

When working with bridge girders, or other straight, slender members, it is often convenient to assume that the length of the girder is effectively infinite. This simplifies engineering calculations by reducing the girder to a two-dimensional cross-section subjected to

in-plane aerodynamic line-loads (Figure 5-1). Depending on the direction of wind, out-of-plane forces and moments may exist, but they generally do not contribute to the load cases that control design and can therefore be considered negligible. In two dimensions, the proportionality expressions for the aerodynamic coefficients become:

$$F' = C_F q L_1 \tag{5-4}$$

$$M' = C_M q L_1 L_2 \tag{5-5}$$

where, F' is a distributed force (force per unit length) and M' is a distributed torque (moment per unit length). Note that two-dimensional aerodynamic coefficients can be used interchangeably in the three-dimensional formulation if the reference length L_0 is taken to be the out-of-plane length of the girder. All further discussions of aerodynamic coefficients in this report will use the two-dimensional formulation unless stated otherwise. The remaining reference lengths (L_1 and L_2) will always be taken as the girder depth, D, so that the force and moment coefficients are defined as:

$$C_F = \frac{F'}{\frac{1}{2}\rho V^2 D} \tag{5-6}$$

$$C_M = \frac{M'}{\frac{1}{2}\rho V^2 D^2} \tag{5-7}$$

Aerodynamic coefficients are sometimes called *shape factors* because they represent the contribution of the geometry of an object (i.e., the way airflow is diverted around it), independent of the scale of the object or the intensity of the flow. Because of the complexity of the differential equations governing fluid flow, the aerodynamic coefficients of a structure are not calculated from first principles but can, instead, be measured directly in a wind tunnel using reduced-scale models.

5.2.2 Terminology Related to Aerodynamic Coefficients

Aerodynamic force on a body is typically resolved into two orthogonal components, drag and lift. These components have corresponding force coefficients: the *drag coefficient* (C_D) and *lift coefficient* (C_L). In this report, drag is defined as the lateral component of force and lift is defined as the vertical component of force, regardless of the angle of the applied wind.

In several subfields of fluid dynamics, it is more conventional to define drag as the component of force along the direction of the wind stream and lift as the component perpendicular to the wind stream. However, this is inconvenient when evaluating wind loads on stationary structures (e.g., bridge girders) because the angle of the wind stream can change over time. Where necessary in this report, the names *stream drag* (C_{SD}) and *stream lift* (C_{SL}) (Figure 5-2) will be used to refer to the force components that are aligned with, and perpendicular to, the wind stream.

Finally, the term *pressure coefficient* (C_P), is an alternative name for $C_{D,}$ and is often used in design codes to indicate that it is to be used to calculate a wind *pressure* load (P), rather than a total force, as in:

$$P = C_P \frac{1}{2} \rho V^2 \tag{5-8}$$

This is advantageous because it obviates the need to explicitly specify the characteristic dimensions that were used to normalize the coefficient. Instead, denormalization occurs implicitly when the pressure load is applied over the projected surface area of the structure. Unfortunately, this approach breaks down when working with drag and lift coefficients together. If drag and lift are both represented as pressure loads, then the areas used to normalize the coefficients will differ (unless by chance the depth and width of the structure are equal). As a result, the magnitudes of the coefficients are not directly comparable—that is, equal coefficients

will not produce loads of equal magnitude—and they cannot be treated mathematically as components of a single force vector, which complicates coordinate transformations and other operations. For this reason, the term pressure coefficient is not used in this report, except when in reference to design codes that use the term.

In this report, the term *torque coefficient* (C_T) refers to the in-plane moment that acts about the centroid of the cross-section. This is a convenient choice of axis because it coincides with the axes of beam elements in most structural analysis software. Loads calculated from C_D, C_L, and C_T can be applied directly to beam nodes (located at the centroid of the cross-section) to correctly model the two-dimensional state of aerodynamic load. However, most design codes represent wind load as a uniform pressure load that produces a resultant force acting at a location called the *center of pressure* (Figure 5-3), which is typically assumed to correspond to the mid-height of the cross-section. For such circumstances, the term *pressure torque coefficient* (C_{PT})—acting about the center of pressure—will be used to differentiate it from the C_T, which always acts about the centroid (Figure 5-4). A summary of the different types of aerodynamic coefficient used in this report is presented in Table 5-1.

5.3 Current Wind Design Practice in Florida

Bridge structures in Florida are designed in accordance with the provisions of the *FDOT Structures Design Guidelines* (SDG; FDOT, 2013). As with most modern design codes, the wind load provisions in the SDG are based on Equation 5-8, with additional scale factors included to adjust the intensity of the wind load according to the individual circumstances of the bridge. Specifically, Section 2.4 of the SDG gives the equation:

$$P_Z = 2.56\times10^{-6} K_Z V^2 G C_P \tag{5-9}$$

where P_Z is the design wind pressure (ksf, kip per square foot), K_Z is the velocity pressure exposure coefficient, V is the basic wind speed (mph), and G is the gust effect factor. The constant term, 2.56×10^{-6}, represents the quantity $\frac{1}{2}\rho$ from equation 5-8 expressed in derived units of (ksf)/(mph)^2.

Each county in Florida is assigned a basic wind speed, V, adapted from wind maps published by the American Society of Civil Engineers (ASCE, 2006), which are based on statistical analyses of historical wind speed records compiled by the National Weather Service. Statistically, V represents the peak 3-second gust wind speed for a 50-year recurrence interval. In other words, if the average wind speeds during every 3-second time interval were recorded over a period of 50 years, V is the expected value of the maximum speed that would be recorded. It is important to note that this does *not* mean that Florida bridges are only designed to resist 50-year wind loads. Different load combinations use load factors for wind that effectively adjust the recurrence interval up or down. For example, the Strength III limit state, as stipulated by the SDG, includes a wind load factor of 1.4, which increases the recurrence interval to approximately 850 years (FDOT, 2009).

Basic wind speeds published by ASCE are based on measurements taken at an elevation of 33 ft and are not directly applicable to structures at other elevations. Wind that is closer to ground level is slowed by the effect of surface friction, resulting in a vertical wind gradient called the atmospheric boundary layer (Holmes, 2007). The purpose of the velocity pressure exposure coefficient, K_Z, is to modify the wind pressure load to account for differences in elevation. Because surface roughness of the terrain is known to reduce the steepness of the gradient, ASCE divides terrains into three exposure categories, B, C, and D, and provides

equations for each category. However, for simplicity, the SDG conservatively assumes that all Florida structures are in the Exposure C category. As a result, the equation for K_Z in Florida is:

$$K_Z = 2.01\left(\frac{z}{900}\right)^{0.2105} \geq 0.85 \qquad (5\text{-}10)$$

where z is the elevation above ground (ft). Note that K_Z is equal to unity at an elevation of 33 ft (corresponding to the wind speed measurements) and that wind speed is assumed to be constant for elevations of 15 ft or less (Figure 5-5).

Wind is characteristically gusty and turbulent, producing dynamic structural loads that can fluctuate significantly over short periods of time. However, it is simpler and more efficient to design structures to resist static loads. Furthermore, wind tunnel measurements of static force coefficients are typically performed in steady flow (with a major exception being site-specific wind tunnel testing, which models a proposed structure along with its surrounding terrain for the express purpose of capturing turbulent loads). The gust effect factor, G, modifies the static design wind pressure so as to envelope the effects of wind gustiness and dynamic structural response on peak structural demand. For aerodynamically rigid bridge structures, defined as those with spans less than 250 ft and elevations less than 75 ft, the SDG prescribes a gust effect factor of 0.85. By this definition, the vast majority of precast prestressed concrete girder bridges in Florida are considered aerodynamically rigid. It is noted that G actually *reduces* the design wind pressure on rigid bridges, reflecting the fact that peak gust pressures are unlikely to occur over the entire surface area of such structures simultaneously (Solari and Kareem, 1998).

The SDG further provides specific guidance on the calculation of wind loads during the bridge *construction* stage (as opposed to the calculation of wind loads on the completed bridge structure). If the exposure period of the construction stage is less than one year, a reduction factor of 0.6 on the basic wind speed is allowed by the SDG.

Calculation of wind pressure using Equation 5-9 requires that an appropriate pressure coefficient (C_P) be determined for the structure under consideration. Pressure coefficients are provided by the SDG for several broad categories of bridge component as indicated in Table 5-2. In the present study, the pressure coefficients of interest are those for girders *with stay-in-place forms* in place. As Table 5-2 indicates, the SDG provides a single value of C_P, regardless of girder shape, when deck forms are in place: $C_P = 1.1$. The wind tunnel testing conducted in this study was performed to help determine whether $C_P = 1.1$ is an appropriate value, and whether it should depend on the girder type.

5.4 Testing Configurations

To maximize the potential for comparing results from wind tunnel tests with SIP forms to those without forms, the test configurations used in a previous study (BDK75-977-33, Consolazio et al., 2013, no formwork) were used as a guide in determining the wind tunnel test program scope in the present study (with formwork). Consequently, several 'nearly-equivalent' testing configurations—with the sole difference being the presences of SIP forms—were included in the present study. Four different girder cross-sectional shapes (Figure 5-6) were selected as being representative of a wide range of modern Florida bridges:

- **78-inch-deep Florida-I beam (*78" FIB*)**: One of the most common FIB shapes used in bridge design. All FIB shapes have identical flanges, with the differences in girder depth arising from differences in the height of the web. The 78″ FIB was the deepest FIB shape considered in this study.

- **45-inch-deep Florida-I beam (*45" FIB*)**: The 45″ FIB was included in this study to quantify the effect of changing the FIB depth, and to ensure that the resulting design loads would be applicable to a range of FIB shapes.

- **Wide-flange plate girder (*WF plate*)**: Drag coefficients of I-shaped girders have been studied, in the literature, for width-to-depth ratios ranging from 1:1 to 2:1. However, built-up steel plate girders commonly used to support bridge decks tend to be much deeper than they are wide. The WF Plate girder considered in this study has an 8-ft deep web and 2′-8″ wide flanges, resulting in a width-to-depth ratio of 3:1, representing the approximate lower bound for bridge girders.

- **Box girder (*Box*)**: A survey of existing box girder bridges was used to develop a representative 6-ft deep cross-section.

All of these girder sections were tested in multiple girder configurations and with addition stay-in-place formwork present (Figure 5-7a). Additionally, to quantify the influence of overhangs, all bridge cross-sections were tested both with and without maximum feasible overhangs (Figure 5-7b). Fully dimensioned drawings of the girder cross-sections and schematics of each test configuration conducted in this study are included in Appendix B.

Wind tunnel test configurations were defined by type of girder employed (Figure 5-6), and by the following parameters (Figure 5-7):

- **Number of girders**: Wind tunnel tests were performed on 2-girder, 5-girder, and 10-girder configurations.

- **Spacing**: Spacing refers to the horizontal center-to-center distance between girders. Results from previously conducted wind tunnel testing (Consolazio et al., 2013) indicated that girder configurations with larger spacing produced less shielding (i.e., less aerodynamic interference, and thus larger forces) on leeward girders. Therefore, to yield conservative wind tunnel results in the present study, a characteristic *maximum* spacing was determined for each type of girder based on a survey of existing bridge designs and consultations with the FDOT. Each testing configuration for a given type of girder then used only the maximum spacing.

- **Cross-slope**: Most bridge decks are designed with a cross-slope that is 2% or greater in magnitude, and the girders are usually aligned vertically along that slope so that they can evenly support the deck. Therefore, the FIBs and plate girders were tested with a cross-slope that was 2% in magnitude, but negative in sign (Figure 5-7): i.e., a cross-slope of -2%. A negative cross-slope was used because when SIP forms are attached to the top flanges of the girders, the exposed bottom flanges of the girders produce a worst-case (maximum) condition in terms of drag forces generated on the shielded leeward girders. Generally, steel girder bridges can have a greater amount of horizontal curvature than FIB bridges, so higher cross-slopes are often included to improve vehicle handling. To account for the larger magnitude of cross-slope, the WF Plate girders were tested in configurations with -8% cross-slope. In contrast to the ‘I-shaped’ FIB and plate girders, box girders are not generally aligned vertically when supporting a cross-sloped deck. Instead, the girders are typically inclined to follow the bridge cross-slope. As a result, in this study, box girders were only tested in a 0% (un-sloped) configuration, however the range of tested wind angles was increased (relative to the I-shaped girder wind angles), as described below.

- **Wind angle**: In practical bridge construction situations, the direction of wind flow will not, in general, always be perfectly horizontal. To account for the natural variation in wind angle (and at the recommendation of a commercial wind tunnel test facility), each FIB and plate girder bridge configuration was tested at five (5) different wind angles ranging from −5° to +5° in increments of 2.5° (Figure 5-8). In the case of the box girder, a change in wind angle is geometrically equivalent to rotating the girders to match the deck cross-slope (Figure 5-9). As a result, the box girder configurations were tested at −10°, −5°, 0°, +5°, and +10° angles, in order to include the *combined* effects of 5° wind angle and 5° (8.7%) of cross-slope.

- **Overhangs**: In most economical bridge designs, the bridge deck extends transversely beyond the extents of the exterior girders, thus creating an overhang of each side. Since it was desirable to quantify the effects of such overhangs on wind coefficients, overhang formwork was included in many of the configurations tested in the wind tunnel. It should be noted that the overhang formwork *support brackets* described earlier (see Section 3.4) were excluded from the wind tunnel tests because they were not expected to influence the wind coefficients. However, the top surface of the overhang formwork, which was expected to influence the wind coefficients, was included. A constant 'total overhang width' (W_{OHT}) of 5 ft (Figure 5-10), as measured from the centerline of the top girder flange to edge of the overhang formwork (*not* the edge of the concrete deck), was used for all girder types. However, due to differences in girder top flange widths, the 'overhang *formwork* width' (W_{OHF}), which was the extension of formwork *beyond* the edge of the girder top flange (Figure 5-10), varied for the girder types tested.

A summary of the scope of the wind tunnel test program is provided in Table 5-3. Note that it was not feasible to instrument (measure wind forces) at every girder position in every configuration tested. Instead, the girder positions (G1, G2 ... G10.) that were instrumented were strategically chosen to maximize the usefulness of the measured data.

5.5 Testing Procedure

The Boundary Layer Wind Tunnel Laboratory at the University of Western Ontario (UWO) was contracted to fabricate the test specimens and to perform all wind tunnel measurements. Based on the size of the UWO wind tunnel, the girder models were constructed at reduced scale (Table 5-4), with air flow properties similarly adjusted so that the resulting forces would be applicable at full-scale. All testing was performed in smooth flow, with turbulence intensities less than 0.5%. Because the tested cross-sections were sharp-edged, it was expected that the measured wind forces would not be sensitive to Reynolds number and the force

coefficients are applicable over a broad range of wind speeds. In a previous study (Consolazio et al., 2013), the assertion that wind forces would not be sensitive to Reynolds number was verified by UWO by performing selected tests at multiple Reynolds numbers. Results from those tests did not reveal any obvious Reynolds number sensitivities.

The scaled girder models were all 7-ft long (equivalent to 175-ft and 196-ft girders at full scale) and were constructed to be fully rigid, without exhibiting any aeroelastic effects. An adjustable frame was used to keep the girders properly oriented relative to each other in each test configuration. To measure wind-induced girder forces at varying wind angles of attack, the entire bridge cross-sectional assembly was rotated in-place relative to the wind stream.

To maximize the utility of the data collected during the wind tunnel testing, it was desirable to *individually* quantify the aerodynamic forces (drag, lift, torque) that acted on each girder within the bridge cross-section. In order to accomplish this goal, each girder in the bridge had to be structurally independent from the rest of the girders—i.e., transmission of lateral load from one girder to the next had to be prevented. Simultaneously, however, air flow between adjacent girders also had to be prevented in order to model the blockage effects associated with the presence of SIP forms.

The approach used to satisfy both of these requirements was to attach bent plates (Figure 5-11) to the top flanges of the girders in the bridge cross-section. The plates represented both the SIP forms and, where present, the overhang formwork. Structural independence was achieved by only extending the SIP form plates to the midpoint between adjacent girders (Figure 5-11) and leaving a small gap so that force transmission to the adjacent plate was not possible. As such, each SIP form plate cantilevered from a girder top flange to the midpoint of the girder spacing on each side (for an interior girder). To model the air flow blockage effects of

the SIP forms, but without transmitting force across the gaps, a flexible adhesive tape (i.e., an adhesive membrane) was used to seal and span across the gaps. In tests where overhangs were present, the top plates were further extended (cantilevered) out to the extents of the overhang formwork.

Wind forces on the girders in each test configuration were measured individually with a high-precision load balance that recorded the time-averaged horizontal load (drag), vertical load (lift), and torque (overturning moment). These loads were then normalized to produce the aerodynamic coefficients for drag (C_D), lift (C_L), and torque (C_T). Finally, the torque coefficient was adjusted so that it represented the torque about the centroid of the section, rather than the torque about the point of measurement (which was at mid-height for the I-shaped girders and at an arbitrary point for the box girders).

Table 5-1. Parameter values used in the database-production parametric study

Symbol	Coefficient name	Description
C_D	Drag	Component of force in horizontal (lateral) direction
C_L	Lift	Component of force in vertical direction
C_{SD}	Stream Drag	Component of force parallel to wind stream
C_{SL}	Stream Lift	Component of force perpendicular to wind stream
C_P	Pressure	Alternative name for C_D
C_T	Torque	Torque measured about centroid
C_{PT}	Pressure Torque	Torque measured about center of pressure

Table 5-2. Pressure coefficients in *FDOT Structures Design Guidelines* (FDOT, 2013)

Bridge component	C_P
Substructure	1.6
Girders with deck forms	1.1
Completed superstructure	1.1
I-shaped bridge girders	2.2
Box and U-shaped girders	1.5

Table 5-3. Summary of wind tunnel tests

Section	Overhangs included	Cross-slope	Spacing (ft)	Number of girders	Instrumented girder position	Test Angles
78” FIB	-	-2%	13	10	1, 2, 3	0°, ±2.5°, ±5°
78” FIB	Yes	-2%	13	10	1, 2, 3, 5, 10	0°, ±2.5°, ±5°
Box	-	0%	22	2	1, 2	0°, ±5°, ±10°
Box	Yes	0%	22	2	1, 2	0°, ±5°, ±10°
WF Plate	-	-8%	14	5	1, 2, 3	0°, ±2.5°, ±5°
WF Plate	Yes	-8%	14	5	1, 2, 3, 4, 5	0°, ±2.5°, ±5°
45” FIB	-	-2%	13	5	1, 2	0°, ±2.5°, ±5°
45” FIB	Yes	-2%	13	5	1, 2, 3	0°, ±2.5°, ±5°

Table 5-4. Wind tunnel test scaling

Section	Model scale	Reynolds number
WF Plate	1:25	77000
78″ FIB	1:28	56000
45″ FIB	1:28	33000
Box	1:25	58000

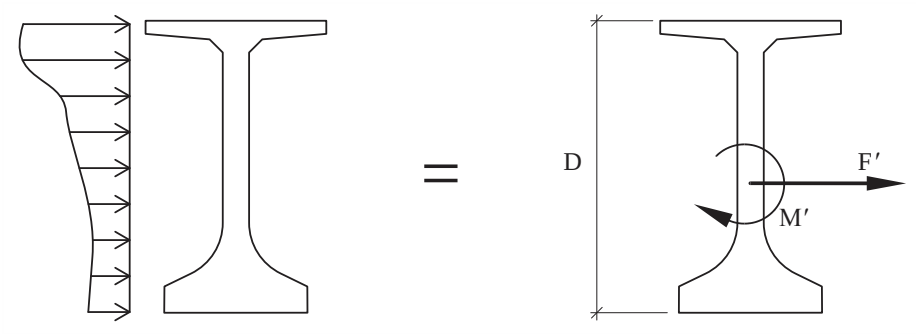

Figure 5-1. Two-dimensional bridge girder cross-section with in-plane line loads

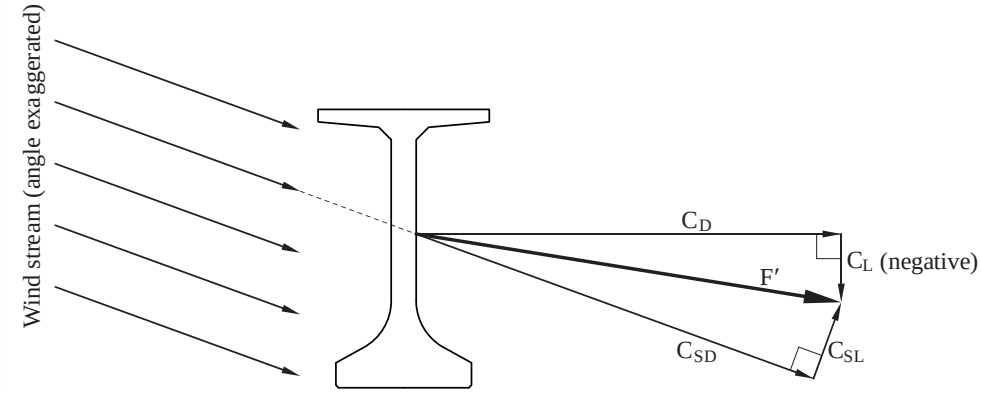

Figure 5-2. Definition of C_D, C_L, C_{SD}, and C_{SL} (shown in positive direction except when noted)

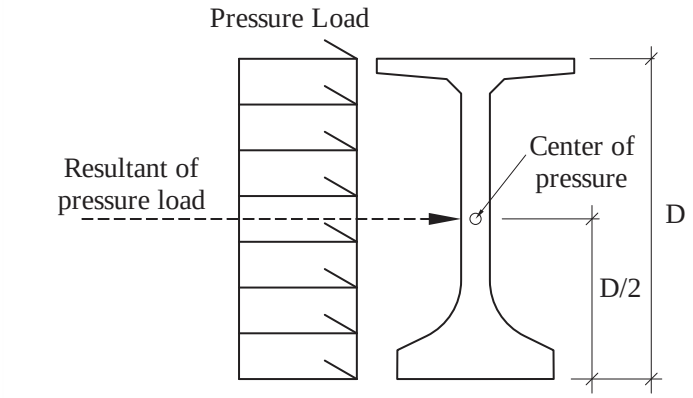

Figure 5-3. Center of pressure of a bridge girder

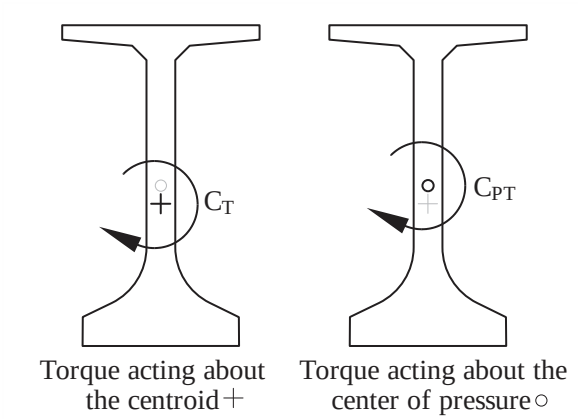

Figure 5-4. Definition of C_T and C_{PT} (shown in positive direction)

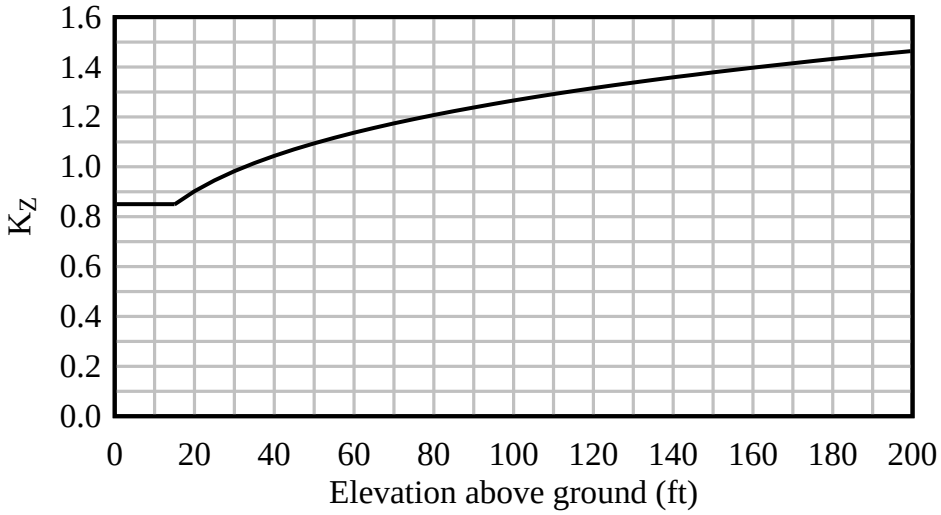

Figure 5-5. Velocity pressure exposure coefficient used by FDOT

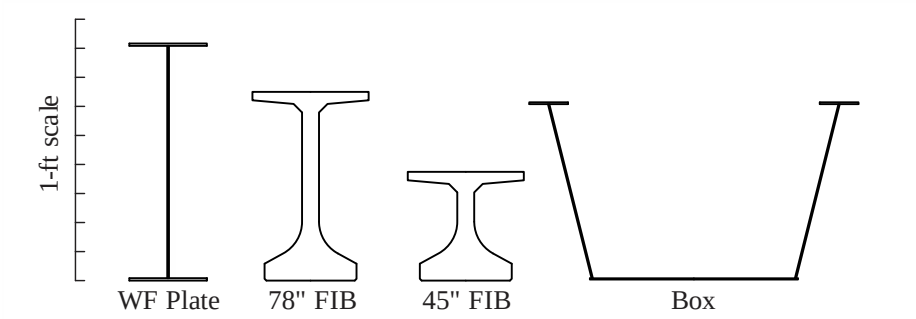

Figure 5-6. Girder cross-sections used in study

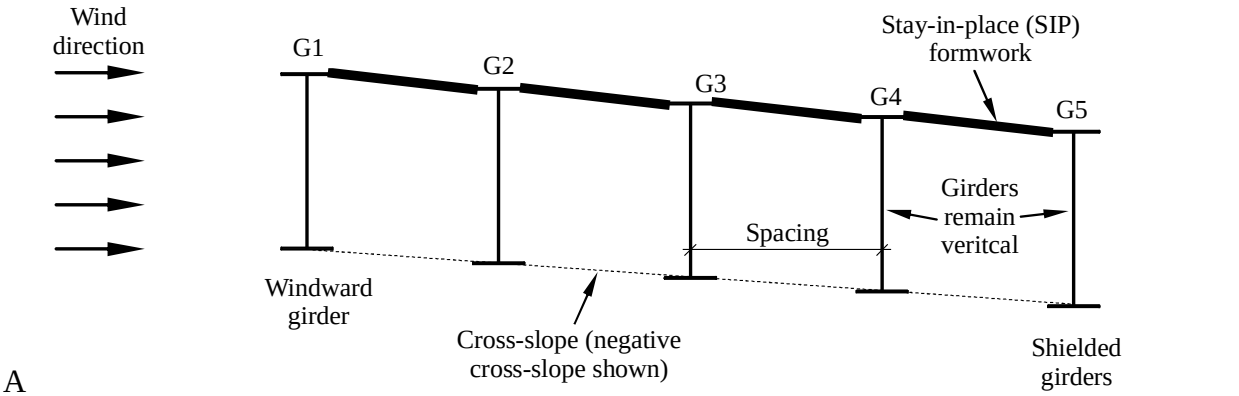

A

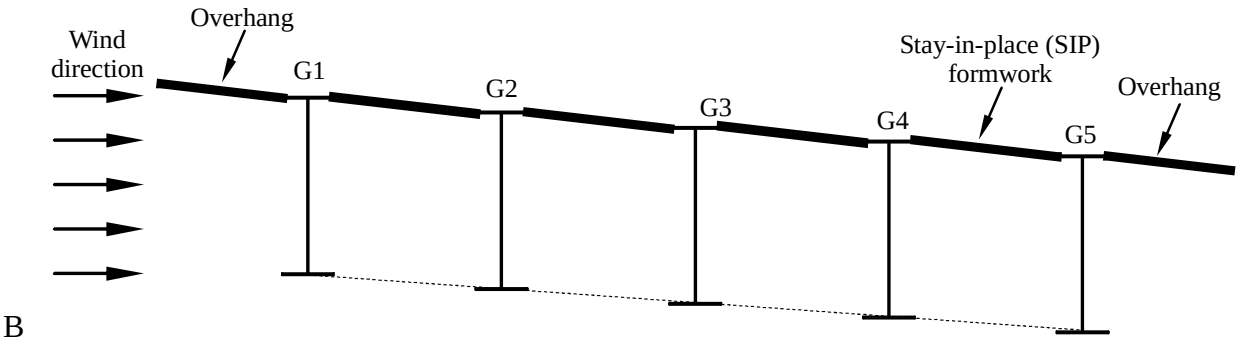

B

Figure 5-7. Parameters definitions for each testing configuration. A) with SIP formwork. B) with SIP formwork and overhangs

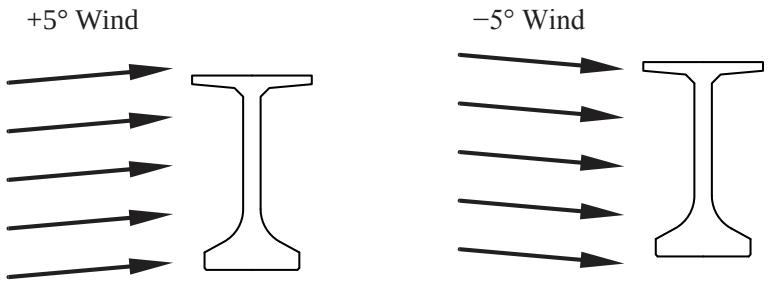

Figure 5-8. Wind angle sign convention

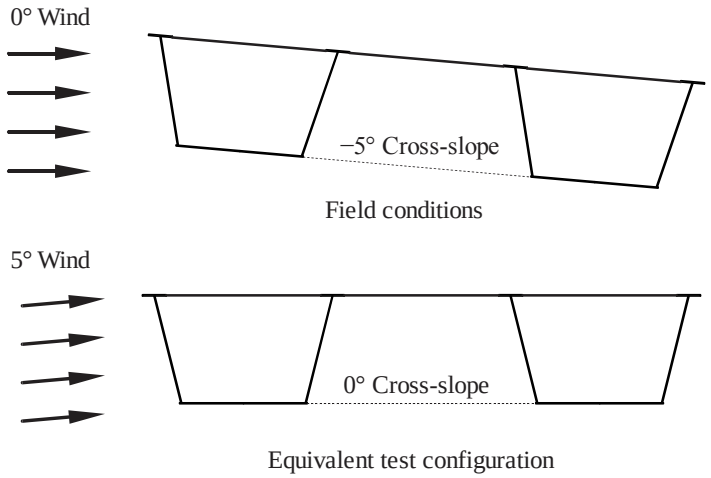

Figure 5-9. Equivalence between wind angle and cross-slope for box girders

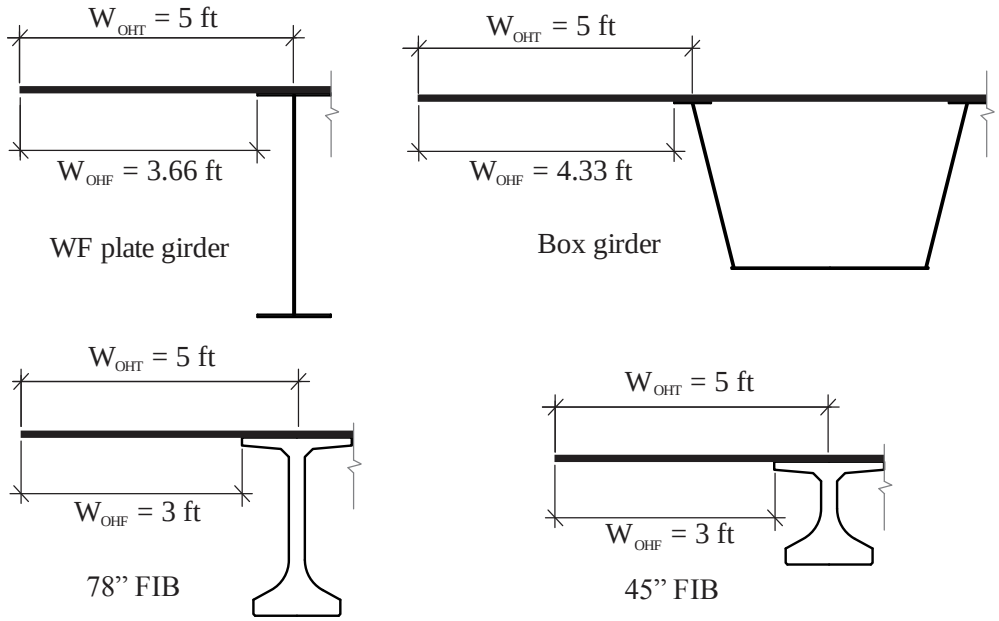

Figure 5-10. Overhang dimensions used in wind tunnel study

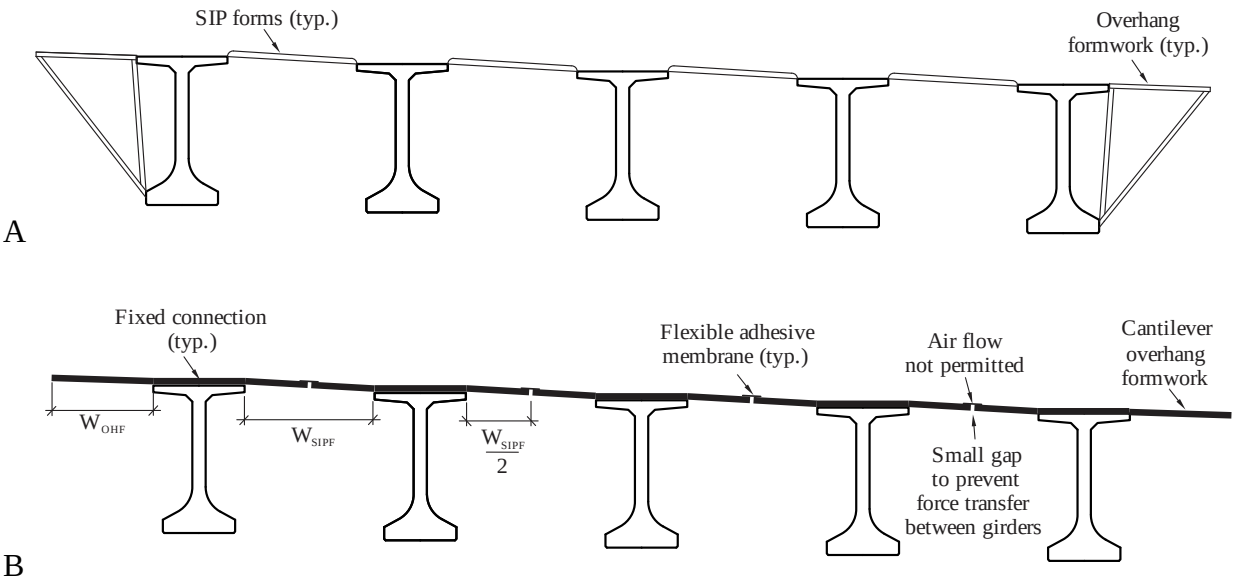

Figure 5-11. Formwork and overhang attachment methodology. A) Typical construction schematic. B) Wind tunnel testing setup.

CHAPTER 6
WIND TUNNEL TESTING RESULTS AND ANALYSIS

6.1 Overview

Wind tunnel tests were performed on the bridge girder test configurations described in Chapter 5. Several groups of laterally spaced girders were tested to quantify shielding effects, identify trends, and evaluate the aerodynamic influence of stay-in-place formwork and overhangs. The complete set of wind tunnel test data, reported using terminology defined in Chapter 5, is available in Appendix C. From analysis of the results, simplified calculation procedures were developed for determining global drag coefficients for I-shaped girder bridges (i.e., FIBs and plate girders) and bridges constructed using box girders.

6.2 Key Findings from the Wind Tunnel Test Program

After processing the wind tunnel data into a form consistent with the terminology defined in Chapter 5—which is also consistent with terminology used in a previous wind tunnel study (BDK75-977-33, Consolazio et al., 2013)—the following key findings and data trends were identified.

6.2.1 Influence of Stay-In-Place Forms and Overhangs on Drag Coefficients

Representative example comparisons of drag coefficients (C_D) for systems consisting *only* of bare girders and drag coefficients for systems consisting of girders with SIP forms and with overhang formwork are presented in Figure 6-1 for wide flange (WF) plate girders, and in Figure 6-2 for FIB78 girders. Data shown in these figures—which represent variations in wind angle, girder type, and bridge width (number of girders)—serve to illustrate the influence that the addition of both SIP forms and overhang formwork had on drag coefficients. (Note: data for FIB45 and box girder sections exhibit similar trends to those illustrated for the WF plate girder and FIB78 sections, but are omitted here for brevity.)

In Figure 6-1, all data presented correspond to a *magnitude* of cross-slope equal to 8%. As noted in Chapter 5, in the present study, only negative cross-slopes were investigated since these conditions produce the most conservative drag coefficients when SIP forms are present. In contrast, in study BDK75-977-33, the cross-slope was a positive value +8%. However, since these earlier tests were conducted without SIP forms or overhang formwork (bare girders only), and because the WF plate girders have doubly symmetric cross-sectional shapes, the results obtained in BDK75-977-33 for +8% also correspond to a cross-slope of -8%. Hence, the C_D data presented in Figure 6-1 from the previous study (at +8%) and the present study (at -8%) are, in fact, comparable.

In general, the data presented in Figure 6-1 and Figure 6-2 indicate that the introduction of SIP forms and overhang formwork does not alter the fundamental C_D trend that was first identified in BDK75-977-33, that is: a large positive C_D value at windward girder position G1; one or more leeward (shielded) girder positions (G2, G3, ...) with *negative* C_D values; and then subsequent increases of C_D values typically producing +C_D values for girders farther downstream. With regard to the windward girder at position G1, introducing SIP forms and overhang formwork *always* produced an increase in the C_D value when corresponding cases—identical in every way except for the presence of SIP forms and overhang formwork—were compared. For leeward (shielded) girder positions, introducing SIP forms and overhang formwork generally produced a slight decrease in the C_D values.

In Figure 6-3 and Figure 6-4, the effects on C_D values produced *only* by adding SIP forms, but *not* overhang formwork, are illustrated. For a majority of the data shown, adding SIP forms has the effect of *reducing* the C_D values for the windward girder (position G1) and for the first shielded leeward girder (position G2); both of these trends will tend to reduce the total

(global) drag force on the bridge cross section. Results for shielded girders farther downwind, however, are mixed.

In Figure 6-5 and Figure 6-6, the effects on C_D values produced by adding overhang formwork to systems that already have SIP forms are illustrated. That is, Figure 6-5 and Figure 6-6 isolate solely the effects of adding overhang formwork. (This is in contrast to Figure 6-1 and Figure 6-2, which illustrated the combined effects of adding *both* SIP forms and overhang formwork). With regard to the windward girder at position G1, introducing overhang formwork *always* produced an increase in the C_D value when matched cases—identical in every way except for the presence of overhang formwork—were compared. In contrast, however, adding overhang formwork had only minor effects on the C_D values for shielded downwind girders.

6.2.2 Lift Coefficients for Girders and Overhangs

When girder lift coefficients (C_L) from the current study, which included SIP forms in all cases, were compared to corresponding lift coefficients from study BDK75-977-33, which included only bare girders, it was found that the addition of SIP forms increased the measured lift coefficients at every girder position measured, and for every condition tested. From this observation, it is clear that the addition of SIP forms altered the flow of wind around the bridge cross-section. Further, when lift coefficients (C_L) for systems with SIP forms *and* overhangs were compared to lift coefficients for systems having only SIP forms (but without overhangs), it was evident that the addition of overhangs further increased the lift coefficients, especially for the windward girder (position G1).

In addition to quantifying lift coefficients for the girders, it was also of interest to quantify lift coefficients for the overhang formwork—i.e., the width of formwork **(**W_{OHF}**)** extending beyond the girder flange tip; recall Figure 5-10. Unfortunately, including direct

measurements of uplift forces on the overhang formwork was not feasible within the scope of the wind tunnel testing program. However, it was possible to *estimate* the overhang formwork lift coefficients ($C_{L,OHF}$) from the wind tunnel data that were measured. For each condition tested (girder type and wind angle), the lift coefficient attributable to the presence of the overhang formwork ($C_{L,OHF}$) was computed as:

$$C_{L,OHF} = C_{L,G1,SIP+OH} - C_{L,G1,SIP} \tag{6-1}$$

where $C_{L,G1,SIP+OH}$ was the lift coefficient measured at the windward girder (position G1) when SIP forms and overhangs were included, and $C_{L,G1,SIP}$ was the lift coefficient measured at the windward girder when SIP forms were included, but overhangs were omitted. Overhang lift coefficients estimated in this manner are summarized in Table 6-1.

Since the overhang formwork lift coefficients ($C_{L,OHF}$) reported in Table 6-1 have been estimated by taking differences of *girder* lift coefficients (C_L), and since the girder lift coefficients reported throughout this study are normalized relative to the girder depth (D), by definition, the overhang formwork lift coefficients are then also normalized by the girder depth (D). Therefore, to compute overhang formwork lift forces from the coefficients reported in Table 6-1, the $C_{L,OHF}$ values must first be *de-normalized* by the girder depth (D) as:

$$F_{L,OHF} = \frac{1}{2}\rho K_Z V^2 G C_{L,OHF} D \tag{6-2}$$

or alternately, and more conveniently, expressed as:

$$F_{L,OHF} = 2.56\times10^{-6} K_Z V^2 G C_{L,OHF} D \tag{6-3}$$

where $F_{L,OHF}$ is the overhang formwork lift force per ft of girder span length, 2.56×10^{-6} represents the quantity $\frac{1}{2}\rho$ in Eqn. (6-2) expressed in units of (ksf)/(mph)^2, V is the basic wind speed (mph), K_Z is the velocity pressure exposure coefficient, G is the gust effect factor, $C_{L,OHF}$ is taken from Table 6-1, and D is the girder depth in ft. It is important to note that since only a single overhang formwork width (W_{OHF}) was tested for each girder type (Table 6-1), the lift forces computed using the coefficients provided in Table 6-1 are specific to widths tested. Additionally, the type of data measured in the wind tunnel test program does not provide insight regarding the form of the lift pressure distributions (e.g., uniform, triangular, nonlinear, etc.) that acted on the overhang formwork during testing.

6.2.3 Torque Coefficients

Representative example comparisons of torque coefficients (C_T) for systems consisting *only* of bare girders, and torque coefficients for systems consisting of girders with SIP forms and with overhang formwork are presented in Figure 6-7 for wide flange (WF) plate girders, and in Figure 6-8 for FIB78 girders. (Sign convention: a positive torque induces a clockwise girder rotation for wind moving from left to right.) The most significant trend exhibited by the data was that the addition of overhang formwork significantly increased the torque on the windward girder (position G1). For the leeward (shielded) girder positions (G2, G3, ...), torque coefficients were considerably smaller than for the windward girder. When moving from bare girders to girders with SIP forms, moderate increases in torque coefficients were produced, but they were not nearly as pronounced as when overhang formwork was added.

6.3 Analysis of Wind Tunnel Testing Results

To quantify the full (global) wind force acting on a bridge system, the total of all girder drag coefficients must be considered. A calculation procedure was therefore developed for determining a *global pressure (drag) coefficient*—defined as the summation of the drag coefficients of all girders in the bridge cross-section. Both I-shaped girder systems (FIBs and plate girders) and box girder systems were considered in the development process.

6.3.1 Calculation of Global Pressure Coefficient for Systems with I-shaped Girders

Current standard practice specified in the *FDOT Structures Design Guidelines* (SDG; FDOT, 2013) involves determining a global pressure coefficient (for a system of multiple girders with SIP forms and possibly overhang formwork), computing an applied pressure using Eqn. (5-9), and then applying that pressure to the projected area of the bridge. This method, referred to as the 'projected area method', assumes a zero degree (horizontal) wind angle. As such, the horizontal wind pressure is applied to the vertical projected depth (D_{proj}, Figure 6-9) of the bridge. The global pressure coefficient used in this process, for bridge girders with SIP formwork in place (referred to as $C_{P,SIPF}$ in this section), is specified in the FDOT SDG as 1.1 (Table 6-2).

Magnitudes of the wind loads on shielded girders are highly dependent on the interaction between the system cross-slope angle ($\theta_{cross\text{-}slope}$) and the wind angle ($\theta_{wind}$). As the absolute difference between those angles increases, a greater portion of the shielded girders are exposed to direct wind flow, resulting in a roughly proportional increase in girder drag force. Consequently, a strong predictor of total (global) wind load on a girder system is the *projected area* of the system (i.e., the total unshielded area). To appropriately capture this trend, global drag coefficients must be a function of the *projected depth* (D_{proj}).

Because the projected depth is a function of θ_{wind}, which fluctuates randomly over time, engineering judgment must be used in selecting a design value of θ_{wind}, such that it represents the maximum expected angle during the exposure period. For conservatism, the sign of θ_{wind} must be chosen to be in opposition to that of $\theta_{cross\text{-}slope}$, so that the maximum angle difference (θ_{max}) is computed as:

$$\theta_{max} = \left|\theta_{wind}\right| + \left|\theta_{cross\text{-}slope}\right| \tag{6-4}$$

θ_{max} can then be used to calculate the *projected depth*, D_{proj}, of the girder system, as:

$$D_{proj} = D + (n-1)(S)(\tan(\theta_{max})) \tag{6-5}$$

where D is the girder depth, n is the number of girders in the system, and S is the girder spacing (Figure 6-10). In this formulation, wind streamlines are assumed to be straight and the shielding effects of girder flanges are ignored as they are not expected to significantly shield leeward girders.

In contrast to the study BDK75-977-33 (Consolazio et al., 2013), the presence of SIP forms in the girder systems influences the controlling wind direction. For bridges with a negative cross-slope configuration, positive wind angles produce larger system level drag coefficients than do negative wind angles. (This is due to the SIP forms shielding downstream girders when the wind angles of attack are more negative than the cross-slope). Consequently, only wind angles that were in opposition to the cross-slope were considered in the cases shown below. For example, in the -8% cross-slope (-4.57 degrees) WF plate girder systems, only -2.5, 0, +2.5, and +5 degree wind angles were included. In the -2% cross-slope (-1.15 degrees) FIB systems, 0, +2.5, and +5 degree wind angles were included.

Furthermore, in addition to SIP forms, the presence of *overhang formwork* was found to marginally increase the total (global) system-level drag forces for I-shaped girders. To account for this increase, the vertical projected depth of the *windward* overhang formwork was included in the projected depth formulation, as:

$$D_{proj} = D + (n\text{-}1)(S)(\tan(\theta_{max})) + W_{OHF}\left(\tan(\theta_{max})\right) \quad (6\text{-}6)$$

where W_{OHF} is the horizontal width of the overhang formwork (recall Figure 5-10). In the remainder of this report, using Eqn. (6-6) to compute the projected depth (instead of the D_{proj} illustrated in Figure 6-9), will be referred to as the '*modified projected area method*'.

Within the scope of the wind tunnel tests, it was not feasible to instrument every girder positions for drag coefficient measurement. For reference, the following data were measured directly during the wind tunnel tests:

- **WF-plate girder (5-girders)**: Fully instrumented for the cases with overhang formwork. Positions G1-G3 were instrumented for cases without overhang formwork.
- **FIB78 (10-girders)**: Positions G1-G3 were instrumented in both the non-overhang and overhang formwork setups. Positions G5 and G10 were instrumented in the systems with overhang formwork.
- **FIB45 (5-girders)**: Positions G1-G2 were instrumented in both the non-overhang and overhang formwork setups. Position G3 was instrumented in the systems with overhang formwork.

The following process was used to estimate drag coefficients at non-measured positions:

- **WF-plate girder**: Girder positions that were measured in overhang formwork cases were used as an estimate for non-instrumented positions in systems without overhang formwork. An example case, at zero degree wind angle, is provided in Figure 6-11 to illustrate this estimation process.
- **FIB78**: Positions G5 and G10 were experimentally measured in the systems with overhang formwork and used as estimates in the non-measured positions in systems without overhang formwork. Other intermediate drag coefficients were linearly interpolated between the range of G3-G5 and G5-G10. An example case, at zero degree wind angle, is provided in Figure 6-12 to illustrate the linear interpolation process.

- **FIB45**: Position G3 was measured in the systems with overhang formwork and was used to estimate the corresponding position for the systems without overhang formwork. The last (most leeward) position in 5-girder FIB45 systems was estimated using the proportionality between the first to the last position (i.e., $C_{D,Last}/C_{D,First}$) experimentally measured in the FIB78 systems. When transitioning from a -5 degree wind angle to a +5 degree wind angle, the ratio of first girder to last girder drag coefficients decreases; that proportionality was reflected in the FIB45 estimations. The following calculation was performed:

$$C_{D,Last,FIB45} = C_{D,First,FIB45}\left(\frac{C_{D,Last,FIB78}}{C_{D,First,FIB78}}\right) \tag{6-7}$$

  where the last position (G5) in a FIB45 system was estimated using the proportionality between the first and last measured drag coefficient in the FIB78 systems. Similar to the FIB78 estimation process, Position G4 was linearly interpolated between G3-G5 (Figure 6-13).

To assess the level of conservatism produced by use of the modified projected area calculation method (using Eqn. (6-6) to compute D_{proj}) for I-shaped girders, a 'conservatism ratio' was defined as the calculated (predicted) lateral wind force divided (normalized) by the summation of girder drag forces measured during the wind tunnel study (or estimated, for non-instrumented girders positions, as described above). Defined in this manner, the conservatism ratio was ≥ 1.0 when the modified projected area method was conservative, and < 1.0 when the method was unconservative.

However for convenience, it was desired to compute the conservatism ratio in terms of pressure (drag) coefficients rather than the total wind forces corresponding to those coefficients. To do so, it was recognized that in the modified projected area method, $C_{P,SIPF}$ is used to compute a pressure that is then applied to the *projected depth* (D_{proj}) of the structure. In contrast, the *girder* drag coefficients reported from wind tunnel testing ($C_{D,\exp}$) are normalized (referenced) to the *girder depth* (*D*), not the *projected* depth (D_{proj}). Therefore, to compute a

proper conservatism ratio based on the ratio of pressure (drag) coefficients (rather than forces), it was necessary to define:

$$\delta = \left(\frac{D_{proj}}{D} \right) \tag{6-8}$$

Using this definition, the conservatism ratio could be properly defined in terms of pressure (drag) coefficients as $\left(\delta C_{P,SIPF}\right) / \left(\sum C_{D,\exp}\right)$. Ratios computed in this manner for all I-shaped girders are presented in Figure 6-14. It is evident in the figure that using a pressure coefficient of $C_{P,SIPF}$ = 1.1 (from Table 6-2) produced *unconservative* results in many cases. Note that in some cases, the systems were tested in *horizontal wind* (zero degree wind angle), meaning that the modified projected area approach used the same assumption as currently recommended by the SDG (Figure 6-9). To ensure that conservative force predictions were obtained (i.e., normalized values greater than 1.0), it was determined—via calibration—that the pressure coefficient for girders with formwork in place ($C_{P,SIPF}$) needed to be revised to 1.4 (see again, Figure 6-14).

The goal of this method was to provide conservative predictions of global pressure coefficients. However, with a design pressure coefficient of 1.4, FIB girder global pressure coefficients are overly-conservative in comparison to WF plate girder systems (Figure 6-14). To produce a more refined prediction of FIB-girder global pressure coefficients, a reduction factor was developed for use in the modified projected area approach. An ideal global C_P reduction factor (β_{ideal}) could be calculated as:

$$\beta_{ideal} = \frac{\Sigma C_{D,\exp}}{\delta C_{P,SIPF}} \tag{6-9}$$

where the sum of experimentally determined girder drag coefficients in a girder system ($C_{D,exp}$) is normalized by the predicted global pressure coefficient. In Figure 6-15, ideal reduction factors

are plotted against maximum angles (absolute differences between the wind angle and cross-slope). To envelope the data, an upper bound linear curve fit was applied:

$$\beta = 1.05 - 0.07(\theta_{max}) \leq 1 \tag{6-10}$$

where β is the reduction factor to be applied in the calculation of FIB girder global pressure coefficients, and θ_{max} has units of degrees. Additionally, since β is a *reduction* factor, it's computed value must be less than 1.0, thus creating a bi-linear curve.

Application of the reduction factor (β) to the prediction of FIB global pressure coefficients produces conservatism levels that are appropriate for design purposes (Figure 6-16) with an average conservatism ratio (across all three girder types: WF plate girder, FIB45 and FIB78) of 1.16. Note that the revised design pressure coefficient $C_{P,SIPF}$ = 1.4 was used in these calculations and wind angles (θ_{wind}) were included when computing the maximum angle difference (θ_{max}).

An alternative calculation procedure for determining global drag coefficients was also developed by implicitly including wind angle in the projected depth calculation. Similar to the currently prescribed method in the FDOT SDG for global drag coefficients, wind load was taken as the pressure of the wind acting horizontally on a vertical projection over the exposed area of the structure. In other words, it was assumed that the maximum difference angle (θ_{max}) is equivalent to the cross-slope angle ($\theta_{cross\text{-}slope}$), and that the wind angle (θ_{wind}) was taken as zero-degrees. Then:

$$\theta_{max} = \left|\theta_{cross\text{-}slope}\right| \tag{6-11}$$

By normalizing predicted global drag coefficients (determined using Eqn. 6-11 to define θ_{max}) by measured global drag coefficients at variable wind angles, the level of conservatism was

evaluated. As evident in Figure 6-17, the level of conservatism produced by this approach was not desirable when a design pressure coefficient $C_{P,SIPF}$ = 1.1 was used.

Therefore, to ensure that conservative force predictions were achieved (i.e., normalized values greater than 1.0, Figure 6-18), it was determined through calibration that the pressure coefficient needed to be $C_{P,SIPF}$ = 1.8 (rather than the values of 1.1 or 1.4 previously noted), if wind angles are not explicitly included in the determination of maximum difference angle θ_{max}.

6.3.2 Calculation of Global Pressure Coefficient for Systems with Box Girders

Currently, the *FDOT Structures Design Guidelines* (SDG, FDOT, 2013) specify that a $C_{P,SIPF}$ = 1.1 be applied to both I-shaped girder and box girder superstructures *when deck forms are in place* (Table 6-3). Similar to the I-shaped girder global pressure coefficient calculation procedure described in the previous section, the accuracy of the projected area method was compared to the experimentally determined global drag coefficients for box girders. Recall from Chapter 5 that box girders were tested in the wind tunnel at 0°, ±5° and ±10° wind angles with the girders aligned with the cross-slope (Figure 6-19). Given the matching alignment of the girders and the cross-slopes, these test configurations were geometrically equivalent to zero-degree (horizontal) wind angles with 0% (0 degree), ±8.7% (±5 degree), and ±17.6% (±10 degree) cross-slopes.

Fully measured global drag coefficients for box girders with SIP forms are plotted as a function of wind angle in Figure 6-20. For I-shaped girders, positive wind angles (that opposed the negative cross-slope) always produced higher global drag forces. In contrast, clearly defined trends were not evident for the box girder data in terms of wind angle (i.e., positive wind angles did not necessarily produce global drag forces that exceed those produced at negative wind

angles). Consequently, *all* box girder cases (positive and negative angles) with SIP forms were included in the development of a global pressure coefficient prediction method.

To develop such a prediction method, projected depths were calculated for each case by considering the entire superstructure. In the I-shaped girder global pressure prediction method described earlier, flange shielding was considered negligible and girders were assumed to behave as flat, vertical plates. In contrast, the equivalent 'full-scale' width of the bottom 'flange' of each box section tested was seven (7) ft across and therefore could not be idealized as a vertical plate. Consequently, the projected depth could not be defined simply in terms of girder spacing (S) and angle. Instead, the projected depth of box girder systems was defined by projecting the entire geometry of the boxes (including bottom flange width) onto a vertical plane (Figure 6-21a). Additionally, when overhang formwork was present in the cross-section (Figure 6-21b), the vertical projection of the *windward* overhang was included in the projected depth [analogously to the $W_{OHF}\left(\tan(\theta_{max})\right)$ term previously noted in Eqn. (6-6)]. The leeward overhang was omitted since it is 'hidden' behind the projected depth of the leeward box.

Using this projection method, and $C_{P,SIPF}$ = 1.1, per Table 6-3, both cases (without and with formwork overhangs) at zero degree maximum difference angles (θ_{max}) were *under-predicted* (Figure 6-22), i.e., unconservative relative to measured wind tunnel data. Additionally, the predicted global drag force was significantly more *unconservative* (greater error) for the box girder bridge with overhang formwork present. This is important since at zero degree wind and 0% cross-slope, the box girder depth (D) and the projected depth (D_{proj}) and equal. Since the global drag force (and pressure coefficient) was larger when overhang formwork was present—despite the fact that the projected depth (D_{proj}) was no different than the girder depth (D)—this

indicated that use of projected depth *alone* was not adequate to predict the global pressure coefficient (as was the case earlier for I-shaped girders).

Instead, the global pressure coefficient for box girder bridges was formulated to account for the presence, and width, of the overhang formwork. It was found that the minimum global pressure coefficients needed to produce conservative results at zero wind angle were $C_{P,SIPF}$ = 1.19 (SIP forms only) and $C_{P,SIPF}$ =1.48 (SIP forms and overhang formwork). For convenience in design, these values were rounded to $C_{P,SIPF}$ = 1.2 and $C_{P,SIPF}$ = 1.5, respectively. In the wind tunnel test program, it was only feasible to conduct tests at a single overhang formwork width: W_{OHF} =4.33 ft (recall Figure 5-10 and Table 6-1) Therefore, to account for intermediate overhang widths that are likely to be encountered in practice, the pressure coefficient for box girder bridges with SIP forms and overhang formwork was defined using linear interpolation as:

$$C_{P,SIPF} = 1.2 + 0.3\left(\frac{W_{OHF}}{4.33\text{ ft}}\right) \tag{6-12}$$

where W_{OHF} is defined in units of ft. Using the box girder $C_{P,SIPF}$ together with projected depth (D_{proj}), to account for wind angles other than zero degrees, the normalized predicted global pressure coefficients were computed for all conditions tested in the wind tunnel (Figure 6-23) and were found to be conservative (greater than 1.0).

However, for large wind angles, the degree of conservatism was greater than desirable, therefore, a reduction factor (β) was developed in a manner similar to that previously developed for FIB systems. As before, an ideal reduction factor (β_{ideal}) for each test case was determined using Eqn. (6-9), where $C_{P,SIPF}$ was computed from Eqn. (6-12) and D_{proj} as defined in Figure 6-21. In Figure 6-24, the ideal reduction factors are plotted as a function of maximum

difference angle (i.e., absolute value of the difference between the wind angle and cross-slope). To envelope the data, an upper bound linear curve fit was applied:

$$\beta = 1.0 - 0.02(\theta_{max}) \tag{6-13}$$

where θ_{max} is defined in Eqn. (6-4) and has units of degrees, and β is the reduction factor for calculation of box girder global pressure coefficients. Use of the reduction factor (β) produced conservatism levels that are deemed appropriate for design purposes (Figure 6-25).

6.3.3 Recommended Procedure for Calculation of Wind Loads

Using the pressure coefficients for I-shaped girders and box girders that were developed above, an overall procedure for computing lateral wind loads was developed:

1. Establish wind angle θ_{wind}. Establish the angle of wind (θ_{wind}) that will be considered. If wind will be assumed to be horizontal, then set θ_{wind} = 0. Compute the maximum 'angle of difference' between the wind angle and the bridge cross-slope:

$$\theta_{max} = \left|\theta_{wind}\right| + \left|\theta_{cross-slope}\right| \tag{6-14}$$

2. Determine pressure coefficient $C_{P,SIPF}$: For a partially constructed bridge consisting of multiple girders with SIP forms (and possibly overhang formwork), determine the pressure coefficient $C_{P,SIPF}$ from Table 6-4. For box girder bridges, the calculation of $C_{P,SIPF}$ involves the use of the overhang formwork width W_{OHF} (in units of ft.) which is defined in Figure 5-10.

3. Determine the pressure coefficient C_P: Compute the pressure coefficient C_P as:

$$C_P = \beta C_{P,SIPF} \tag{6-15}$$

where β is a reduction factor that takes into account the effects of wind angle:

$$\beta = \begin{Bmatrix} 1.0 & Plate\ girders \\ 1.05 - 0.07(\theta_{max}) \le 1.0 & FIB\ girders \\ 1.00 - 0.02(\theta_{max}) & Box\ girders \end{Bmatrix} \tag{6-16}$$

where θ_{max} has units of degrees.

4. Compute the design wind pressure P_Z. Per current FDOT practice, compute the design wind pressure P_Z using Eqn. (5-9), repeated here for convenience:

$$P_Z = 2.56\times10^{-6} K_Z V^2 G C_P \tag{6-17}$$

where P_Z is the design wind pressure (ksf), K_Z is the velocity pressure exposure coefficient, V is the basic wind speed (mph), G is the gust effect factor, and the constant term 2.56×10^{-6} is in units of (ksf)/(mph)^2. [For additional details, see the *FDOT Structures Design Guidelines* (FDOT, 2013)].

5. Apply the design wind pressure over the projected area of the structure. To compute the projected area for box girder bridges, the projected depth (D_{proj}) should be determined as indicated in Figure 6-21. To compute the projected area for I-shaped girders, the following definition of projected depth (D_{proj}) should be used:

$$D_{proj} = D + (n\text{-}1)(S)(\tan(\theta_{max})) + W_{OHF}\left(\tan(\theta_{max})\right) \tag{6-18}$$

where D is the girder depth, n is the number of girders, S is the girder spacing, $\theta_{max} = \left|\theta_{wind}\right| + \left|\theta_{cross-slope}\right|$, and W_{OHF} is the overhang formwork width (in units of ft.) as defined in Figure 5-10.

6.3.4 Alternate Procedure for Calculation of Wind Loads for I-shaped Girders

For bridges constructed from I-shaped girders, the following alternate procedure for computing lateral wind loads implicitly accounts for the effects of variable wind angles (but without the need for explicitly quantifying θ_{wind}).

1. Establish θ_{max}. Set the maximum 'angle of difference' to the bridge cross-slope: $\theta_{max} = \left|\theta_{cross-slope}\right|$.

2. Determine pressure coefficient $C_{P,SIPF}$. For a partially constructed bridge consisting of multiple I-shaped girders with SIP forms (and possibly overhang formwork), determine the pressure coefficient $C_{P,SIPF}$ from Table 6-5.

3. Determine the pressure coefficient C_P. Set the pressure coefficient:

$$C_P = C_{P,SIPF} \tag{6-19}$$

4. Compute the design wind pressure P_Z. Per current FDOT practice, compute the design wind pressure P_Z using Eqn. (5-9), repeated here for convenience:

$$P_Z = 2.56\times10^{-6} K_Z V^2 G C_P \quad (6\text{-}20)$$

where P_Z is the design wind pressure (ksf), K_Z is the velocity pressure exposure coefficient, V is the basic wind speed (mph), G is the gust effect factor, and the constant term 2.56×10^{-6} is in units of (ksf)/(mph)^2. [For additional details, see the *FDOT Structures Design Guidelines* (FDOT, 2013)].

5. Apply the design wind pressure over the projected area of the structure. To compute the projected area, use the following definition of projected depth (D_{proj}):

$$D_{proj} = D + (n\text{-}1)(S)(\tan(\theta_{max})) + W_{OHF}\left(\tan(\theta_{max})\right) \quad (6\text{-}21)$$

where D is the girder depth, n is the number of girders, S is the girder spacing, $\theta_{max} = \left|\theta_{cross-slope}\right|$, and W_{OHF} is the overhang formwork width (in units of ft.) as defined in Figure 5-10.

6.4 Assessment of Brace Forces due to Wind Loads

In the previous section, a methodology was developed for computing the *global* pressure (drag) coefficient and associated global wind load on a multiple-girder bridge cross-section with SIP forms (and possibly overhang formwork) in place. Such wind loads will typically be used in a *global* strength limit state evaluation for the determination of wind load reactions on the substructure. However, applied wind loads will also induce forces in the individual brace components (diagonals and horizontal elements) and, as such, have the potential to affect the brace design process. It was therefore important to determine how the magnitudes of brace forces caused by wind loads compared to those caused by construction gravity loads (e.g., eccentric construction loads, etc.). If wind-load-induced brace forces were consistently smaller in magnitude than construction-load-induced brace forces, then there would be no need to formulate wind pressure coefficients specifically for use in designing the bracing elements when SIP forms are present.

To carry out this assessment, structural analysis models of bracing systems were created for purposes of analyzing brace forces due to wind loads. Two-dimensional (2-D) bracing

models were analyzed by adapting the modeling methodology previously developed in BDK75-977-33 (see Section 5.6 of Consolazio et al., 2013). In the most-windward bracing panel (i.e., between girders G1 and G2), the largest differences between the G1 and G2 drag coefficients (C_D) were observed. Since such conditions produce the most severe wind-induced brace forces, only braces forces in this panel were compared to forces induced by construction loads.

As previously noted (e.g., in Section 6.2.3), wind tunnel testing revealed that the addition of overhang formwork significantly increased the wind-induced magnitude of torque on the windward girder (G1). However, for *every* wind angle tested, the direction of wind-induced torque (related to C_T) on the overhang was found to be in *opposition* to the torque (i.e., moment) produced on the overhang by the downward acting gravity (self-weight) of the overhang formwork (denoted M_{OHF}). Hence, for all feasible scenarios, the effect of including wind-induced overhang torque would be to *reduce* (i.e., offset) the effect that moment M_{OHF} would have on the development of brace forces. Consequently, for simplicity and conservatism, the worst case loading condition for brace force assessment was taken as the moment M_{OHF} acting without any reduction attributable to wind-induced torque. That is, wind-induced torque was conservatively omitted. [Note that because the bottom of each overhang bracket bears against (makes contact with) the bottom flange of the exterior girder (recall Section 3.4), but is *not* structurally connected to the girder, it is *not* possible for wind-induced torque to exceed M_{OHF} and cause a net increase in torque (and associated brace force). Instead, the maximum effect that wind-induced torque can achieve is to fully cancel out M_{OHF}.] Consequently, in the simplified 2-D models used to assess 'wind-related' brace forces, the maximum differences in wind-tunnel measured drag coefficients (C_D) for G1 and G2 were converted into an equivalent maximum

horizontal-wind force, which was simultaneously applied to the model in conjunction with the maximum gravity-induced overhang moment M_{OHF}.

To be particularly conservative in including the effects of M_{OHF} on brace forces, the overhang formwork dead load (causing M_{OHF}) was assumed to be 20 psf (rather than the 10 psf value noted earlier in Table 3-1), and only worst-case geometric configurations were considered. Maximum feasible braced lengths were chosen for 45" FIB and 78" FIB analysis models based on an 'end-span only' bracing configuration. Consequently, wind pressures were converted into wind loads (drag forces)—for application to the structural analysis models—by multiplying them by a tributary length equal to one-half the maximum feasible girder span length. Additionally, a conservative estimate of maximum 'construction inactive' wind speed was assumed. The FDOT SDG (FDOT, 2013) allows a reduction factor (R_e) of 0.6 to be applied for structures with an exposure period of less than one year. By selecting the maximum 'construction inactive' wind speed in Florida (150 mph), and applying the reduction factor, a construction design wind speed of 90 mph was obtained and used in all analyses.

Maximum brace forces produced by the combined application of wind-induced drag force and maximum feasible overhang moment (M_{OHF}) were found to be *smaller than* the maximum brace forces caused by the application of the full set of construction loads listed in Table 3-1. That is, construction loads—*not* wind loads—were found to produce brace forces that would control the brace design process. Therefore, pressure coefficients for use specifically in determining wind-induced brace forces were not developed in this study. Instead, it is recommended that construction loads be considered the controlling load case for the design of construction-stage girder bracing when SIP formwork is in place.

Table 6-1. Estimated lift coefficients ($C_{L,OHF}$) attributable to overhang formwork

Girder	Min. $C_{L,OHF}$ across all wind angles	Max. $C_{L,OHF}$ across all wind angles	$C_{L,OHF}$ at zero-degree wind angle	Width of overhang formwork (W_{OHF}) (see Figure 5-10)
WF plate	1.32	1.51	1.51	3.66 ft
78″ FIB	0.48	1.43	1.38	3.00 ft
45″ FIB	0.12	1.80	1.68	3.00 ft
Box	0.15	1.55	1.55	4.33 ft

Table 6-2. Pressure coefficient during construction for I-shaped girders (FDOT SDG)

Construction Condition	Pressure Coefficient
Deck forms not in place	$C_P = 2.2$
Stay-in-place (SIP) deck forms in place	$C_{P,SIPF} = 1.1$

Table 6-3. Pressure coefficient during construction for Box girders (FDOT SDG)

Construction Condition	Pressure Coefficient
Deck forms not in place	$C_P = 1.5$
Stay-in-place (SIP) deck forms in place	$C_{P,SIPF} = 1.1$

Table 6-4. Recommended pressure coefficient for bridges during construction

Component type	Pressure Coefficient
I-shaped girders with SIP formwork	$C_{P,SIPF} = 1.4$
Box girders with SIP formwork	$C_{P,SIPF} = 1.2 + 0.3\left(\frac{W_{OHF}}{4.33\text{ ft}}\right)$

Table 6-5. Alternate pressure coefficient for bridges during construction

Component type	Pressure Coefficient
I-shaped girders with SIP formwork	$C_{P,SIPF} = 1.8$

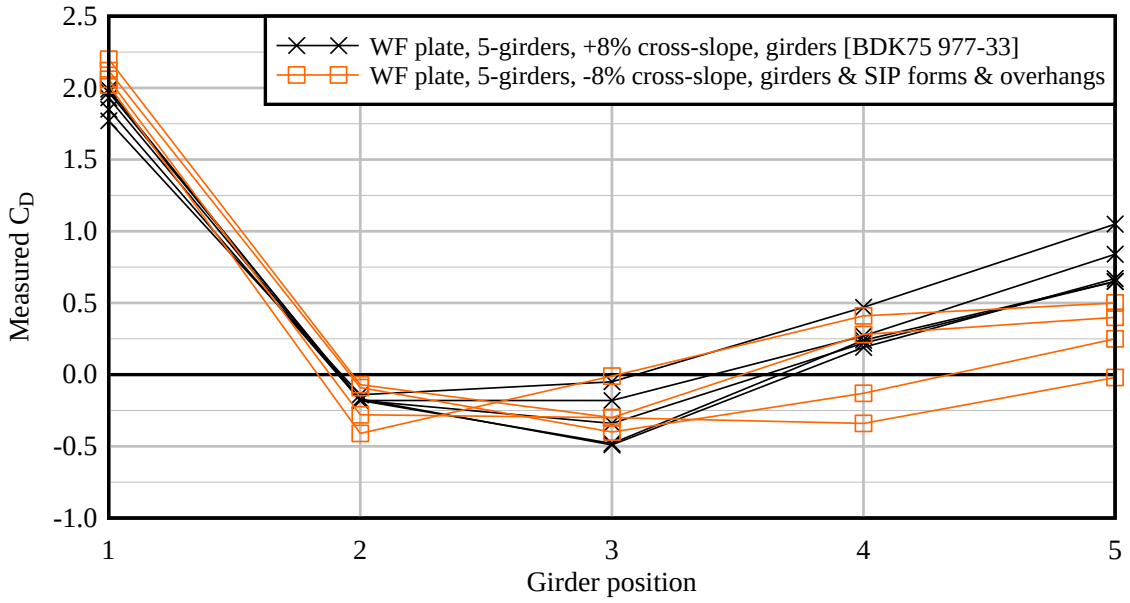

Figure 6-1. Influence on plate girder C_D values from addition of SIP forms and overhangs (All tested wind angles shown)

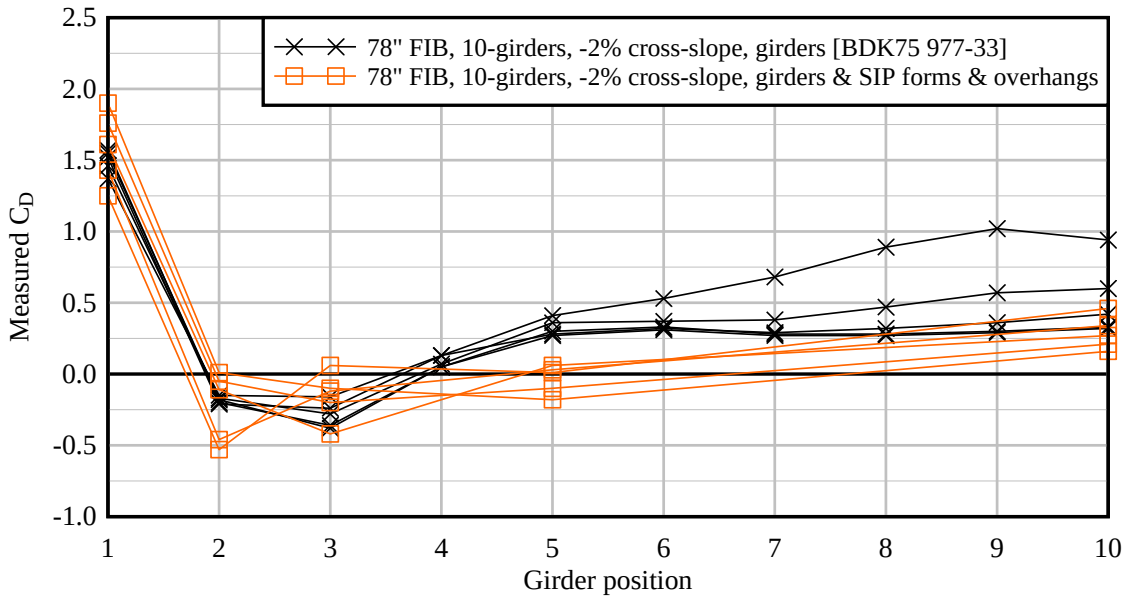

Figure 6-2. Influence on FIB78 C_D values from addition of SIP forms and overhangs (All tested wind angles shown)

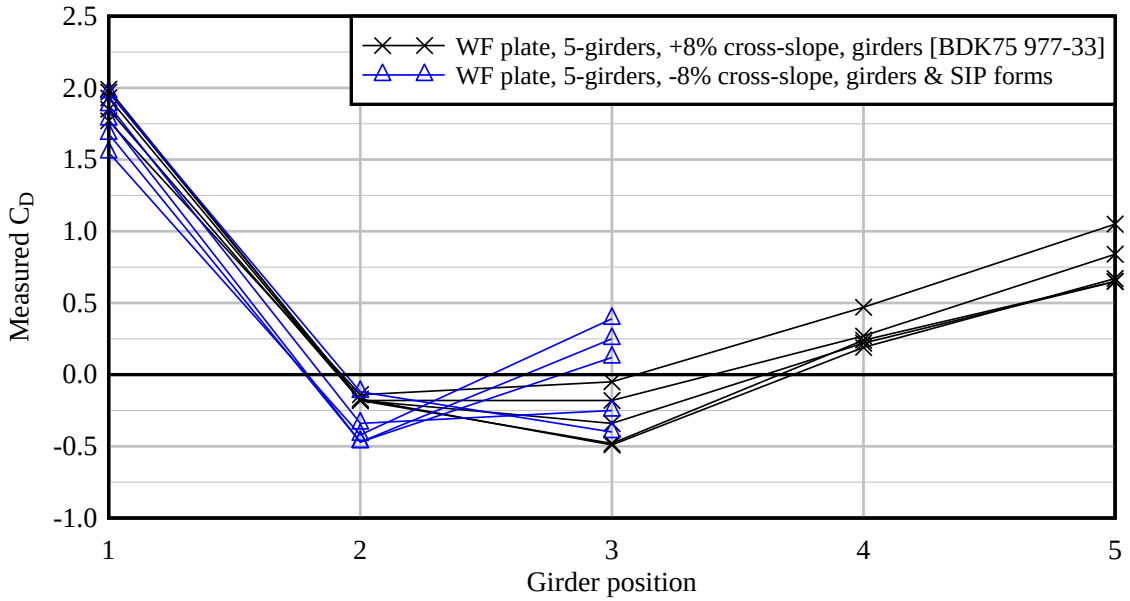

Figure 6-3. Influence on plate girder C_D values from addition of SIP forms (All tested wind angles shown)

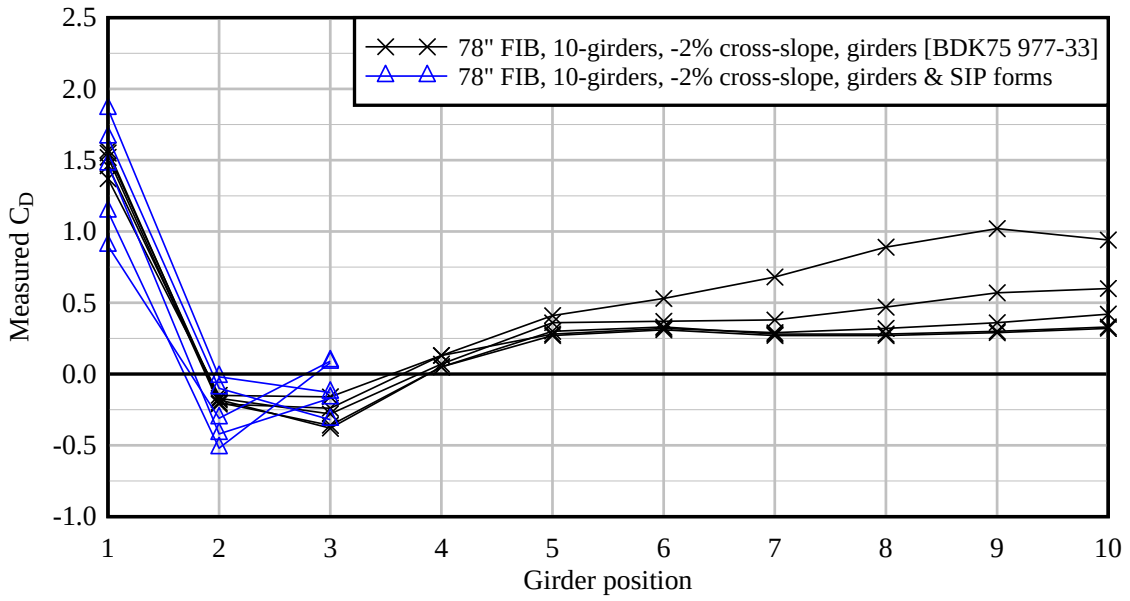

Figure 6-4. Influence on FIB78 C_D values from addition of SIP forms (All tested wind angles shown)

Figure 6-5. Influence on plate girder C_D values from addition of overhangs (All tested wind angles shown)

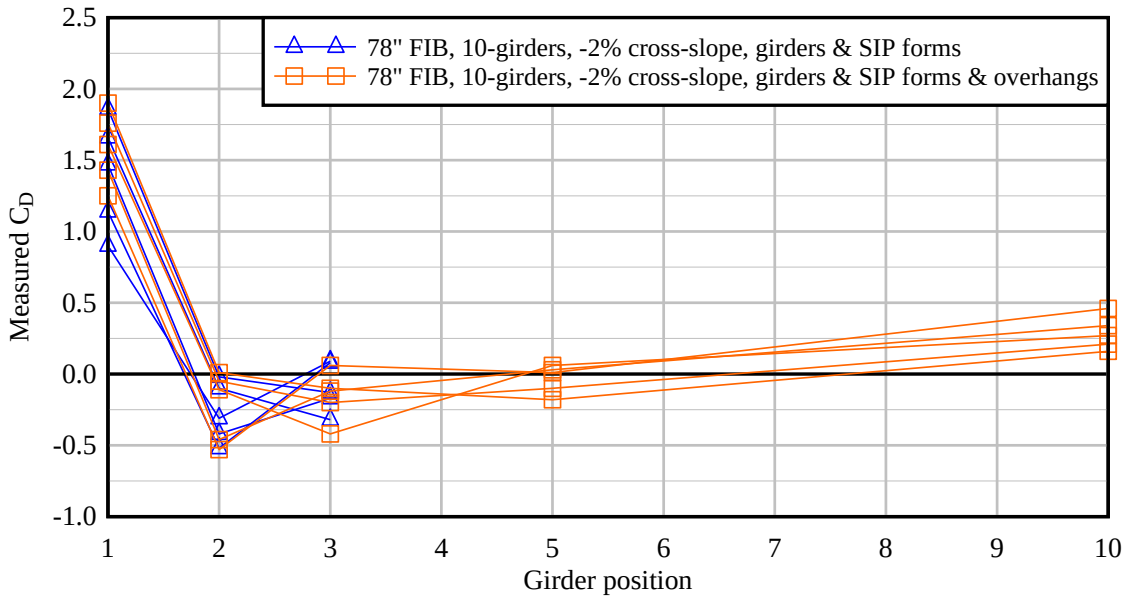

Figure 6-6. Influence on FIB78 C_D values from addition of overhangs (All tested wind angles shown)

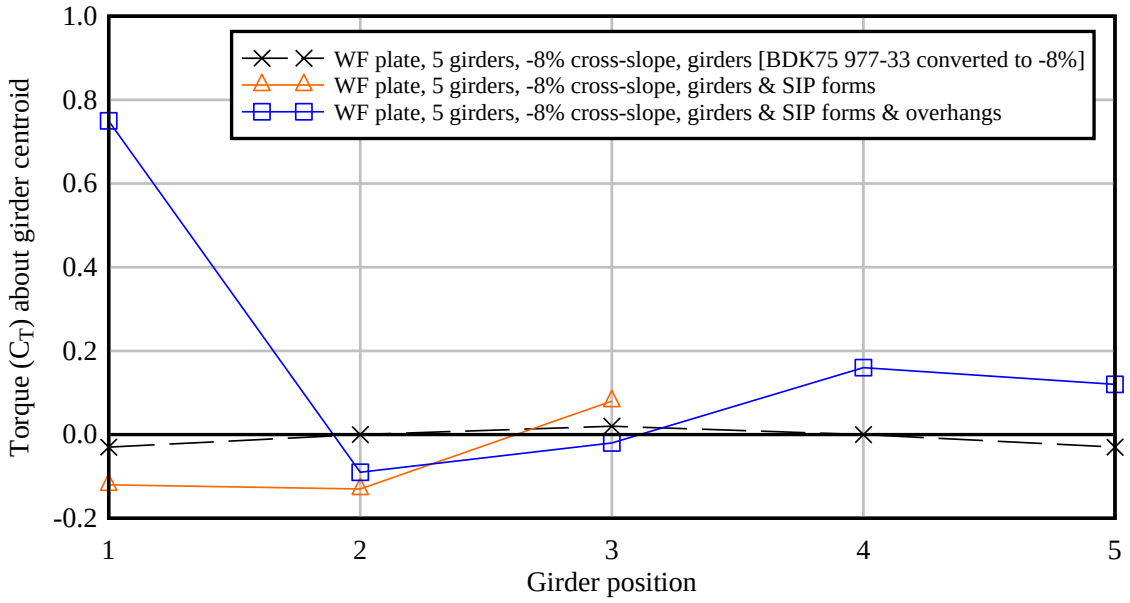

Figure 6-7. Comparison of WF plate girder torque coefficients (All data are for zero degree wind angle)

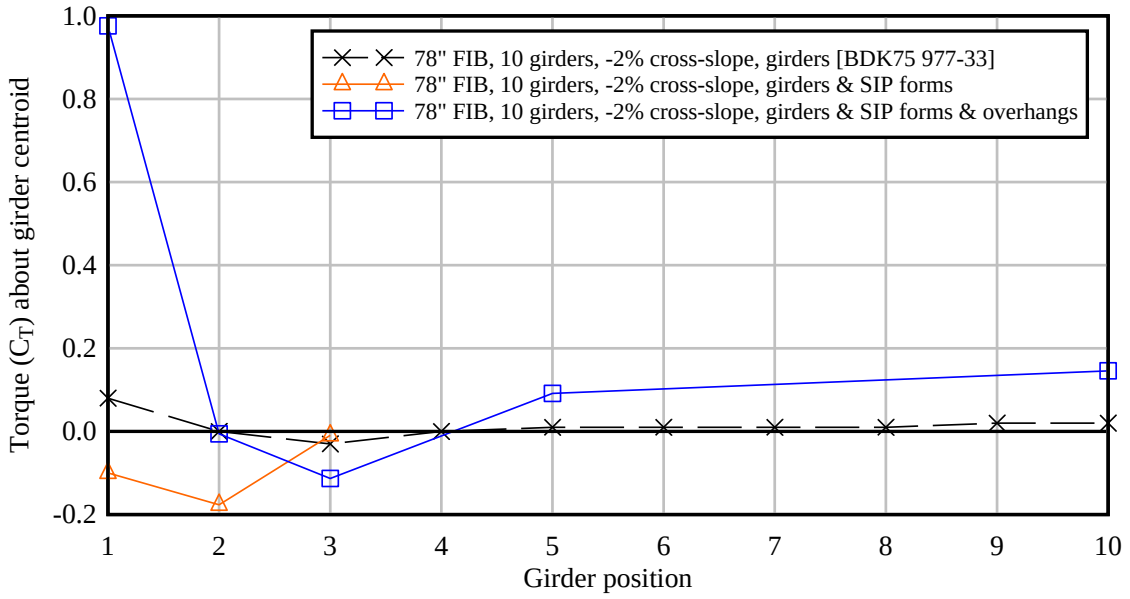

Figure 6-8. Comparison of FIB78 girder torque coefficients (All data are for zero degree wind angle)

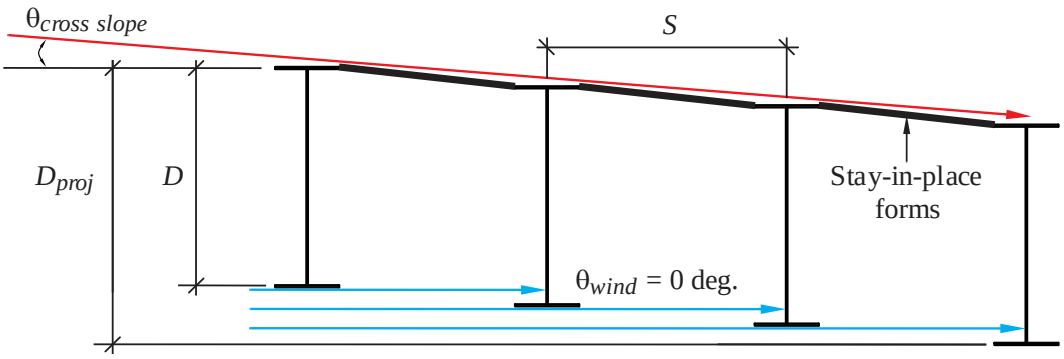

Figure 6-9. Projected area method

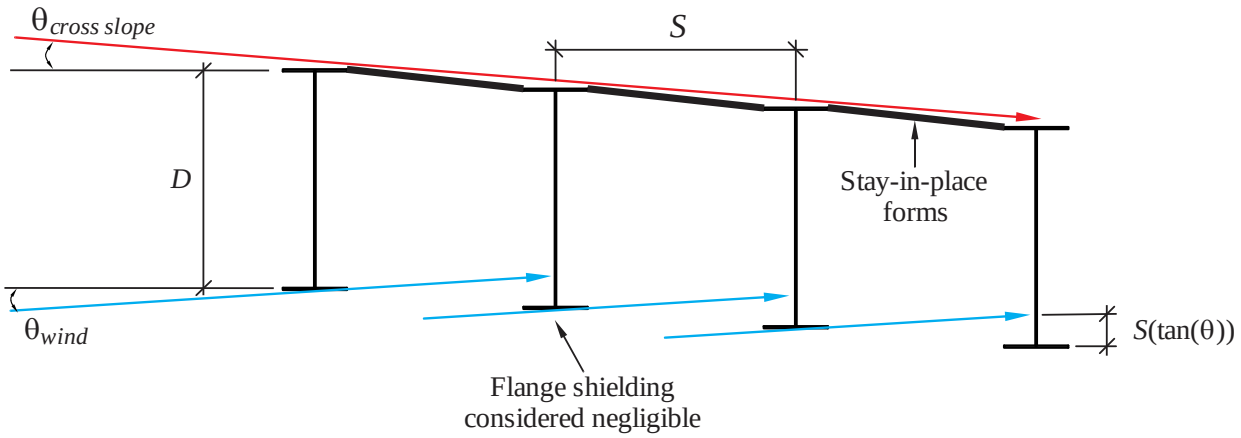

Figure 6-10. Modified projected area method

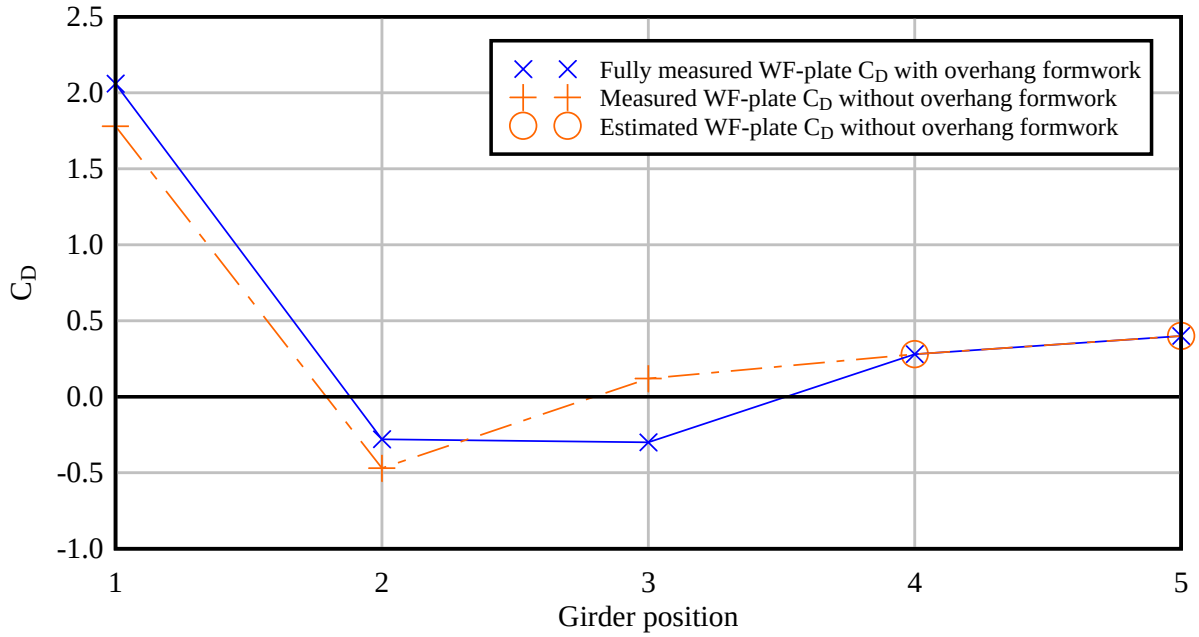

Figure 6-11. Drag coefficients for wide-flange plate girder systems (zero degree wind angle)

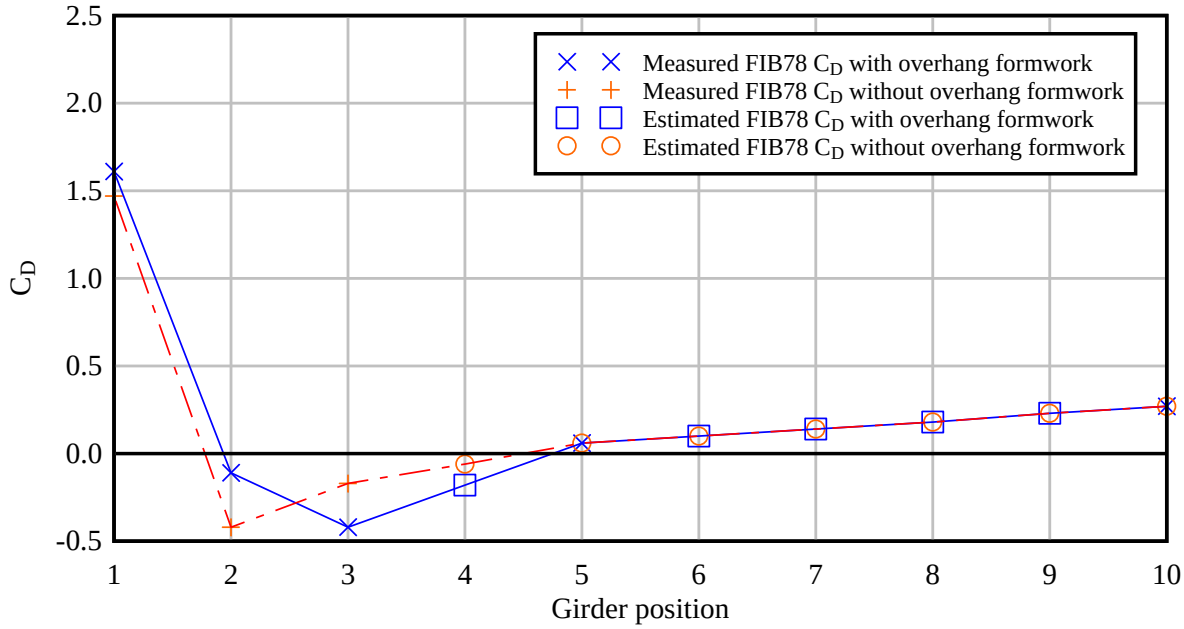

Figure 6-12. Drag coefficients for FIB78 systems (zero degree wind angle)

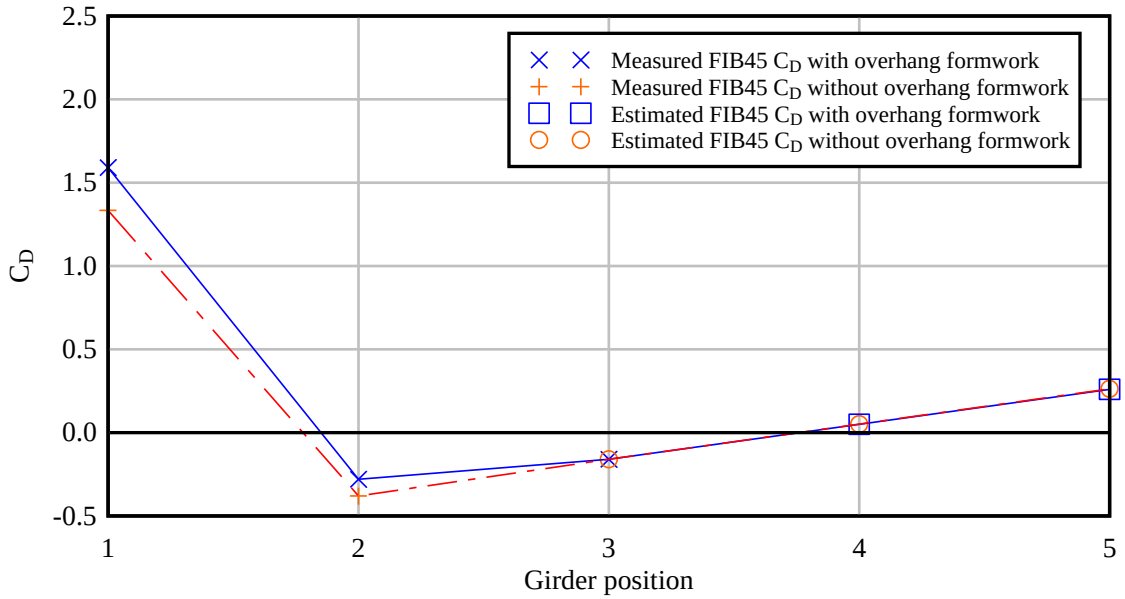

Figure 6-13. Drag coefficients for FIB45 systems (zero degree wind angle)

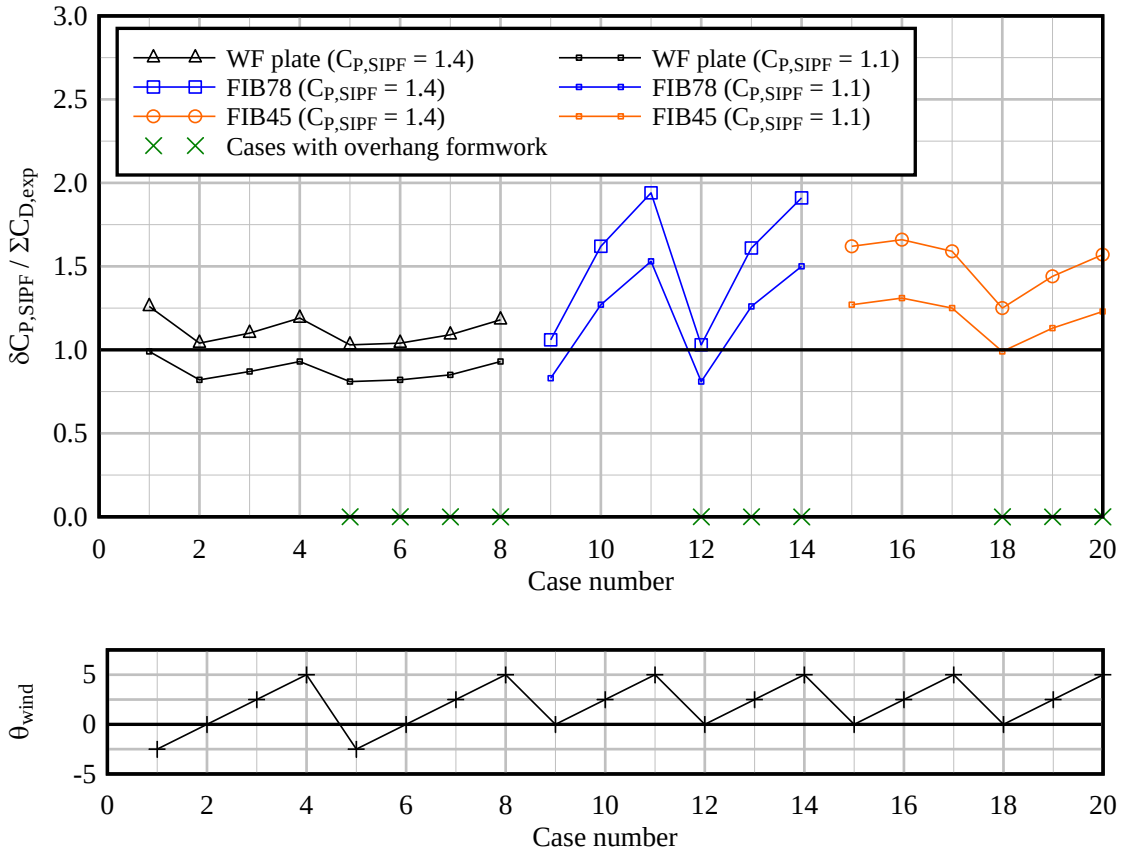

Figure 6-14. Conservatism of modified projected area calculation procedure for I-shaped girders

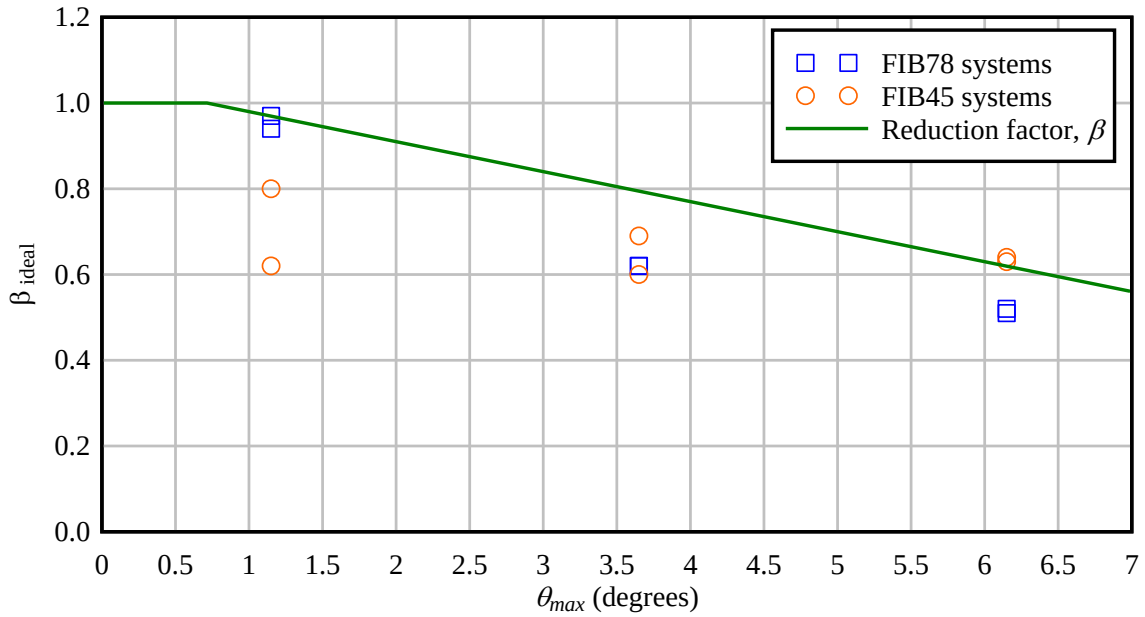

Figure 6-15. Upper bound formulation of reduction factor (β) for FIB systems

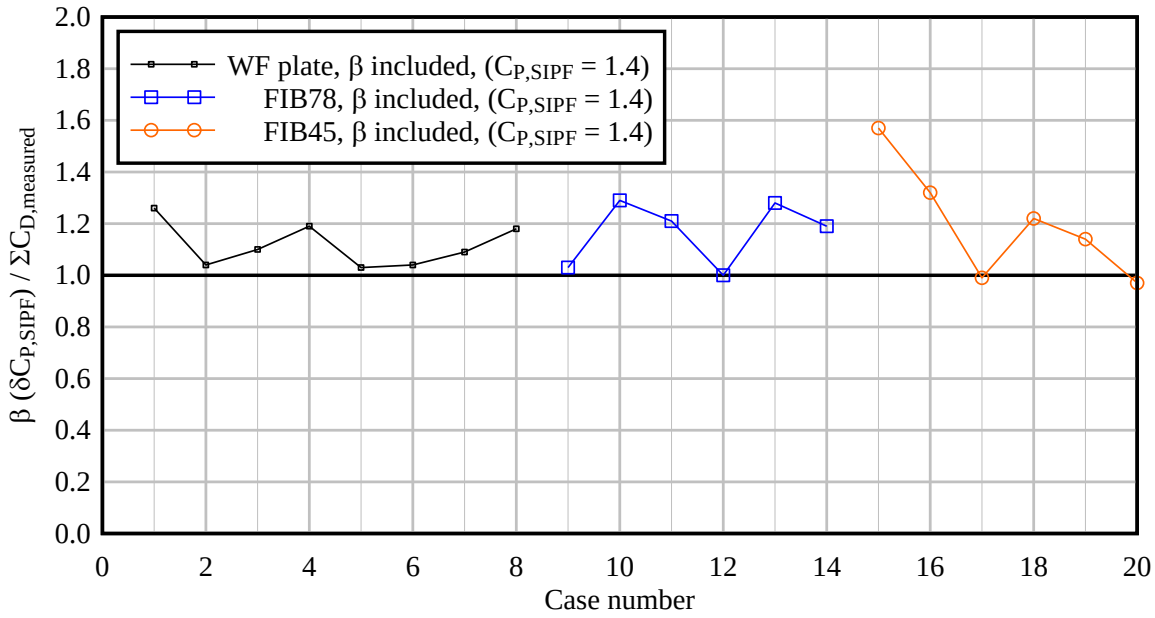

Figure 6-16. Conservatism of modified projected area calculation procedure for I-shaped girders (Reduction factor β applied to FIB systems)

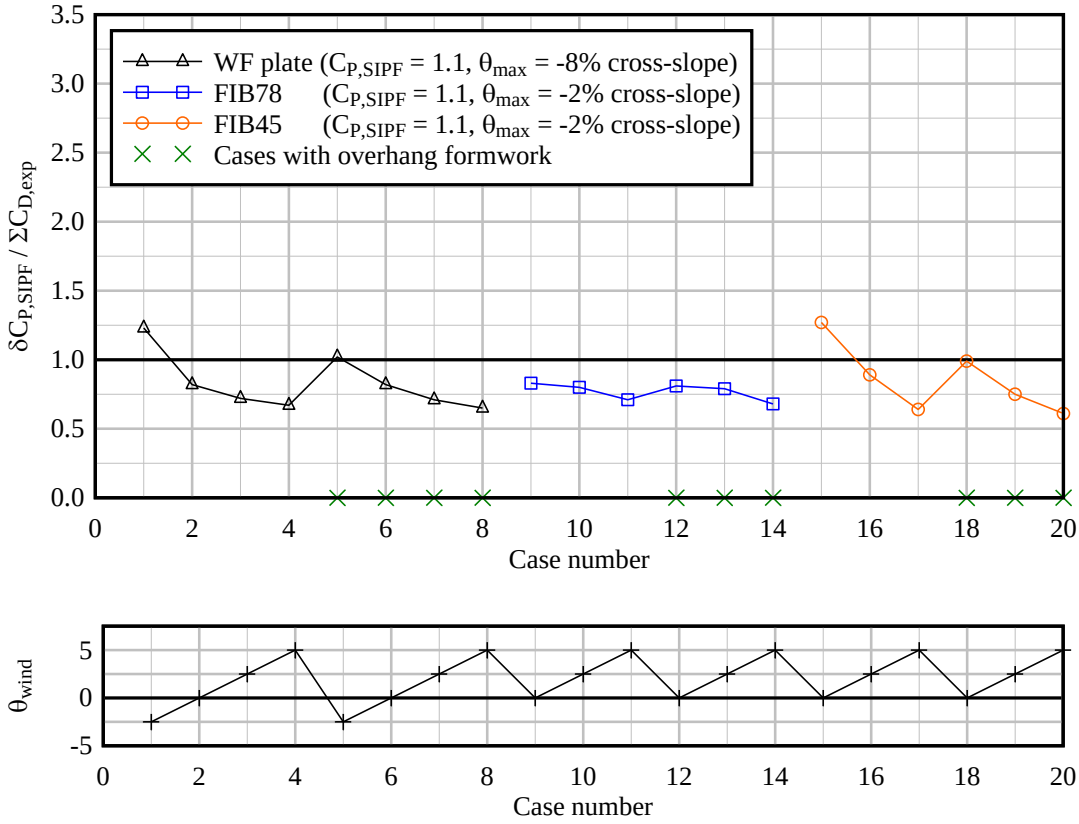

Figure 6-17. Conservatism of alternative projected area calculation procedure for I-shaped girders

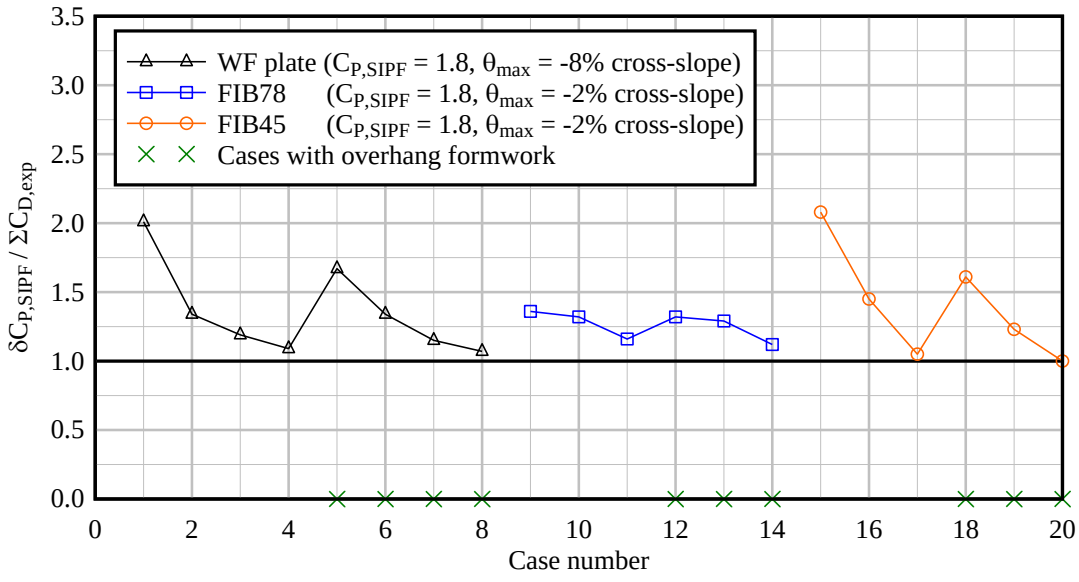

Figure 6-18. Conservatism of alternative projected area calculation procedure for I-shaped girders ($C_{P,SIPF}$ = 1.8 and wind angle not included in calculation of maximum difference angle; i.e., θ_{max}= ($\theta_{cross\text{-}slope}$))

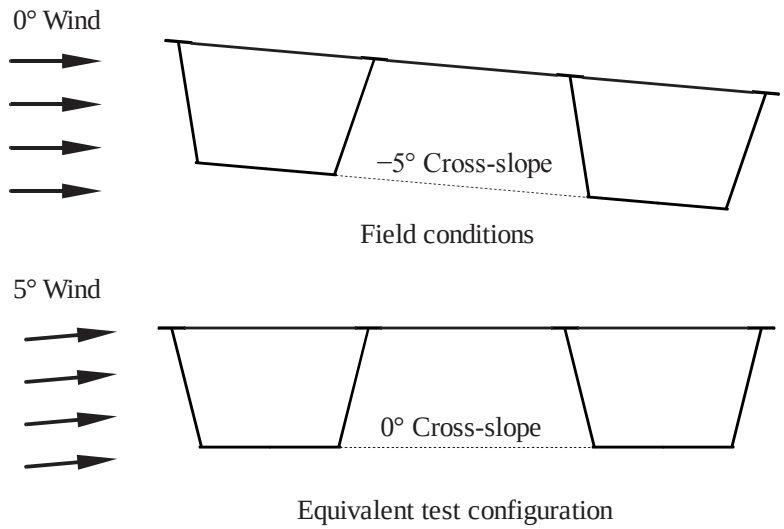

Figure 6-19. Equivalence of box girder cross-slope and wind angle

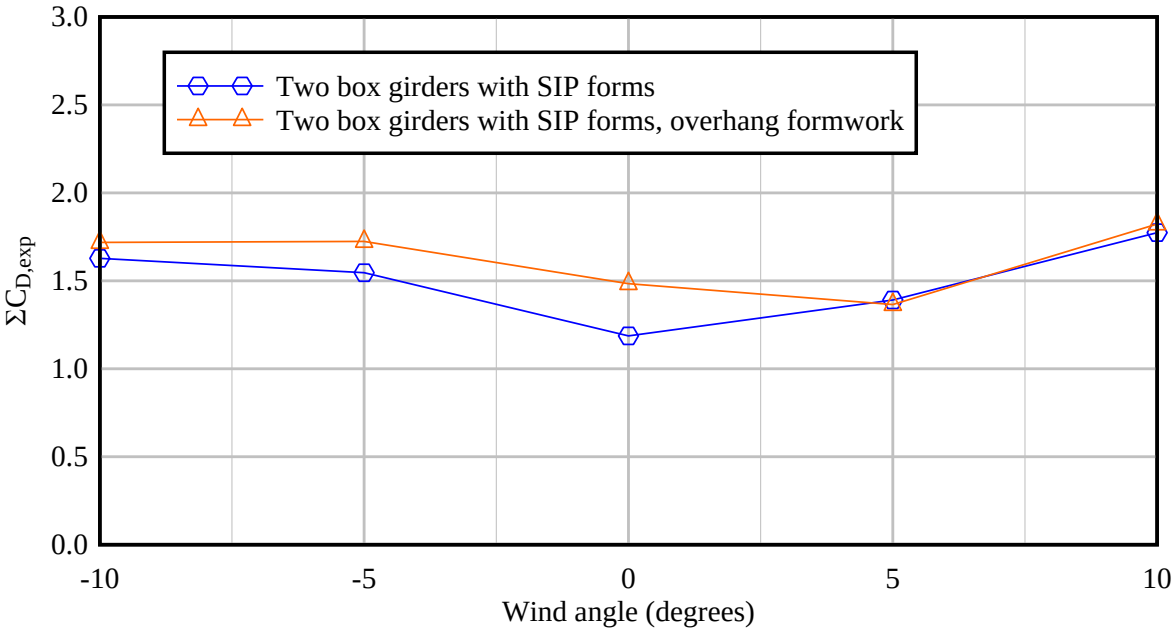

Figure 6-20. Measured global pressure coefficients for box girders

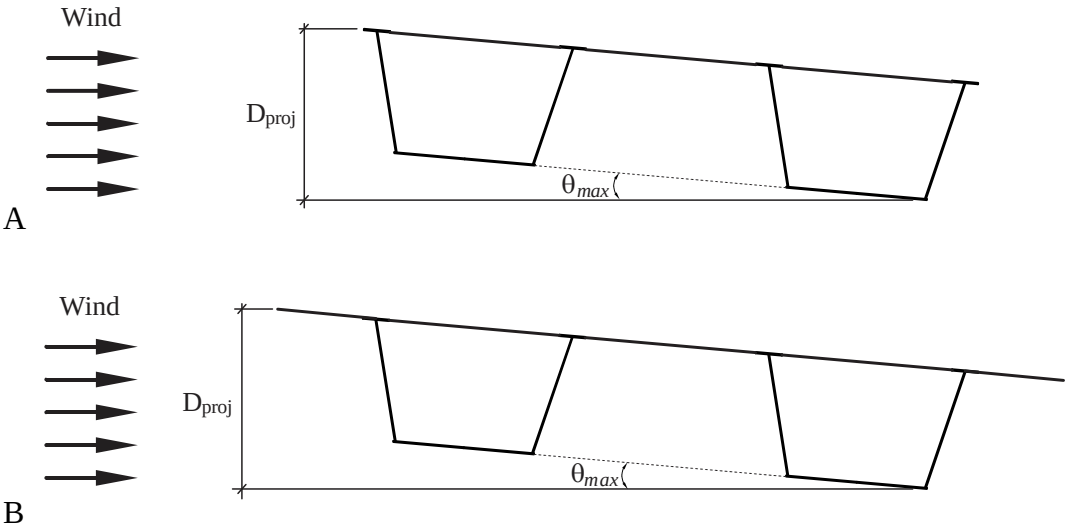

Figure 6-21. Determination of projected depth for box girder bridges. A) without overhang formwork. B) with overhang formwork.

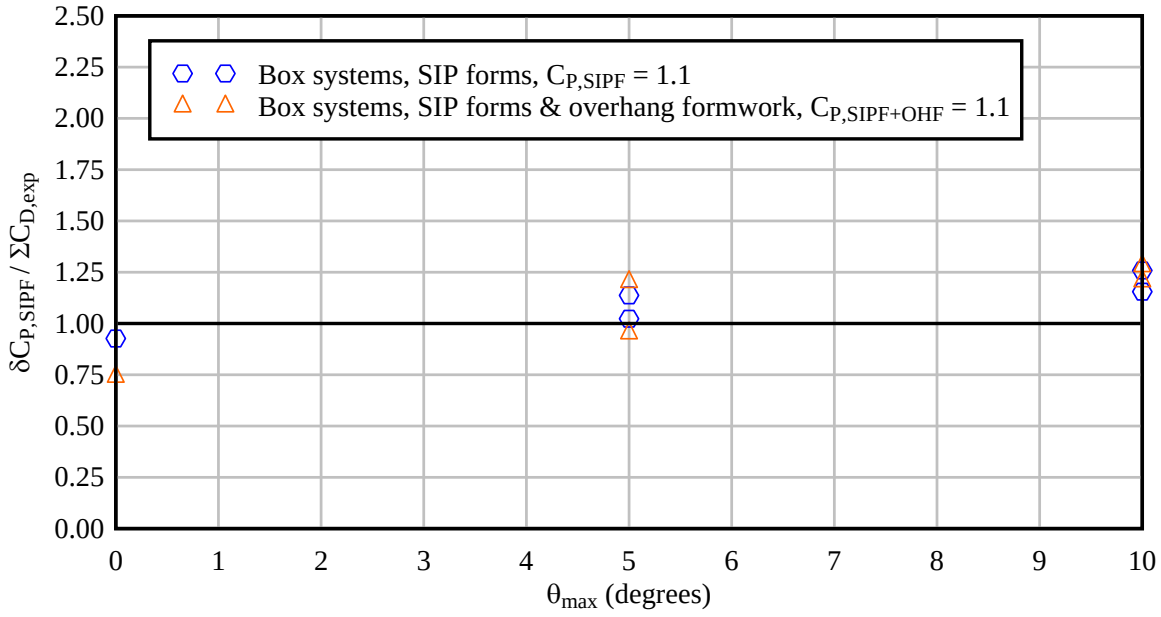

Figure 6-22. Conservatism of projected area calculation procedure for box girders (Using current FDOT $C_{P,SIPF}$ = 1.1 and $C_{P,SIPF+OHF}$= 1.1)

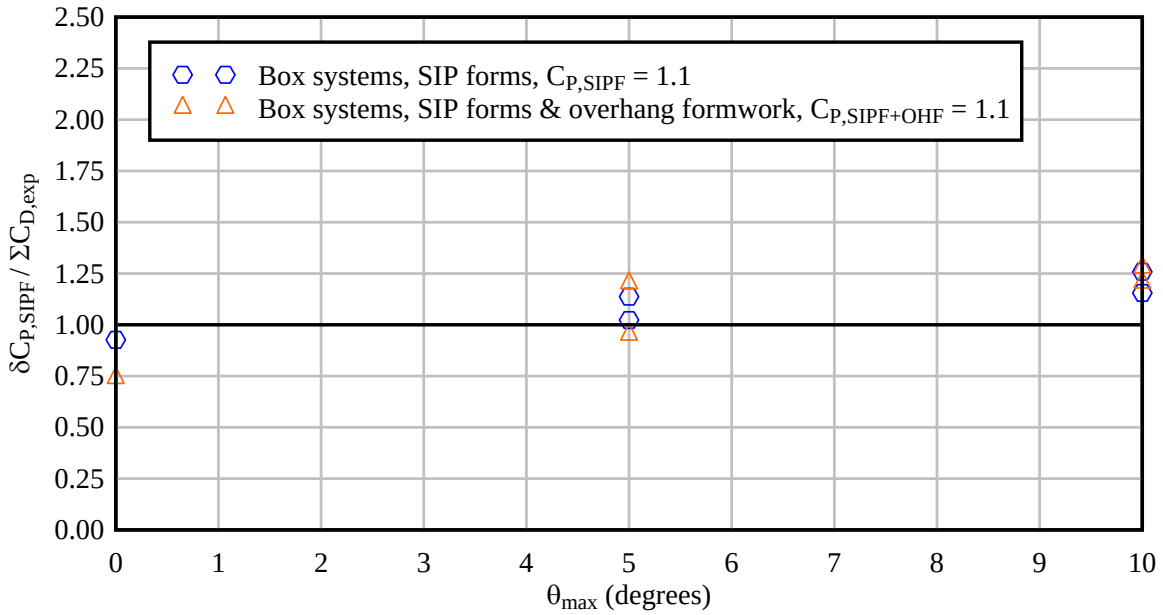

Figure 6-23. Conservatism of projected area calculation procedure for box girders (Using proposed $C_{P,SIPF}$ = 1.2 and $C_{P,SIPF+OHF}$= 1.5)

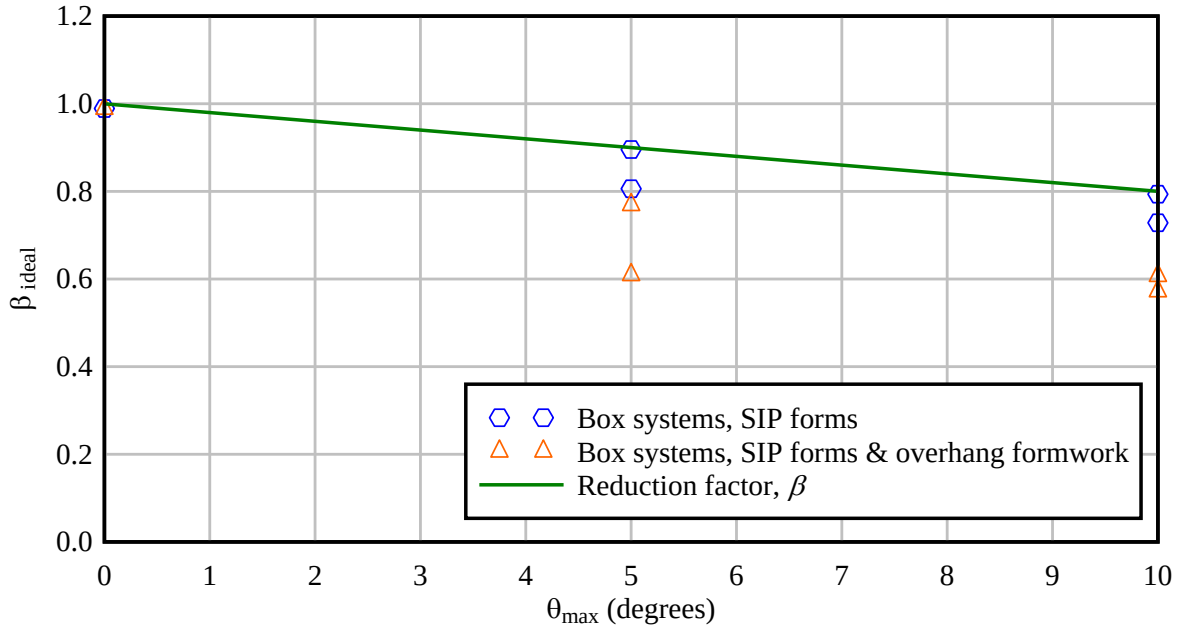

Figure 6-24. Upper bound formulation of a reduction factor (β) for box girders

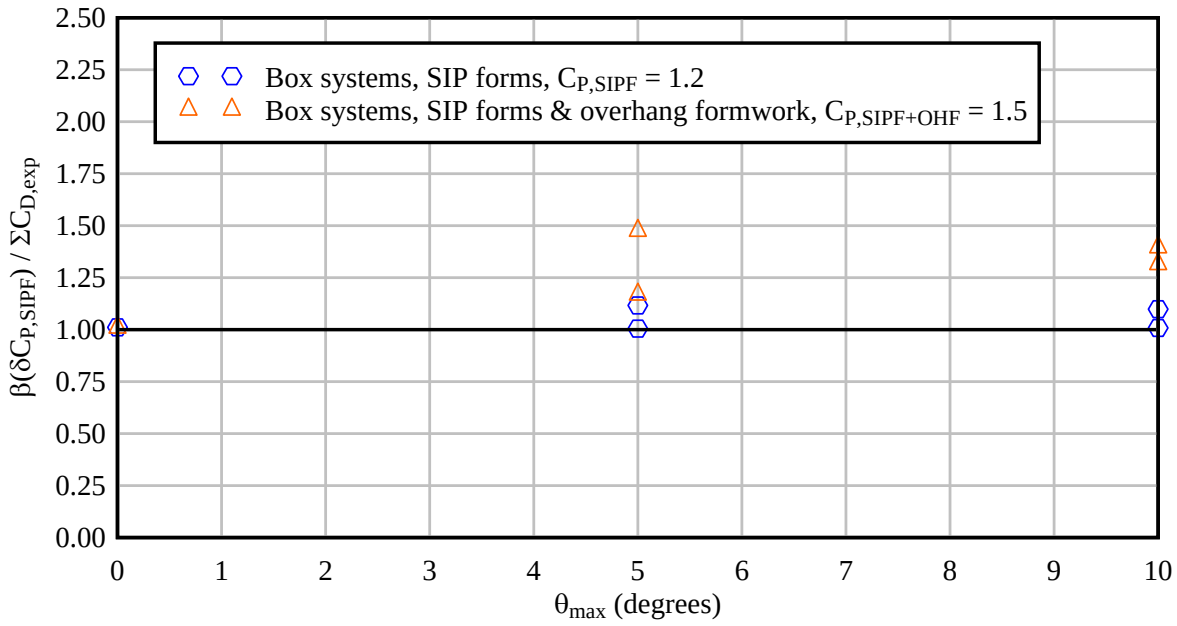

Figure 6-25. Conservatism of projected area calculation procedure for box girders (reduction factor (β) included)

CHAPTER 7
SUMMARY, CONCLUSIONS, AND RECOMMENDATIONS

7.1 Overview

In this study, issues relating to the application of construction gravity loads and lateral wind loads, to bridges under construction, were investigated. For construction gravity loads, a brace force prediction methodology was developed. For lateral wind loads, drag coefficients were measured using wind tunnel testing and a methodology for computing global pressure coefficients and applying the associated lateral wind pressures to bridges under construction was developed.

7.2 Brace Forces due to Construction Loads

Numerical finite element bridge models and analysis techniques were developed for evaluating brace forces induced by construction loads acting on precast concrete girders (Florida-I Beams) in systems of multiple girders braced together. Construction loads considered in this study included: wet concrete deck load, stay-in-place (SIP) form weight, overhang formwork weight, live load, worker line loads, and concentrated loads representing a deck finishing machine.

Preliminary limited-scope sensitivity studies indicated that brace forces were not particularly sensitive to bridge grade, bridge cross-slope, girder camber, or girder sweep; therefore, variations of these parameters were not included in subsequent parametric analyses. Additional sensitivity studies indicated that the typical configuration of K-brace recommended for use the FDOT generally produced marginally larger brace forces than did three alternative K-brace configurations. Consequently, for brace force determination purposes, only the FDOT recommended K-brace configuration was used in the remainder of the study.

A large-scale parametric study, involving more than 450,000 separate three-dimensional structural analyses, was performed to compute maximum brace forces for un-factored (service) and factored (strength) construction load conditions. Maximum end-span brace forces and intermediate-span brace forces quantified from the parametric study were stored into a database. The parametric study included consideration of different Florida-I Beam cross-sections, span lengths, girder spacings, deck overhang widths, skew angles, number of girders, number of braces, and bracing configurations (K-brace and X-brace). Additionally, partial coverage of wet (non-structural) concrete load and variable placement of deck finishing machine loads were considered.

To make the process of accessing and interpolating the brace force database simple and user-friendly, a MathCad-based program was developed that employed automated data-retrieval (from the database) and multiple-dimensional linear interpolation. The accuracy of the database interpolation approach to brace force prediction was found to be suitable for use in design (less than ten percent (10%) error was present in a majority of verification cases assessed). It is therefore recommended that the brace force database and database interpolation program developed in this study be deployed as a methodology for computing brace forces for bracing design in bridges under construction.

7.3 Wind Pressure Coefficients and Corresponding Lateral Loads

Wind tunnel testing was used to quantify wind load coefficients (drag, torque, and lift) for systems of multiple bridge girders (FIB, plate girder, and box) with stay-in-place (SIP) forms and overhang formwork in place. Tests were conducted at multiple wind angles, and corresponding tests with and without overhang formwork were conducted so that the effects of overhang formwork on drag, lift, and torque coefficients could be quantified.

Wind tunnel tests indicated that adding SIP forms to systems of bare girders [as were investigated in a previous study (BDK75-977-33, Consolazio et al., 2013)] had only an incremental influence on individual girder drag coefficients, rather than fundamentally changing the distribution of drag coefficients across the bridge. However, it was found that adding overhang formwork significantly increased the wind-induced torque on the windward girder. Additionally, by making use of lift force data measured for the windward girder, estimates of uplift forces acting on overhang formwork were produced.

Drag coefficients measured at each girder position in bridges with I-shaped girders, and in bridges with box girders, were used to develop conservative methods for computing global (system) pressure coefficients suitable for use in bridge design (particularly, for use in calculating global lateral substructure load due to wind). The developed methodology involves computing global pressure coefficients (using newly proposed values and expressions), computing design wind pressures (using established FDOT methods), and then applying the computed wind pressure to the projected area of the bridge using a newly proposed definition of projected bridge depth.

Finally, by comparing brace forces (note: *not* global substructure forces) caused by construction loads to brace forces caused primarily by wind load, it was found that the construction loads produced significantly larger brace forces and would therefore be very likely to control the design of bracing systems and bracing elements.

APPENDIX A
CROSS-SECTIONAL PROPERTIES OF FLORIDA-I BEAMS

In this study, finite element models Florida-I Beams (FIBs) were analyzed to evaluate temporary bracing forces caused by construction loads. In each model, the FIBs were modeled using *warping beam elements*, a specialized beam element available in the ADINA finite element code, which require the calculation of a comprehensive set of cross-sectional properties. This appendix provides mathematical definitions of all such properties and corresponding numeric values that were calculated for each FIB cross-sectional shape.

Definitions of the cross-sectional properties that are required to use the warping beam element in ADINA are listed in Table A-1. Each property requires the evaluation of an integral over the area of the cross-section, in which the integrands are written in terms of coordinates x and y, referenced to the geometric centroid of the section (Figure A-1). Some properties also require knowledge of the *warping function*, $\psi(x,y)$, which represents the torsionally-induced out-of-plane warping displacements per rate of twist at every point on the cross-section. (The units of ψ are therefore in/(rad/in) or in^2.)

For general cross-sectional shapes (e.g., an FIB), analytical (closed-form) solutions for $\psi(x,y)$ do not exist; instead the warping field $\psi(x,y)$ must be solved numerically. In this study, the calculation of $\psi(x,y)$ for each FIB shape was accomplished by discretizing the cross-sectional shape into a high-resolution mesh of thousands of two-dimensional triangular elements, and then employing a finite element approach to solve the governing differential equation.

In general, solutions for $\psi(x,y)$ change depending on the assumed location of the center of twist. In the literature, the term 'warping function' typically refers to a particular solution (ψ in Table A-1) corresponding to a state of *pure torsion*, i.e., torsion about the shear center. As a result, prior knowledge of the location of the shear center is required to compute several of the

warping beam properties. However, it is possible to calculate the coordinates of the shear center, x_S and y_S (Table A-1), using an alternative solution to the warping function (ψ_C), where the center of twist is assumed to be located at the centroid of the section. Therefore, two different warping functions were computed for each FIB section: first the section centroid was used to compute ψ_C and then the location of the shear center, obtained from ψ_C, was used to compute ψ as well as the remaining cross-sectional properties.

Because all FIB cross-sections are symmetric about the y-axis, I_{xy}, x_S, I_{xr}, and $I_{\omega r}$ have a value of zero (0) by definition. The remaining cross-sectional properties calculated for each FIB shape are summarized in Table A-2.

Table A-1. Definitions of cross-sectional properties required for use of a warping beam element

Property	Integral form	Units	Description
A	$\int_A dA$	in^2	Cross-sectional area
I_{yy}	$\int_A y^2 dA$	in^4	Strong-axis moment of inertia
I_{xx}	$\int_A x^2 dA$	in^4	Weak-axis moment of inertia
I_{xy}	$\int_A (xy) dA$	in^4	Product of inertia
x_S	$-\frac{1}{I_{yy}} \int_A (y\psi_c) dA$	in	X-coordinate of shear center
y_S	$\frac{1}{I_{xx}} \int_A (x\psi_c) dA$	in	Y-coordinate of shear center
J	$\int_A \left(x^2 + y^2 + x\frac{d\psi}{dy} - y\frac{d\psi}{dx} \right) dA$	in^4	St. Venant torsional constant
C_ω	$\int_A \psi^2 dA$	in^6	Warping constant
I_{xr}	$\int_A x\left(x^2 + y^2\right) dA$	in^5	Twist/strong-axis bending coupling term
I_{yr}	$\int_A y\left(x^2 + y^2\right) dA$	in^5	Twist/weak-axis bending coupling term
$I_{\omega r}$	$\int_A \psi\left(x^2 + y^2\right) dA$	in^6	Twist/warping coupling term
I_{rr}	$\int_A \left(x^2 + y^2\right)^2 dA$	in^6	Wagner constant

Table A-2. Cross-sectional properties of Florida-I Beams

Section	A (in^2)	I_{yy} (in^4)	I_{xx} (in^4)	y_s (in)	J (in^4)	C_ω (in^6)	I_{yr} (in^5)	I_{rr} (in^6)
36″ FIB	807	127,700	81,283	3.00	30,864	11,577,000	703,250	86,224,000
45″ FIB	870	226,810	81,540	3.46	31,885	21,835,000	1,521,200	167,760,000
54″ FIB	933	360,270	81,798	3.81	32,939	35,370,000	2,760,500	315,370,000
63″ FIB	996	530,790	82,055	4.07	33,973	52,203,000	4,471,300	562,480,000
72″ FIB	1059	741,060	82,314	4.27	35,041	72,337,000	6,693,800	951,390,000
78″ FIB	1101	904,610	82,484	4.38	35,693	87,610,000	8,473,400	1,314,600,000
84″ FIB	1143	1,087,800	82,657	4.46	36,421	104,350,000	10,504,000	1,781,400,000
96″ FIB	1227	1,516,200	83,002	4.56	37,859	142,280,000	15,336,000	3,107,900,000

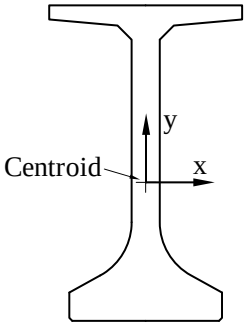

Figure A-1. Coordinate system used in the calculation of cross-sectional properties

APPENDIX B
DIMENSIONED DRAWINGS OF WIND TUNNEL TEST CONFIGURATIONS

This appendix includes dimensioned drawings of every girder configuration that was subjected to wind tunnel testing.

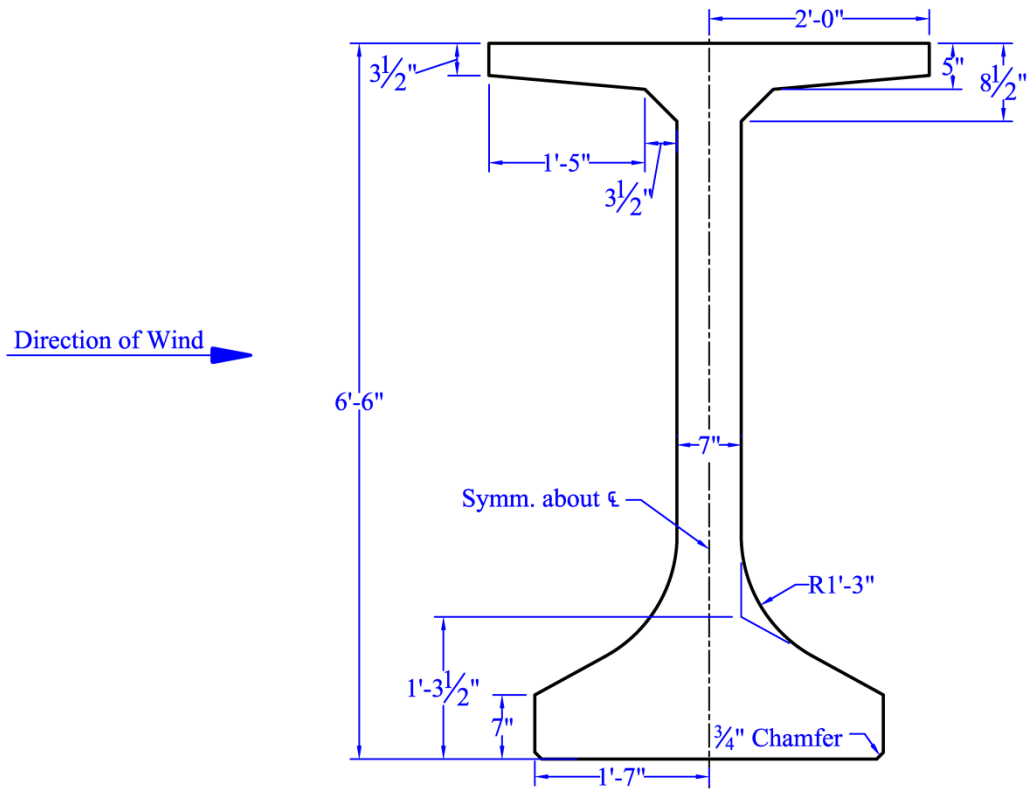

Girder Cross Section

REVISIONS			Determination of Brace Forces Caused by Construction Loads and Wind Loads During Bridge Construction		
Revision 1: 2012-12-17			University of Florida	78" Florida I-Beam Test Section	Sheet 1 of 7

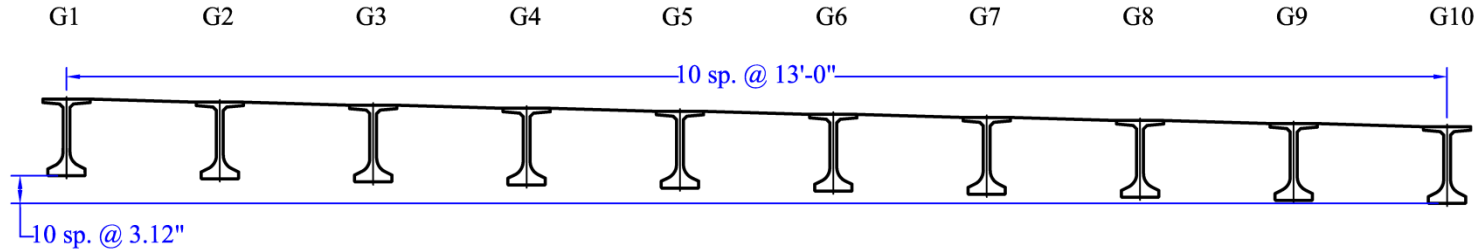

Set A1: 10 Girder Model (-2% Cross Slope)

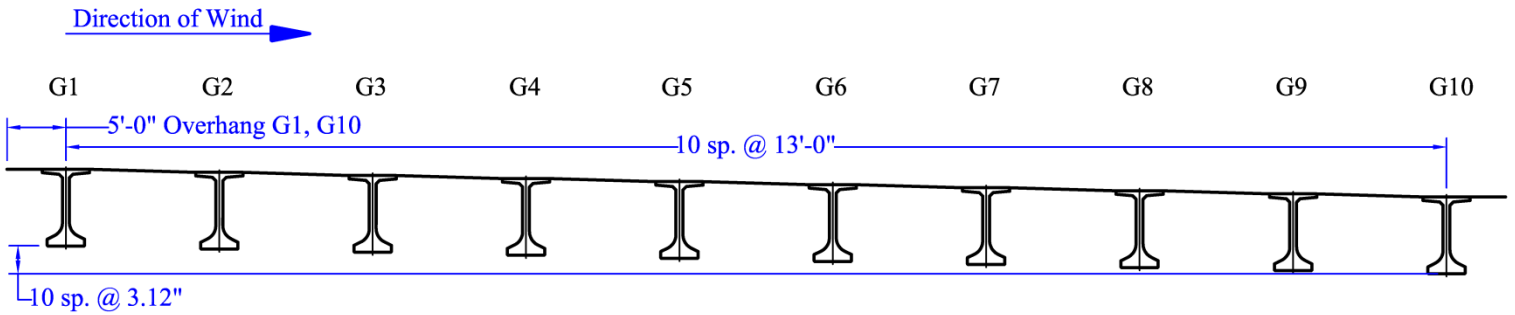

Set A2: 10 Girder Model (-2% Cross Slope, Overhangs Included)

REVISIONS			Determination of Brace Forces Caused by Construction Loads and Wind Loads During Bridge Construction		
Revision 1: 2012-12-17			University of Florida	78" Florida I-Beam Test Section	Sheet 2 of 7

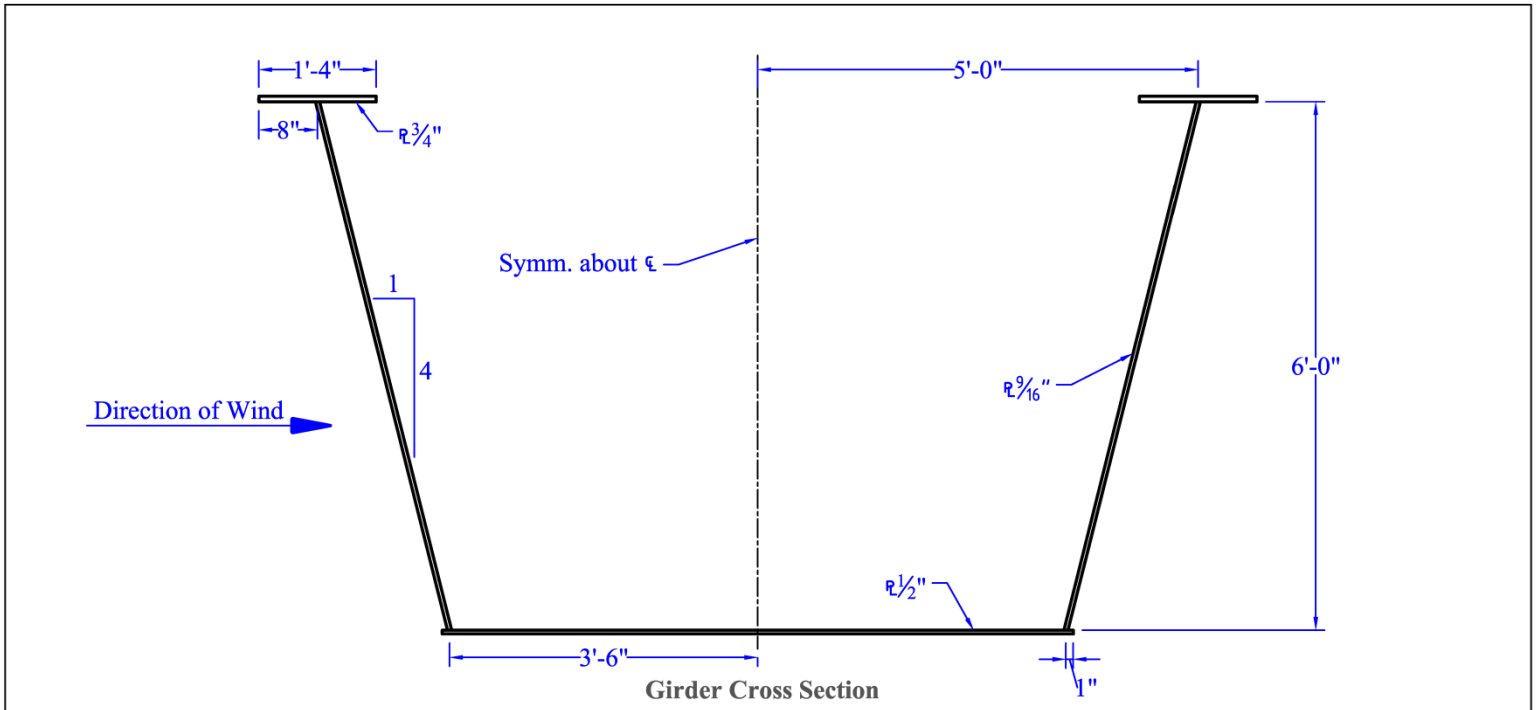

Girder Cross Section

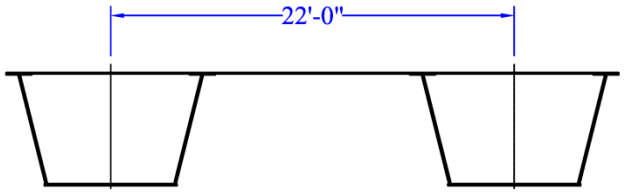

Set B1: 2 Girder Model
(0% Cross Slope)

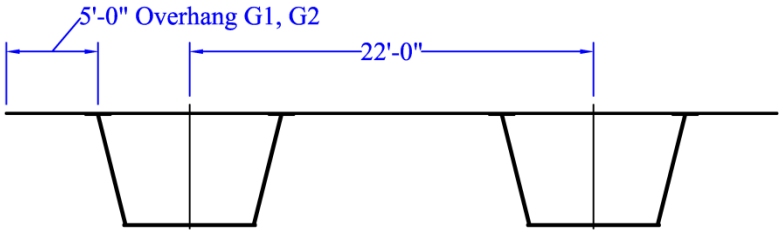

Set B2: 2 Girder Model
(0% Cross Slope, Overhangs Included)

REVISIONS			Determination of Brace Forces Caused by Construction Loads and Wind Loads During Bridge Construction		
Revision 1: 2012-12-17			University of Florida	Steel Box Girder Test Section	Sheet 3 of 7

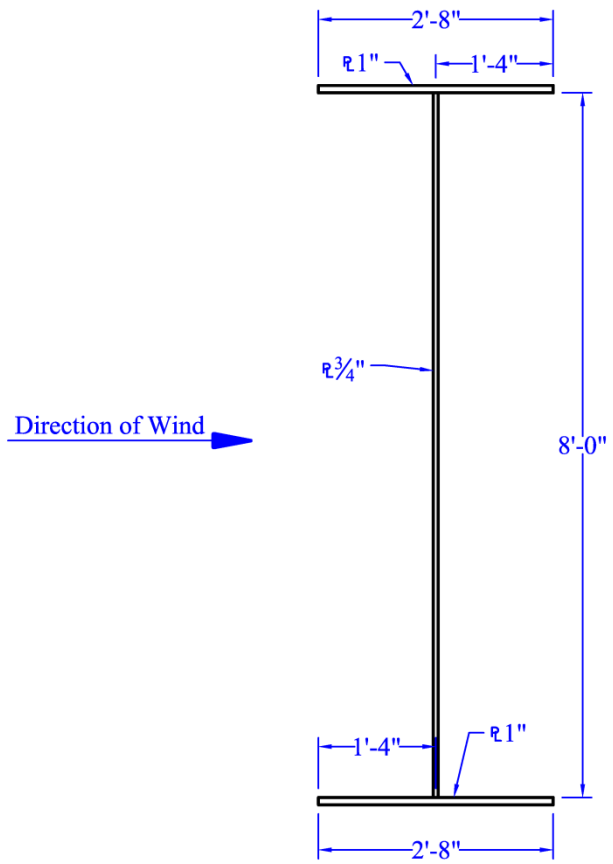

Girder Cross Section

REVISIONS			Determination of Brace Forces Caused by Construction Loads and Wind Loads During Bridge Construction		
Revision 1: 2012-12-17			University of Florida	Wide Flange Steel I-Girder Test Section	Sheet 4 of 7
Revision 2: 2013-07-30					

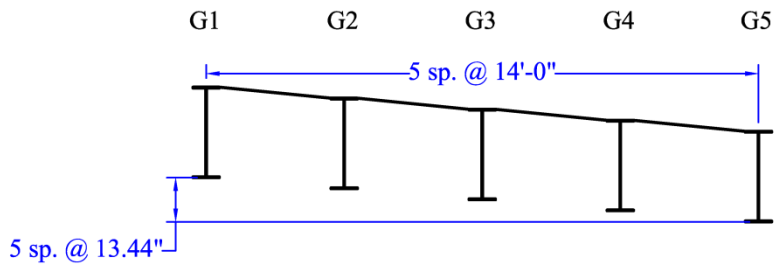

Set C1: 5 Girder Model (-8% Cross Slope)

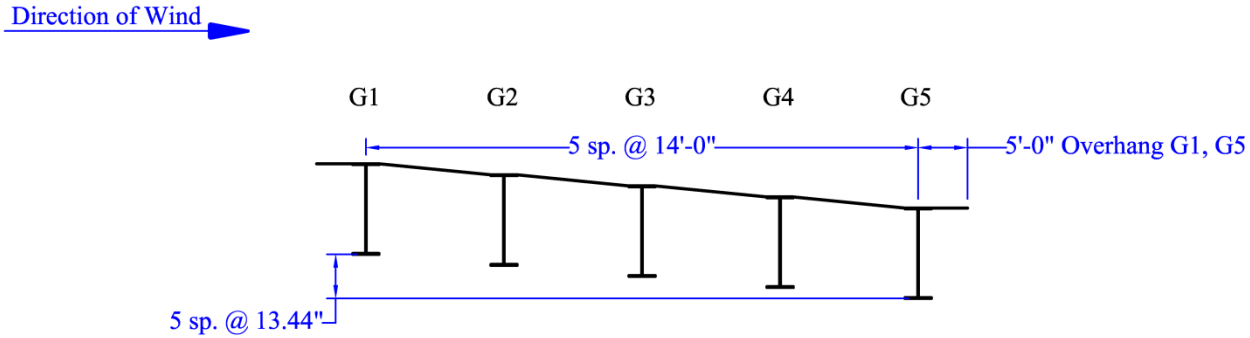

Set C2: 5 Girder Model (-8% Cross Slope, Overhangs Included)

REVISIONS			Determination of Brace Forces Caused by Construction Loads and Wind Loads During Bridge Construction		
Revision 1: 2012-12-17					
Revision 2: 2013-07-30			University of Florida	Wide Flange Steel I-Girder Test Section	Sheet 5 of 7

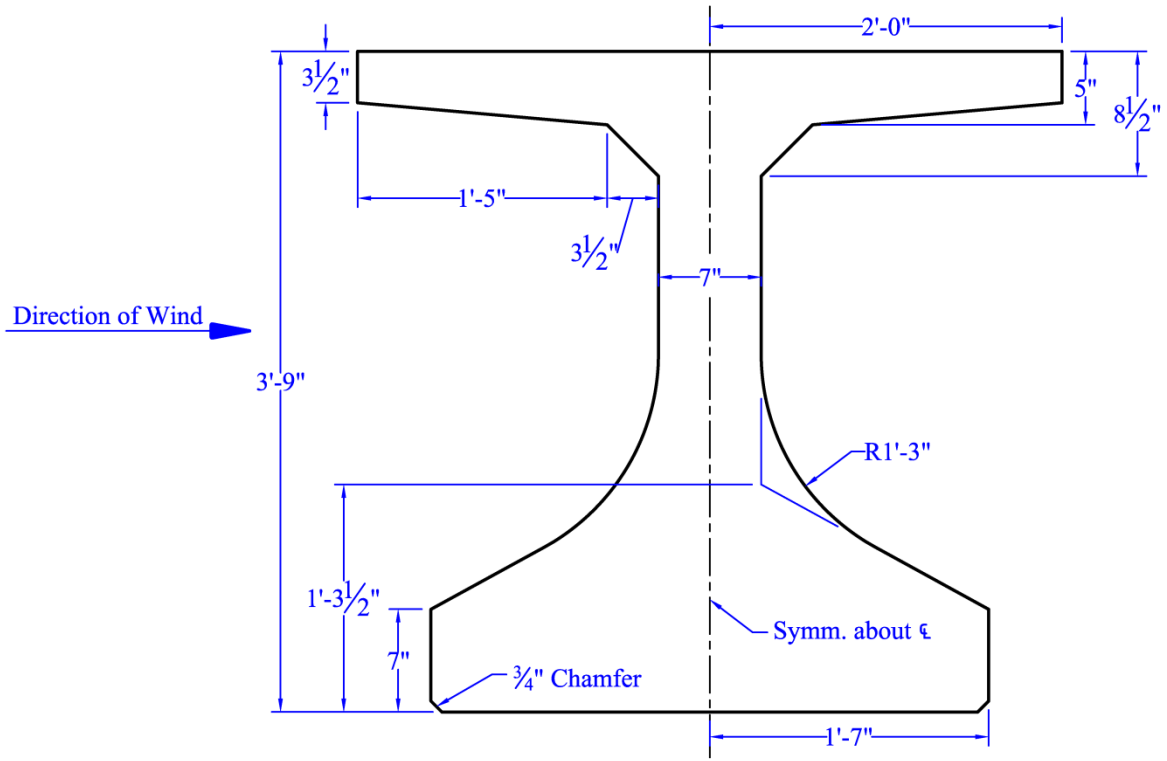

Girder Cross Section

REVISIONS			Determination of Brace Forces Caused by Construction Loads and Wind Loads During Bridge Construction		
Revision 1: 2012-12-17					
Revision 2: 2013-07-30			University of Florida	45" Florida I-Beam Test Section	Sheet 6 of 7

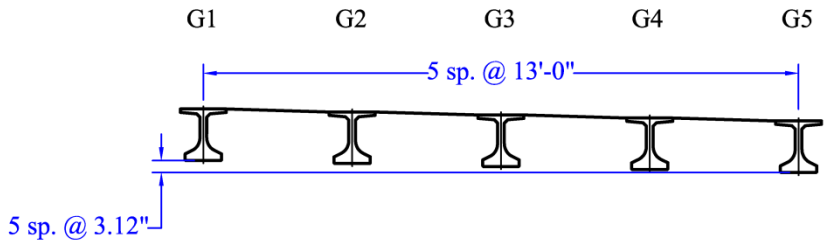

Set D1: 5 Girder Model (-2% Cross Slope)

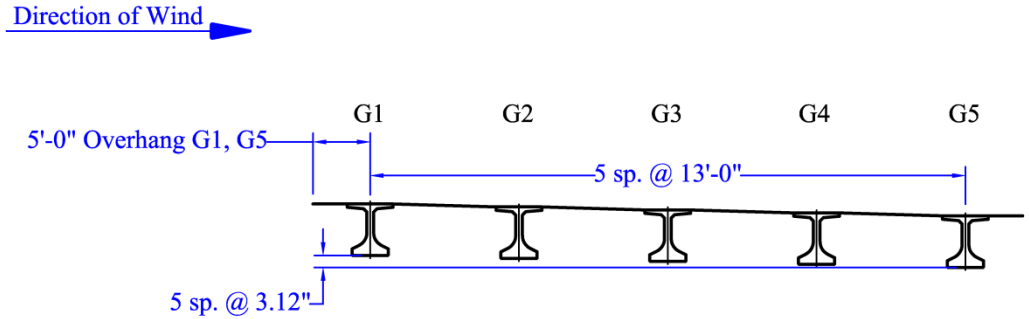

Set D2: 5 Girder Model (-2% Cross Slope, Overhangs Included)

APPENDIX C
TABULATED RESULTS FROM WIND TUNNEL TESTS

This appendix contains results from all of the wind tunnel tests that were performed, including drag, lift, and torque coefficients. The wind tunnel testing scope is given in Table C-1. Note that the wind coefficients in this appendix are converted to measurements at the girder centroid. Results for each test configuration are given an ID code consisting of a letter and a number. The letter describes the cross-section of the girders, and the number indicates if overhangs were included. A second number following a dash is the girder being measured. For example, the designation A2–5 refers to the fifth (5) 78" FIB girder in a configuration with overhangs (indicated by 2) in a group of ten (10).

Table C-1 Summary of wind tunnel tests

Configuration Name	Section	Overhangs included	Cross -slope	Spacing (ft)	Number of girders	Instrumented girder position
A1	78" FIB	-	-2%	13	10	1,2,3
A2	78" FIB	Yes	-2%	13	10	1,2,3,5,10
B1	Box	-	0%	22	2	1,2
B2	Box	Yes	0%	22	2	1,2
C1	WF Plate	-	-8%	14	5	1,2,3
C2	WF Plate	Yes	-8%	14	5	1,2,3,4,5
D1	45" FIB	-	-2%	13	5	1,2
D2	45" FIB	Yes	-2%	13	5	1,2,3

Testing Configuration A1

Cross-section:	78″ FIB
Spacing:	13 ft
Cross-slope:	-2%
Overhangs:	No
Number of girders:	10
Instrumented girders:	1, 2, 3

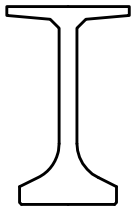

Drag coefficient (C_D)

Wind Angle	A1–1	A1–2	A1–3	A1–4	A1–5	A1–6	A1–7	A1–8	A1–9	A1–10
−5.0°	1.86	-0.02	-0.13	--	--	--	--	--	--	--
−2.5°	1.66	-0.10	-0.32	--	--	--	--	--	--	--
0°	1.47	-0.42	-0.17	--	--	--	--	--	--	--
2.5°	1.14	-0.52	0.08	--	--	--	--	--	--	--
5.0°	0.90	-0.31	0.09	--	--	--	--	--	--	--

Lift coefficient (C_L)

Wind Angle	A1–1	A1–2	A1–3	A1–4	A1–5	A1–6	A1–7	A1–8	A1–9	A1–10
−5.0°	-0.34	-1.96	-1.91	--	--	--	--	--	--	--
−2.5°	0.23	-0.28	-0.68	--	--	--	--	--	--	--
0°	0.69	1.07	1.53	--	--	--	--	--	--	--
2.5°	1.20	2.12	2.50	--	--	--	--	--	--	--
5.0°	1.44	2.69	2.70	--	--	--	--	--	--	--

Torque coefficient (C_T)

Wind Angle	A1–1	A1–2	A1–3	A1–4	A1–5	A1–6	A1–7	A1–8	A1–9	A1–10
−5.0°	0.41	0.10	-0.05	--	--	--	--	--	--	--
−2.5°	0.11	0.14	-0.07	--	--	--	--	--	--	--
0°	-0.10	-0.18	-0.01	--	--	--	--	--	--	--
2.5°	-0.36	-0.23	-0.01	--	--	--	--	--	--	--
5.0°	-0.48	-0.20	-0.04	--	--	--	--	--	--	--

Testing Configuration A2

Cross-section:	78″ FIB
Spacing:	13 ft
Cross-slope:	-2%
Overhangs:	Yes
Number of girders:	10
Instrumented girders:	1, 2, 3, 5, 10

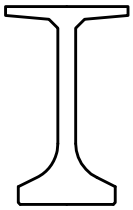

Drag coefficient (C_D)

Wind Angle	A2–1	A2–2	A2–3	A2–4	A2–5	A2–6	A2–7	A2–8	A2–9	A2–10
−5.0°	1.90	0.01	-0.10	--	-0.18	--	--	--	--	0.16
−2.5°	1.76	-0.05	-0.20	--	-0.10	--	--	--	--	0.21
0°	1.61	-0.11	-0.42	--	0.06	--	--	--	--	0.27
2.5°	1.43	-0.46	-0.12	--	0.03	--	--	--	--	0.34
5.0°	1.25	-0.53	0.06	--	0.01	--	--	--	--	0.46

Lift coefficient (C_L)

Wind Angle	A2–1	A2–2	A2–3	A2–4	A2–5	A2–6	A2–7	A2–8	A2–9	A2–10
−5.0°	0.14	-2.16	-1.95	--	-1.18	--	--	--	--	-0.06
−2.5°	1.47	-0.90	-1.10	--	-0.05	--	--	--	--	0.04
0°	2.07	0.56	1.03	--	0.62	--	--	--	--	0.04
2.5°	2.64	1.59	2.48	--	1.50	--	--	--	--	0.02
5.0°	2.85	2.05	2.75	--	2.41	--	--	--	--	0.24

Torque coefficient (C_T)

Wind Angle	A2–1	A2–2	A2–3	A2–4	A2–5	A2–6	A2–7	A2–8	A2–9	A2–10
−5.0°	1.47	0.01	-0.03	--	-0.04	--	--	--	--	0.11
−2.5°	1.11	0.18	-0.05	--	0.08	--	--	--	--	0.14
0°	0.98	-0.01	-0.11	--	0.09	--	--	--	--	0.15
2.5°	0.82	-0.26	-0.07	--	0.05	--	--	--	--	0.13
5.0°	0.67	-0.28	-0.03	--	-0.04	--	--	--	--	0.17

Testing Configuration B1

Cross-section:	Box
Spacing:	22 ft
Cross-slope:	0%
Overhangs:	No
Number of girders:	2
Instrumented girders:	1, 2

Drag coefficient (C_D)

Wind Angle	B1–1	B1-2
−10.0°	1.68	-0.05
−5.0°	1.74	-0.20
0°	1.71	-0.52
5.0°	1.67	-0.28
10.0°	1.55	0.22

Lift coefficient (C_L)

Wind Angle	B1–1	B1-2
−10.0°	-0.98	-1.34
−5.0°	0.01	-1.54
0°	1.04	-0.97
5.0°	1.19	0.88
10.0°	1.16	0.97

Torque coefficient (C_T)

Wind Angle	B1–1	B1-2
−10.0°	1.82	-0.71
−5.0°	1.56	-0.97
0°	0.64	-0.60
5.0°	0.53	0.29
10.0°	0.40	0.36

Testing Configuration B2

Cross-section:	Box
Spacing:	22 ft
Cross-slope:	0%
Overhangs:	Yes
Number of girders:	2
Instrumented girders:	1, 2

Drag coefficient (C_D)

Wind Angle	B2–1	B2–2
−10.0°	1.73	-0.01
−5.0°	1.80	-0.08
0°	1.80	-0.32
5.0°	1.92	-0.55
10.0°	1.88	-0.06

Lift coefficient (C_L)

Wind Angle	B2–1	B2–2
−10.0°	-0.83	-1.98
−5.0°	0.71	-1.77
0°	2.59	-1.34
5.0°	2.08	0.39
10.0°	1.89	0.75

Torque coefficient (C_T)

Wind Angle	B2–1	B2–2
−10.0°	2.76	-0.35
−5.0°	3.54	-0.41
0°	2.70	-0.42
5.0°	2.75	-0.08
10.0°	2.58	0.07

Testing Configuration C1

Cross-section:	WF Plate
Spacing:	14 ft
Cross-slope:	-8%
Overhangs:	No
Num. of girders	5
Instrumented girders:	1, 2, 3

Drag coefficient (C_D)

Wind Angle	C1–1	C1–2	C1–3	C1–4	C1–5
−5.0°	1.97	-0.12	-0.40	--	--
−2.5°	1.88	-0.34	-0.25	--	--
0°	1.78	-0.47	0.12	--	--
2.5°	1.68	-0.47	0.25	--	--
5.0°	1.55	-0.42	0.39	--	--

Lift coefficient (C_L)

Wind Angle	C1–1	C1–2	C1–3	C1–4	C1–5
−5.0°	0.08	-0.06	-0.39	--	--
−2.5°	0.30	0.57	1.08	--	--
0°	0.38	0.91	1.49	--	--
2.5°	0.39	1.01	1.53	--	--
5.0°	0.45	1.31	1.50	--	--

Torque coefficient (C_T)

Wind Angle	C1–1	C1–2	C1–3	C1–4	C1–5
−5.0°	0.00	0.00	-0.03	--	--
−2.5°	-0.08	-0.09	0.01	--	--
0°	-0.12	-0.13	0.08	--	--
2.5°	-0.12	-0.13	0.09	--	--
5.0°	-0.15	-0.11	0.13	--	--

Testing Configuration C2

Cross-section:	WF Plate
Spacing:	14 ft
Cross-slope:	-8%
Overhangs:	Yes
Num. of girders	5
Instrumented girders:	1, 2, 3, 4, 5

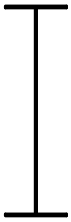

Drag coefficient (C_D)

Wind Angle	C2–1	C2–2	C2–3	C2–4	C2–5
−5.0°	2.20	-0.07	-0.30	-0.34	-0.02
−2.5°	2.12	-0.09	-0.40	-0.13	0.25
0°	2.06	-0.28	-0.30	0.28	0.40
2.5°	2.02	-0.41	-0.01	0.41	0.50
5.0°	1.95	-0.46	0.17	0.46	0.59

Lift coefficient (C_L)

Wind Angle	C2–1	C2–2	C2–3	C2–4	C2–5
−5.0°	1.44	-0.69	-1.30	-0.85	-0.11
−2.5°	1.76	0.33	0.13	0.12	0.06
0°	1.88	0.67	1.27	1.02	0.27
2.5°	1.79	0.81	1.52	1.24	0.37
5.0°	1.76	0.93	1.55	1.24	0.41

Torque coefficient (C_T)

Wind Angle	C2–1	C2–2	C2–3	C2–4	C2–5
−5.0°	0.83	0.10	-0.09	-0.10	-0.05
−2.5°	0.79	0.03	-0.04	0.03	0.05
0°	0.75	-0.09	-0.02	0.16	0.12
2.5°	0.72	-0.13	0.03	0.16	0.14
5.0°	0.69	-0.14	0.06	0.14	0.15

Testing Configuration D1

Cross-section:	45″ FIB
Spacing:	13 ft
Cross-slope:	-2%
Overhangs:	No
Num. of girders	5
Instrumented girders:	1, 2

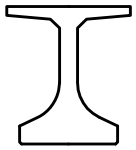

Drag coefficient (C_D)

Wind Angle	D1–1	D1–2	D1–3	D1–4	D1–5
−5.0°	1.65	-0.11	--	--	--
−2.5°	1.51	-0.23	--	--	--
0°	1.33	-0.38	--	--	--
2.5°	1.05	-0.22	--	--	--
5.0°	0.89	-0.01	--	--	--

Lift coefficient (C_L)

Wind Angle	D1–1	D1–2	D1–3	D1–4	D1–5
−5.0°	-1.09	-2.78	--	--	--
−2.5°	0.23	-1.60	--	--	--
0°	0.95	1.02	--	--	--
2.5°	1.68	2.86	--	--	--
5.0°	1.93	3.21	--	--	--

Torque coefficient (C_T)

Wind Angle	D1–1	D1–2	D1–3	D1–4	D1–5
−5.0°	1.44	-0.07	--	--	--
−2.5°	0.25	0.07	--	--	--
0°	-0.36	0.06	--	--	--
2.5°	-0.89	-0.32	--	--	--
5.0°	-1.14	-0.17	--	--	--

Testing Configuration D2

Cross-section:	45″ FIB
Spacing:	13 ft
Cross-slope:	-2%
Overhangs:	Yes
Num. of girders	5
Instrumented girders:	1, 2, 3

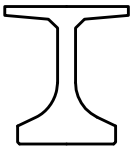

Drag coefficient (C_D)

Wind Angle	D2–1	D2–2	D2–3	D2–4	D2–5
−5.0°	1.69	-0.13	-0.18	--	--
−2.5°	1.66	-0.18	-0.20	--	--
0°	1.59	-0.28	-0.16	--	--
2.5°	1.49	-0.32	0.15	--	--
5.0°	1.41	-0.38	0.36	--	--

Lift coefficient (C_L)

Wind Angle	D2–1	D2–2	D2–3	D2–4	D2–5
−5.0°	-0.97	-2.96	-2.13	--	--
−2.5°	0.90	-2.34	-1.20	--	--
0°	2.63	-0.58	-0.16	--	--
2.5°	3.48	1.69	1.91	--	--
5.0°	3.64	2.30	2.86	--	--

Torque coefficient (C_T)

Wind Angle	D2–1	D2–2	D2–3	D2–4	D2–5
−5.0°	3.03	-0.01	-0.05	--	--
−2.5°	3.48	-0.18	-0.09	--	--
0°	2.59	0.19	-0.16	--	--
2.5°	2.27	-0.31	0.39	--	--
5.0°	2.06	-0.55	0.47	--	--

LIST OF REFERENCES

AASHTO (American Association of State Highway and Transportation Officials) (2008). *Guide Design Specification for Bridge Temporary Works*, AASHTO, Washington, D.C.

AASHTO (American Association of State Highway and Transportation Officials) (2010). *LRFD Bridge Design Specifications: 5th Edition*, AASHTO, Washington, D.C.

ADINA (2012). *Theory and Modeling Guide, Volume 1: ADINA Solids & Structures*, ADINA R&D, Inc, Watertown, MA.

ASCE (American Society of Civil Engineers) (2006). *ASCE 7–05: Minimum Design Loads for Buildings and Other Structures*, ASCE, New York, NY.

Çengel, Y. and Cimbala, J. (2006). *Fluid Mechanics: Fundamentals and Applications*, McGraw–Hill Higher Education, Boston, MA.

Clifton, S. and Bayrak, O. (2008). *Bridge Deck Overhang Construction*, Technical Report IAC: 88-5DD1A003-2, University of Texas, Austin, TX.

Consolazio, G., Gurley, K., and Harper, Z. (2013). *Bridge Girder Drag Coefficients and Wind-Related Bracing Recommendations*, Structures Research Report No. 2013/87322, University of Florida, Gainesville, FL.

FDOT (Florida Department of Transportation) (2009). *Temporary Design Bulletin C09–07*, FDOT, Tallahassee, FL.

FDOT (Florida Department of Transportation) (2010). *Standard Specifications for Road and Bridge Construction*, FDOT, Tallahassee, FL.

FDOT (Florida Department of Transportation) (2013). *Structures Manual Volume I: Structures Design Guidelines*, FDOT, Tallahassee, FL.

FDOT (Florida Department of Transportation) (2014a). *Design Standard No. 20005: Prestressed I-Beam Temporary Bracing*, FDOT, Tallahassee, FL.

FDOT (Florida Department of Transportation) (2014b). *Instructions for Design Standard No. 20010: Prestressed Florida-I Beams*, FDOT, Tallahassee, FL.

FDOT (Florida Department of Transportation) (2014c). *Design Standard No. 20510: Composite Elastomeric Bearing Pads – Prestressed Florida-I Beams*, FDOT, Tallahassee, FL.

Holmes, J. (2007). *Wind Loading of Structures: 2nd Edition*, Taylor & Francis, New York, NY.

PCI (2010). *PCI Design Handbook: 7th Edition*, Precast/Prestressed Concrete Institute, Chicago, IL.

Solari, G. and Kareem, A. (1998). "On the Formulation of ASCE 7–95 Gust Effect Factor", *Journal of Wind Engineering and Industrial Aerodynamics*, Vol. 77, pp. 673–684.

Young, W. C. and Budynas, R. G. (2002). *Roark's Formulas for Stress and Strain: 7th Edition*, McGraw–Hill, New York, NY.

BIOGRAPHICAL SKETCH

Sam Edwards was born in Amelia Island, Florida, in 1989. In August 2007, he started his career at the University of Florida, where he received the degree of Bachelor of Science in civil engineering in May 2012. He then enrolled in graduate school at the University of Florida where he received a Master of Engineering in civil engineering in May 2014, with an emphasis in civil structures.